Thermal and Mechanical properties of Al/AlN interpenetrating phase composites with different preform porosity

プリフォーム多孔体の構造が Al/AlN 相互貫入複合材料の熱的，機械的性質に与える影響

Department of Mechanical Science and Engineering
Graduate School of Engineering
Hiroshima University, Japan

Advisor: Prof. Gen Sasaki

Yan Xiao

July 2024

Contents

Chapter 1 Background and Objective

Chapter 2 Microstructure and mechanical properties of Al/AlN

interpenetrating phase composites with different preform porosity

Chapter 3 Thermal expansion behavior and analysis of Al/AlN interpenetrating phase composites with different preform porosity

Chapter 4 Thermal conductivity of Al/AlN interpenetrating phase composites with different preform porosity

List of Figures

List of Tables

Chapter1

Background and Objective

1.1 Introduction

In the contemporary world, rapid advancements and technological innovations in materials science and engineering continually reshape human lifestyles and work environments. The progress in science and technology, along with the advancements in aerospace, the automobile industry, construction, and electronics, imposes higher standards for material performance. Traditional materials, in turn, manifest various limitations that hinder their ability to meet the progressively intricate and diverse requirements. Consequently, there is a growing urgency in the research and development of novel materials. Composites, emerging as a new material type, garner significant attention[1–6].

Composite materials are novel materials with unique properties formed by combining materials of diverse properties (polymers, metals, inorganic, and non-metallic) through a specialized process[7–9]. Based on the type of reinforcing phase, composites can be categorized into various types including particles, fibers, whiskers, and three-dimensional continuous structures. Particles, whiskers, and fibers are typically randomly dispersed within the traditional composite matrix, resulting in a discontinuous reinforcing phase, which increases the likelihood of uneven distribution and particle agglomeration during composite preparation[10–13]. Interpenetrating phase composite (IPC) represents a novel composite material where the matrix and reinforcing phase form continuous and interpenetrating structures in three-dimensional space. This arrangement facilitates stress transfer and dispersion between phases, inhibiting crack propagation, and consequently enhancing the mechanical properties of the composite material. The types of reinforcing phases, matrix, as well as the morphology and properties of interfaces significantly influence the properties of composites possessing a three-dimensional continuous network structure. This innovative composite material exhibits superior mechanical and wear-resistant properties compared to traditional composites, offering extensive application prospects in aerospace, automotive, and other fields[14–18].

The three-dimensional interpenetrating network structure of metal-ceramic composites finds wide applications across various classes of metal and ceramic materials. These composites exhibit excellent electrical conductivity, thermal conductivity, mechanical properties, and high-temperature resistance[19–23]. Organically combining metals and ceramics to construct a three-dimensional interpenetrating network structure is expected to leverage the synergistic effects of both materials and overcome their individual deficiencies, resulting in enhanced performance. Within the metal-ceramic IPCs, predominant ceramic phases include Al_2O_3, SiC, ZrO_2, Si_3N_4, TiC, TiB2, and SiO_2, while dominant metal phases comprise Al, Ag, Mo, Ni, Cu, Cr, and Fe[24–33]. Limited research has been conducted on Al / AlN IPCs. Al is renowned for its lightweight nature, high strength-to-weight ratio, and excellent thermal conductivity, rendering it a versatile matrix material in composite systems[7,34,35]. Conversely, AlN, with its high thermal conductivity, exceptional thermal shock resistance, and electrical insulation properties, effectively complements aluminum, rendering Al/AlN IPCs an attractive area of research for numerous industrial and technological applications[36–38]. Hence, comprehensive investigation into the microstructure, mechanical, and thermal properties of Al/AlN IPCs is of paramount importance.

1.2 Interpenetrating phase composites

1.2.1 Concept of interpenetrating phase composites

Interpenetrating phase composite materials (IPCs) constitute a novel class of materials characterized by distinctive microstructures. At the microscale, each constituent phase forms a distinct three-dimensional continuous network structure, intertwining and interlacing with one another (as depicted in

Fig. 1-1). IPCs may not comprise independently existing particulate phases, thereby eliminating the traditional differentiation between inclusions and matrix at the microstructural level. Removal of any constituent phase from the material does not preclude the formation of a porous structure capable of withstanding external loads by the remaining phases[39–41]. While prevalent in biological organisms like the shell of abalone, the dactyl club of mantis shrimp[42,43], the shell of bivalve mollusk[44,45] and branches[46,47], interpenetrating phase composite materials are comparatively less common in synthetic material research.

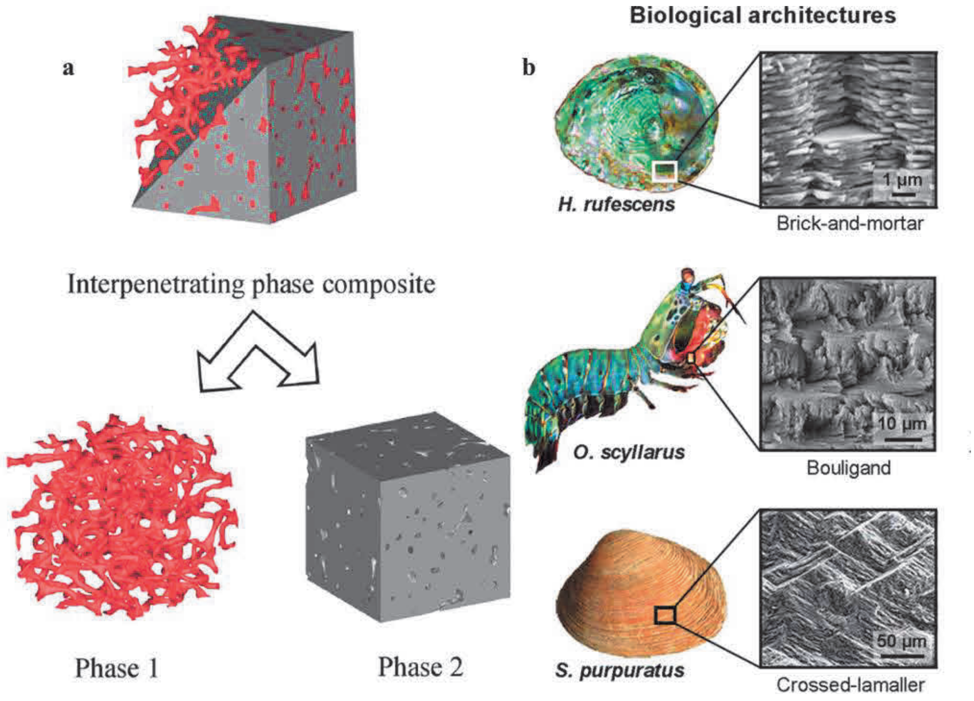

Fig. 1-1 Examples of IPCs: a. Schematic diagram of IPCs[48], b. interpenetrating phase structures in nature[49].

IPCs can be broadly categorized based on their phase composition as follows: Metal-polymer, ceramic-polymer, polymer-polymer, ceramic-metal, metal-metal, etc. Metal-polymer IPCs generally exhibit favorable mechanical properties and thermal conductivity, making them suitable for applications demanding wear resistance and effective thermal management. Nonetheless, disparities in the coefficient of thermal expansion between the metal and polymer may induce interfacial stresses, thereby compromising the material's long-term stability[50–52]. The ceramic-polymer IPCs merges ceramics' high hardness with polymers' flexibility, rendering it apt for crafting wear- and impact-resistant components. Nevertheless, the brittleness of ceramics and the limited thermal stability of polymers might curtail their application in high-temperature settings[53,54]. Polymer-polymer IPCs can attain distinct physical and chemical properties, like enhanced chemical resistance or electrical insulation, through the amalgamation of diverse polymers. Nonetheless, this amalgamation may come at the cost of other attributes, such as thermal conductivity or mechanical strength[55,56]. Metal-metal IPCs can be alloyed with various metals to optimize their properties, such as enhancing strength or electrical conductivity. Nonetheless, processing them can be challenging and they tend to incur higher costs compared to single-metal materials[57–59]. Ceramic-metal IPCs typically exhibit exceptional resistance to high temperatures, thermal properties, and mechanical strength, rendering them ideal for applications in aerospace and similar fields. However, they can be heavier than single materials[60,61].

1.2.2 Preparation of interpenetrating phase composites

There are several broad methods of preparation of IPCs:

(1) In situ method

The in-situ reaction method employs chemical reactions occurring in the same location to synthesize composites directly, forming three-dimensional interpenetrating network structures at the microscopic scale. This approach is primarily employed in the fabrication of metal-ceramic IPCs. The composites exhibit excellent compatibility between its reactive phase and other phases, along with stable interfacial bonding[21,62].

There are 3 main types of situ reaction impregnation methods: 1) Direct Oxidation method: This method involves simultaneously impregnating the preform with molten metal and oxidizing it. This pioneering process for composite material synthesis was developed by the Lanxide Company in the USA[63]. 2) Replacement reaction method: This method involves an in-situ reaction between the prefabricated body and the molten metal during the infiltration process, yielding a metal/ceramic composite material characterized by a three-dimensional interpenetrating network structure. This method is commonly employed to fabricate Al/Al_2O_3 IPCs[64]. 3) Chemical reaction method: In the chemical reaction method, the reinforcing phase powders within the prefabricated body undergo direct synthesis of the ceramic reinforcing phase, utilizing the substantial heat released during the chemical reaction. Chen et al. fabricated TiC/Mg composites exhibiting a three-dimensional interpenetrating network structure using this method[65]. The in-situ reaction method offers several advantages: simplicity in process, rapid infiltration and solidification, high efficiency, superior material properties, low production costs, and near net size molding. However, there are drawbacks, such as limited flexibility, challenges in controlling filling speed, issues with slag collection and exhaust, difficulty in controlling ceramic body morphology, tendency for composite structures to develop sharp corners and holes, and the limitation to obtaining nano-scale ceramic reinforced phases, thereby restricting the material's full performance potential.

(2) Squeeze casting method

Squeeze casting involves creating a preform that matches the part's shape, inserting it into a mold, pouring molten matrix alloy, applying pressure to facilitate liquid infiltration into the preform, and sustaining this pressure during solidification, ultimately yielding a composite material (depicted in Fig. 1-2). The squeeze penetration process comprises three discernible stages[66,67]. In the initial stage, the externally applied pressure must surpass the threshold capillary resistance of the precast body to facilitate melt penetration. This stage is succeeded by a continuous phase of melt flow, during which the pressure escalates proportionally with the duration of melt infiltration until the preform is filled with the alloy. The phase concludes upon reaching the penetrating -through pressure. Subsequently, any remaining air is expelled through the micropores and replaced by the molten alloy, marking the final stage of the process. The primary parameters in this process include the preheating temperature of the precast body, the injection temperature of the metallic fluid, and the pressure level.

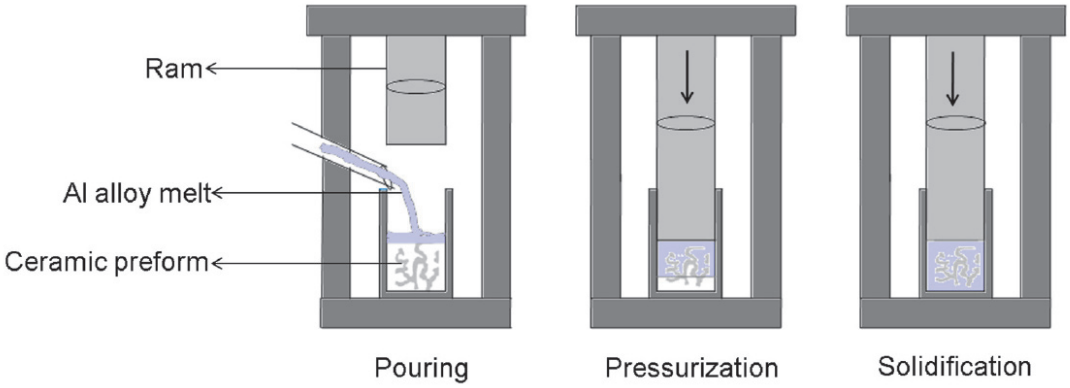

Fig. 1-2 Schematic diagram of the squeeze casting process[39].

This method offers several advantages, including a simple process, good stability, uncomplicated equipment, low investment, short production cycle, and easy scalability. However, there are drawbacks to consider. These include the necessity for high-pressure equipment and the requirement for well-sealed high-pressure molds, resulting in higher production costs. Additionally, preform must possess a certain level of mechanical strength. Furthermore, the production of complex-shaped parts, particularly small, thin-walled electronic packaging components, is severely restricted.

(3) Pressureless infiltration method

Pressureless infiltration refers to the process of preparing composite materials with a network structure. This process involves the spontaneous immersion of molten metal into solid, porous preform through capillary action and gravity, without the application of external pressure (Fig. 1-3). It is a widely employed and efficient technique for fabricating composites with a high-volume fraction of reinforcing phases. Well wettability between the molten material and the preformed body is crucial for ensuring the efficient operation of the process.[68,69] The primary process parameters include alloy composition, impregnation temperature, impregnation duration, and ambient atmosphere. This method offers several advantages: a simple process requiring no high-pressure equipment, enabling the production of large and complex structures. However, there are several drawbacks associated with this method, such as the propensity for shrinkage holes, weak interfacial bonding, extended impregnation time, and susceptibility to variations in material properties, affecting the melting and infiltration process.

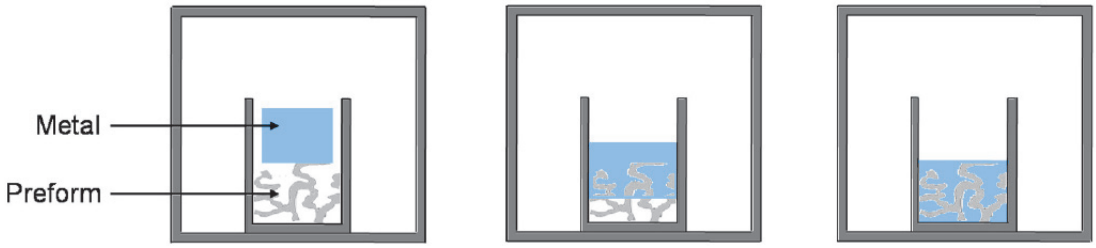

Fig. 1-3 Schematic diagram of the pressureless infiltration process[39].

(4) Gas pressure infiltration

The gas pressure infiltration technique uses gas pressure to aid in impregnating the melt into the open preform, illustrated in Fig. 1-4 schematically. Initially, the vacuum chamber containing the preforms and metal blanks is evacuated. Then, the temperature is elevated to a specified level. Once the alloy has fully melted and coated the preform, gas is introduced under a specific pressure to facilitate the infiltration of the melt into the preform[70–72]. This method requires an initial vacuum of adequate strength to evacuate air from the porous preform, ensuring the smooth infiltration of the melt into its pores. Temperature, applied pressure, and vacuum are critical process parameters in gas pressure infiltration. Advantages encompass the capacity to address wettability issues between the melt and the precast part, shorter processing times, diminished reactions at the interface, and the eradication of porosity and shrinkage. The drawbacks entail the requirement for high-pressure equipment and elevated costs.

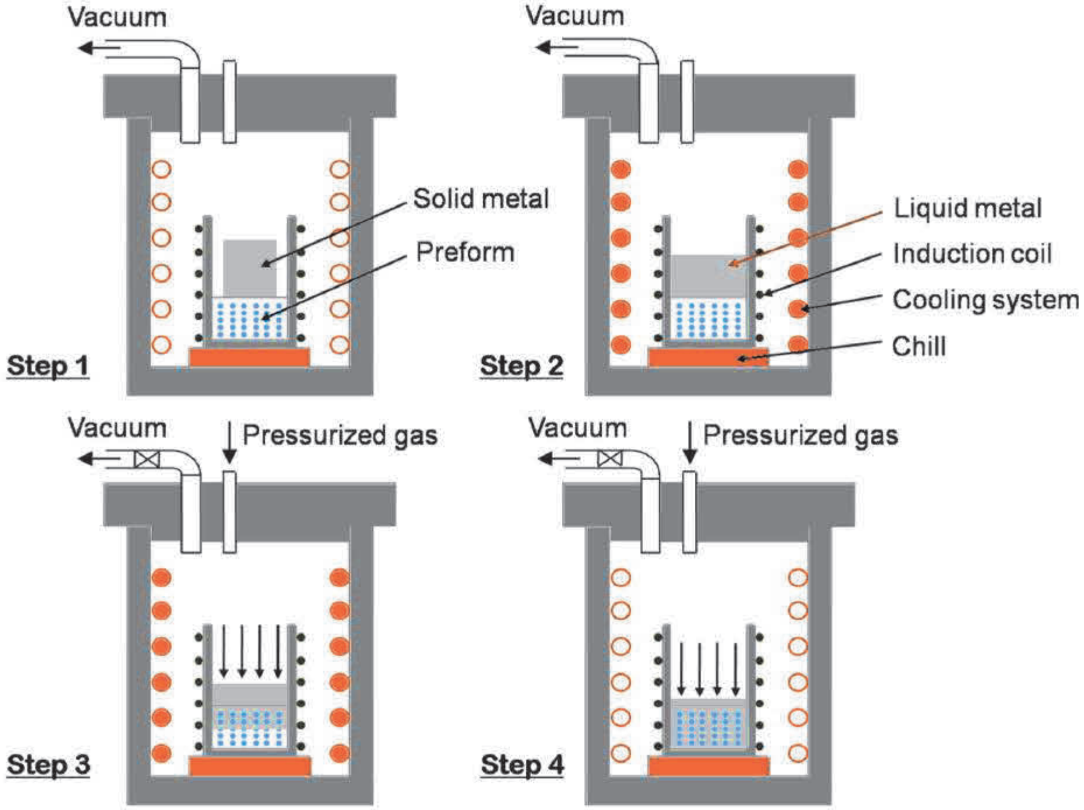

Fig. 1-4 Schematic diagram of the gas-pressure infiltration process[39].

(5) Vacuum infiltration method

Vacuum infiltration technology primarily utilizes negative pressure created under vacuum conditions to infiltrate molten material into a preformed structure (Fig. 1-5). The melt is initially heated to the specified temperature and melted. A continuous flow of inert gas is then introduced into the preform. Subsequently, vacuum is applied, immersing the preform in the melt. The composite is cooled to room temperature upon completion of the infiltration process[73,74]. Vacuum infiltration offers significant advantages including a broad range of applications, a streamlined production process, and easy parameter control. However, the drawback lies in the low solidification rate, resulting in undesirable interfacial reaction byproducts and accelerated grain growth within the metal phase.

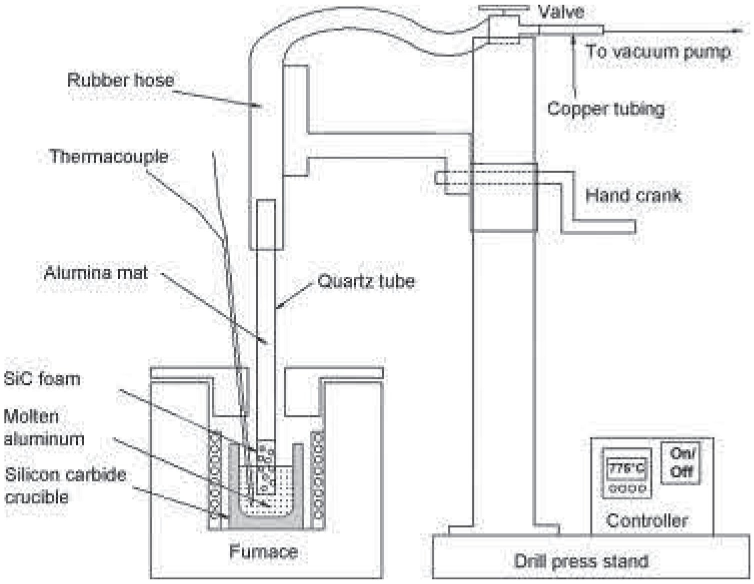

Fig. 1-5 Schematic diagram of the vacuum infiltration process[75].

1.2.3 Application of interpenetrating phase composites

The primary motivation for the interest in IPCs stems from the effective preservation of properties from each constituent phase, leading to superior overall properties unattainable with single-phase materials. The structure of 3D interpenetrating network composites, where reinforcements and tougheners permeate and intersect in three dimensions, dictates their properties, including exceptional mechanical, thermal, abrasion, and vibration damping characteristics.

Taking metal-ceramic IPCs as an example, significant advancements in porous ceramics in recent years have catalyzed notable progress in the research and development of metal-ceramic IPCs. This is because the primary method for preparing such IPCs involves molten metal infiltrating the porous ceramic preform. The plastic toughness of the continuous metal network in three dimensions hinders crack expansion, while the robust ceramic network efficiently bears and transfers loads with its low coefficient of thermal expansion ensuring dimensional stability at high temperatures.

Consequently, it exhibits superior strength and toughness, alongside excellent resistance to abrasion and fatigue. Additionally, it possesses a lower coefficient of thermal expansion and thermal hysteresis compared to conventional particle-reinforced composites, thereby leading to an extended service life during thermal cycling. Metal-ceramics, owing to their unique properties, find extensive applications across various sectors including automotive, electronics, and aerospace[39,76,77]. They are utilized in diverse components such as emergency brake pads for automotive systems, piston tops, cylinder liners, and connecting rods in internal combustion engines, as well as in turbo compressors. Additionally, they serve as heatsink substrates in electronic packaging, nuclear shielding materials, and electrode materials for batteries. Furthermore, their high energy absorption capacity makes them valuable in mitigating vibrations in seismic structures.

By combining the high strength and toughness of metals with the high damping properties of polymers, metal-polymer IPCs can be engineered as specialty materials with high strength, low modulus, and high damping characteristics. This material's design flexibility and interpenetrating structure result in unique mechanical and physical properties, making it suitable for various applications such as impact resistance, damping, electromagnetic shielding, and phase change, which find extensive use in aviation, aerospace, transportation, energy, and construction industries[78–81].

In engineering applications, these materials serve as impact-resistant materials for protecting transportation vehicles from impacts, such as automotive bumper tubes filled with aluminum foam/epoxy IPCs. Their lightweight, compact size, low energy consumption, and ease of maintenance make them promising impact protection devices in the transportation sector. In industrial manufacturing, gear sets composed of aluminum foam/epoxy composites can exhibit damping ratios 8 to 20 times higher than those of cast iron components. In earthquake-resistant building engineering, metal/polymer interpenetrating composites are employed to fabricate diverse types of dampers. These dampers outperform conventional vibration-absorbing materials and viscous fluid dampers in terms of energy dissipation and damping properties, effectively mitigating the collision between neighboring buildings under seismic waves with varying spectral characteristics and intensities. Due to its high damping, high thermal conductivity, and low density, this material is exceptionally suitable for manufacturing electronic equipment enclosures and compatible electronic devices, serving as an excellent electromagnetic shielding material[50,51,82,83].

Metal/metal IPCs can address the wettability issue between two phases in composite preparation, owing to the minor property differences between components, facilitating the fabrication of 3D network composites with flawless interfaces via a straightforward process. In recent years, additive manufacturing, primarily 3D printing, has significantly advanced the research and production of metal/metal IPCs[57].

Various performance requirements can be achieved by combining different metals. For instance, Ti-Mg composites IPCs desirable properties for biomedical applications. Ti possesses low density, high strength, corrosion resistance, excellent biocompatibility, and non-magnetic properties, making it of significant interest in the biomedical field[84]. Mg also exhibits high specific strength, good damping properties, and biodegradability[85,86]. Therefore, Ti-Mg IPCs are highly suitable for biodegradable implants[87]. Besides its biomedical applications, NiTi-Mg IPC is also preferred in automotive manufacturing for its outstanding damping properties. NiTi and Mg are lightweight metals known for their good damping properties. Particularly, Mg exhibits outstanding high-temperature damping properties, while NiTi possesses remarkable shape memory, strain rate sensitivity, and high-temperature strength[88–90]. This combination results in NiTi-Mg IPC demonstrating superior high-temperature damping capabilities compared to its room-temperature counterparts[91]. Stainless steel-aluminum IPCs also hold promising applications in ballistic protection. The distinct impedance properties of both phases, along with their unique three-dimensional interpenetrating structure, enable them to efficiently reflect impact vibrations and undergo minimal deflection and spalling damage in comparison to laminated composites[92].

Ceramic/polymer IPCs show promising potential in dental material applications owing to their biocompatibility, adequate strength, modulus of elasticity, and excellent wear resistance[54,93]. Polymer-Polymer IPCs exhibit remarkable utility in photovoltaics and soft robotics owing to their lightweight nature, exceptional flexibility and elasticity, heightened stability, and outstanding electrical insulation properties[94].

1.3 Porous ceramics

1.3.1 Classification and structural characteristics of porous ceramics

Porous ceramics are the predominant choice for IPCs preforms, and the rapid advancement in porous ceramics research in recent years has significantly propelled IPCs research forward. Porous ceramics are obtained through high-temperature treatment, resulting in a significant number of closed or interconnected pores within the ceramic material structure. These materials offer low bulk density, high specific surface area, formidable strength, as well as corrosion and high-temperature resistance. Porous ceramics can be categorized into two types based on their pore structure: honeycomb ceramics and foam ceramics[95–97].

Honeycomb ceramics are typically structured in two-dimensional arrays of pore units, such as cylinders and tetrahedrons. Current research is primarily focused on foam ceramics, which are generally classified as either open-cell or closed-cell ceramics based on the presence of solid walls within the pores. If the solid phase material forming the foam only occupies the corners of the pores, the material exhibits open pores distributed in three dimensions. Additionally, pore units can take forms such as tetrahedral, trigonal, tetragonal, hexagonal, octahedral, dodecahedral, or icosahedral, with interconnected pores, known as open-cell ceramics, characterized by high permeability. Conversely, if the material features a solid closed surface and independent pores, it is classified as closed-cell ceramic material. Generally, porous ceramics contain both open and closed pores.

1.3.2 Preparation method of porous ceramics

The manufacturing process of porous ceramics directly impacts pore morphology, size, distribution, and connectivity. Common preparation methods include:

(1) Direct foaming method

The direct foaming method involves preparing porous ceramic materials by incorporating a blowing agent into the ceramic components, which generates volatile gases or foams through heat treatment or chemical reactions[98]. During experimentation, the foam exhibits thermodynamic instability owing to its high surface free energy, necessitating rapid curing in the slurry to achieve a high-strength ceramic body.

(2) Foaming agent addition method

Pore-forming agents are added to ceramic powders to occupy space during billet molding, subsequently removed at high temperatures, leaving voids in the sintered ceramic body, thus creating porous ceramic material (Fig. 1-6). Commonly used organic foaming agents include polyvinyl alcohol, starch, walnut shell powder, etc[99]. Carbon powder is another commonly used agent. This process can yield porous ceramic materials of diverse shapes and pore types; however, particle agglomeration during mixing often results in uneven pore distribution.

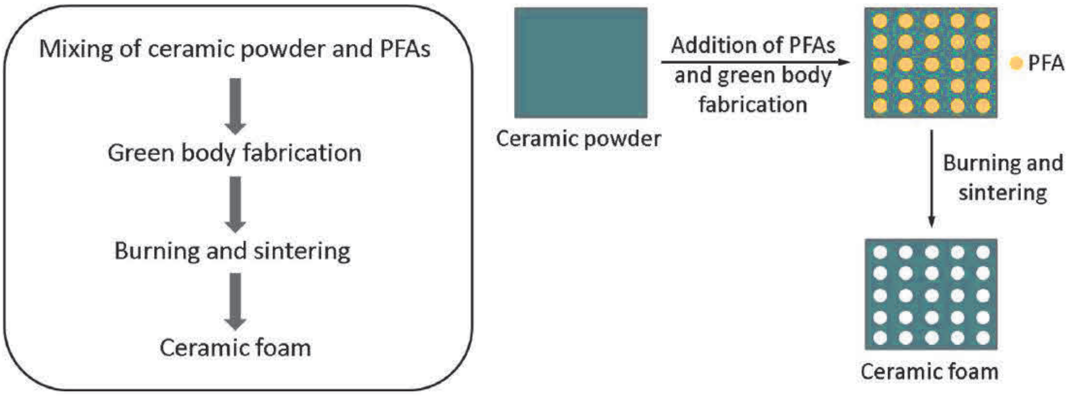

Fig. 1-6 Process flow chart along with the schematic for foaming agent addition method[39].

(3) Freeze-casting method

The freeze-casting method, also referred to as the ice templating method or freeze-drying method, is a versatile technique employed for producing open porous ceramics[100,101]. The process entails the preferential nucleation and growth of ice crystals under a defined thermal gradient (temperature below zero) applied to directionally freeze an aqueous solution containing a ceramic slurry. As ice crystals form and grow in the slurry, they repel suspended ceramic particles, creating a natural isolation of particles between crystals at the advancing solidification front. Upon completion of solidification, sublimation takes place under reduced pressure, converting the solid solvent into a gaseous state. Consequently, a porous ceramic foam is obtained, directly replicating the structure of the frozen solvent. The final sintering process is crucial for achieving sufficient strength and structural integrity (Fig. 1-7).

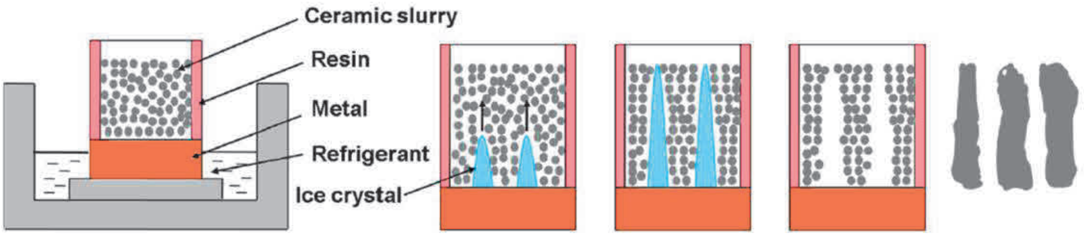

Fig. 1-7 Schematic diagram of the freeze casting method[39].

(4) Organic foam impregnation method

The organic foam impregnation method utilizes prefabricated organic foam as a template[102]. Ceramic slurry is then uniformly applied onto the foam's surface or the foam template is directly submerged in the slurry, excluding air to ensure full wetting of the foam template. Subsequently, drying and high-temperature sintering remove the organic foam template while densifying the ceramic skeleton, yielding porous ceramic materials (Fig. 1-8). The organic foam impregnation method shares similarities with 3D printing technology. It utilizes the shape of the organic foam template to define the shape and uniform distribution of pores. This method is primarily employed in fabricating porous network structures of ceramic materials. However, it is unsuitable for preparing porous ceramic materials with intricate pore shapes and low porosity.

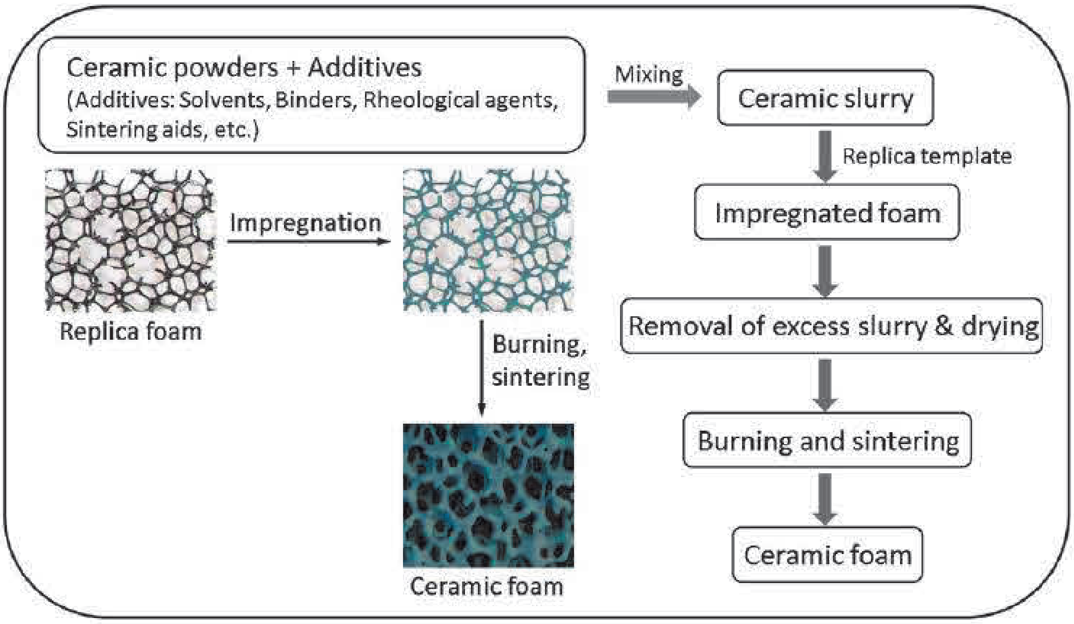

Fig. 1-8 Process flow chart and schematic for organic foam impregnation method[39].

(5) Gel-casting method

The gel-casting method entails incorporating organic monomers or cross-linking agents into a suspension containing flowable ceramic powders, along with catalysts, initiators, or heat. These triggers cross-linking or polymerization of the organic monomers, resulting in a three-dimensional interpenetrating network structure of the organic polymer skeleton (Fig. 1-1-9). Subsequently, the material is dried, demolded, and subjected to high-temperature sintering to produce porous ceramic materials[103]. This method resembles the organic foam impregnation technique. However, in gel-casting, the formation of a skeleton occurs via cross-linking or polymerization of organic monomers, whereas in organic foam impregnation, it relies on pre-positioning the organic skeleton, resulting in differing pore shapes. The holes formed via gel injection molding exhibit a more intricate and orderly alignment.

Fig. 1-1-9 Schematic process flow diagram to fabricate nanofibrous aluminum borate porous ceramics by gel-casting method[104].

(6) 3D printing method

3D printing is an advanced method for preparing porous ceramics, enabling the precise construction of complex three-dimensional structures by layering materials. Initially, special printing inks containing ceramic powders must be prepared. Then, following a computer-aided design (CAD) model, the 3D printer applies the ink layer by layer in a predetermined path, either spraying or extruding it, progressively forming the model's shape. With each layer curing and stacking, a green body with a predetermined pore structure is formed. Finally, a sintering process is employed to eliminate all organic components and fuse the ceramic particles, resulting in a durable porous ceramic material[96,105]. The advantages of 3D printing technology include design flexibility and the capability to fabricate intricate pore structures unattainable with traditional methods, rendering it apt for manufacturing porous ceramic materials tailored for specific functionalities and high porosity.

Various methods employed in the preparation of porous ceramics exert varying impacts on their properties and applications. Grasping the pros and cons of different methods facilitates the selection of an optimal preparation approach tailored to specific application requirements. Table 1-1-1 provides a summary of the benefits and drawbacks associated with the above-mentioned methods.

Table 1-1-1 Summary of advantages and limitations of different preparation methods.

Method	Advantages	Limitations
Direct foaming	Simpletechnique,high porosity	Mainly closed pores
Foaming agent addition	Simple preparation process, controlled porosity	Poor uniformity of pore distribution
Freeze-casting	Strong structural control, environmentally friendly	Process parameter sensitivity
Organic foam impregnation	High porosity, open pores	Shape and density are not easily controlled
Gel-casting	Uniform distribution of pores	Low productivity and difficult to control process conditions
3D printing	Flexibility in design and ability to create complex pore structures	Costly and slow to prepare

1.3.3 Applications of Porous Ceramics

Porous ceramic materials find extensive applications in diverse fields including environmental protection, aerospace, biomedical, and new material synthesis due to their large specific surface area, excellent thermal and chemical stability, high mechanical strength, biocompatibility, and moldability. This subsection summarizes the applications of porous ceramic materials in the relevant fields:

(1) Filtration and separation devices

Porous ceramics find extensive applications in water purification, separating acidic and alkaline solutions, various viscous liquids, and gas mixtures due to their high porosity, ease of processing, resistance to abrasion, corrosion, high temperatures, and deformation. Moreover, porous ceramics offer advantages over metals and polymers in separating highly corrosive fluids, high-temperature fluids, and other specialized fluids[106–110].

(2) Sound-absorbing materials

Porous ceramic materials leverage their porous structure to dissipate the air pressure induced by sound waves, thereby achieving sound absorption and noise reduction. Sound-absorbing and noise-reducing porous ceramics require small pore sizes (20 μm-150 μm), generally exceeding 60% porosity, and exhibit high mechanical properties. Due to its widespread use, which can incur high costs, these materials find application predominantly in environments such as subway tunnels, theaters, and upscale residences[111–113].

(3) Thermal insulation

Porous ceramic materials prepared via the direct foaming method exhibit high porosity, primarily comprising closed cells, resulting in low thermal conductivity that effectively inhibits heat transfer, rendering them eco-friendly thermal insulators. In aerospace applications, porous ceramics can serve as durable thermal insulation layers at the aircraft's forefront, thereby mitigating flight expenses. Naturally, within a specific porosity range, thermal insulation performance improves with increasing porosity; however, strength tends to diminish[114–116]. Therefore, the toughness of porous ceramic materials warrants careful consideration.

(4) Catalyst carriers

Porous ceramics with high specific surface area, thermal stability, and excellent adsorption properties are effective catalyst carriers. The porous ceramic surface is coated with a layer of the appropriate catalyst. When the reaction fluid flows through, it fully interacts with the catalyst, significantly enhancing its catalytic effectiveness[117–119]. For instance, it can be installed in exhaust gas treatment devices to decompose automotive exhaust and industrial wastewater.

(5) Biomedical

Porous ceramic materials, including calcium phosphate, zirconium oxide, and silicon carbide, exhibit excellent biocompatibility, non-toxicity, lightweight, and stable physical and chemical properties. For instance, calcium phosphate and zirconium oxide are employed in dental applications, while silicon carbide is utilized for artificial bones, with documented clinical efficacy[120–122].

(6) Preforms for interpenetrating composites

With the trend toward greater structural and functional integration in new materials, traditional reinforcing phases such as particles, fibers, and whiskers are no longer suitable for highly demanding fields. Consequently, researchers highly favor porous ceramics with a three-dimensional interpenetrating network structure as the new reinforcing materials[39,123]. Specifically, metal or metal alloys are fused into pre-fabricated porous ceramics through infiltration, aiming to produce metal-ceramic composites featuring three-dimensional interpenetrating networks, enhancing their ability to disperse internal stresses and withstand external impacts more effectively. To achieve this goal, it is crucial for the porous ceramics to possess an open porosity accounting for over 95% of the total porosity and for the pores to be interconnected, ensuring favorable macroscopic properties.

1.4 properties of metal/ceramic interpenetrating phase composites

1.4.1 Mechanical properties of metal/ceramic interpenetrating phase composites

IPCs exhibit outstanding overall performance owing to their distinctive three-dimensional continuous network structure. This structure ensures effective interpenetration and support between the matrix and reinforcement, thereby preserving the integrity of each phase’s performance. Metal/ceramic IPCs, being among the most prevalent types, hold significant potential in automotive, aerospace, and electronic packaging industries, garnering considerable attention from researchers. Gao et al.[124] utilized foam replication-reaction sintering to fabricate porous TiC ceramics. Homogeneous mixing of Ti into TiC particles and Ti plating onto the TiC surface improved the bonding between ceramic particles. Subsequently, TiC/stainless steel IPCs were prepared via the melt infiltration method, exhibiting excellent mechanical properties with hardness, tensile strength, and fracture toughness measured at 4.11 GPa, 481 MPa, and 28.9 MPa $m^{1/2}$, respectively. It was observed that the plated network ceramics not only enhanced strong bonding between particles but also reacted with the steel to form a microscopic lock-in microstructure. The double-locked 3D structure promotes the accumulation of interfacial dislocations, facilitating crack deflection and organizing crack diffusion. The interaction between macroscopic and microscopic dual-locked structures in the composites is considered the primary driver for performance enhancement.

Vaucher et al.[125] fabricated SiC ceramic foam preforms with varying pore sizes (10, 35, 50 μm). Subsequently, they employed squeeze casting to produce three-dimensional network composites of foam SiC ceramic and aluminum alloy. The researchers investigated the uniaxial tensile and four-point bending properties of these composites and observed a slight interfacial reaction. Furthermore, they noted an increase in the composite's microhardness, yield strength, and tensile strength with decreasing pore size. Additionally, the modulus of elasticity and hardness of the composites exceeded those of the aluminum alloy.

Schukraft et al.[126] utilized in-situ computed X-ray tomography to investigate the compressive damage behavior of Al_2O_3/AlSi10Mg. They employed 3D reconstruction techniques to construct a finite element model for simulation. The study revealed that the damage behavior progresses through three stages: damage initiation, damage mechanism transformation, and shear failure. During the damage initiation stage, the primary observations were crack formation and interfacial debonding between the ceramic and metal phases. This was followed by the damage mechanism transition stage, characterized by crack extension and coalescence, accompanied by increased plastic deformation of the metal phase. Finally, in the shear failure stage, the failure process was completely dominated by the metal phase, resulting in shear failure. Compared to traditional metal-ceramic composites, these composites exhibit higher damage tolerance and residual strength, primarily due to crack bridging and the high metal content of the metallic phase.

Roy et al.[127] used energy-dispersive synchrotron X-ray diffraction to investigate the internal load transfer mechanism in Al12Si/ Al_2O_3 composites. They calculated the average lattice strain for each of the three crystalline phases (alumina, aluminum solid solution, and pure silicon) by measuring the strain along and transverse to the loading direction. Results showed that under applied compressive stresses of about 100 MPa, all three phases experienced elastic deformation, with lattice macrostrains increasing steadily with stress. The aluminum phase undergoes plastic deformation at compressive stresses exceeding 100 MPa, leading to decreased load carrying capacity, with a greater proportion of the load borne by the harder and stronger alumina phase. At higher applied compressive stresses, the compressive stress-to-stress ratio of the alumina phase decreases further, whereas the compressive stress of the aluminum solid solution phase increases to uphold stress equilibrium in the composite.

Imbeni et al.[128] discovered that Al/Al_2O_3 IPCs exhibits superior wear resistance compared to conventional particle-reinforced Al/Al_2O_3 composites. Liu et al.[16] also observed this phenomenon when examining the wear resistance of IPCS with various ceramic preforms. They observed that initially, metal was deposited on the abraded surface during the abrasion process. Subsequently, this metal layer was abraded away, leading to considerable material loss. Eventually, ceramic pillars emerged and protruded from the surface, providing resistance against further wear until reaching a steady state. Unlike ceramic particles in particle- or short-fiber-reinforced metal matrix composites, which tend to dislodge from the matrix during frictional wear, leading to unstable wear characteristics, ceramic preforms within ceramic/metal composites possessing 3D interpenetrating networks are more resistant to dislodgement during wear; furthermore, hardened micro-convexities developed on the worn surface serve as load-bearing entities, effectively impeding the plastic deformation of the matrix alloy and thus reducing adhesive wear. Furthermore, the hardened micro-convexities developed on the worn surface can bear loads, prevent plastic deformation of the matrix alloy, and diminish adhesive wear. As the pore size of the ceramic preform decreases, the number of micro-convex bodies on the wear surface increases, resulting in enhanced wear resistance.

Rio et al. [129]investigated the potential application of co-continuous NiAl- Al_2O_3 composites as high-temperature materials. Comparison with composites reinforced with continuous ceramic fibers revealed that the co-continuous NiAl- Al_2O_3 composites retain high strength and exhibit exceptional resistance to thermal cycling damage. This resilience stems from the hydrostatic stress experienced by IPCs after thermal cycling, contrasting with the typically biased stress distribution in conventional composites.

1.4.2 Thermal properties of metal/ceramic interpenetrating phase composites

Metal/ceramic IPCs holds significant promise in electronic packaging owing to its low coefficient of thermal expansion and high thermal conductivity. Consequently, its thermal performance has been extensively investigated.

Li et al. [130]fabricated a series of composite materials, incorporating particles and interpenetrating networks, all with identical SiC content ranging from 45% to 70%. Upon comparison, they observed that the IPCs with equivalent content exhibited lower CTE. They attributed this discrepancy to the distinct geometries of the reinforcements. Specifically, they noted that particle-reinforced composites demonstrated inferior inter-particle bonding among ceramic constituents, thereby impeding the restriction of aluminum matrix movement during thermal expansion. In contrast, the continuous SiC ceramics within IPCs displayed robust bonding, effectively constraining matrix mobility and mitigating expansion.

Roy et al.[123] investigated the thermal expansion behavior of Al12Si/Al2O3 IPCs. Prefabricated bodies with various ceramic contents were prepared through the addition of a pore-forming agent. IPCs were then produced via the pneumatic pressure immersion infiltration method. Their findings indicated that increasing the ceramic content reduced the thermal strain and CTE of the composites. However, the thermal expansion behavior resembled that of particle-reinforced composites, with a CTE higher than the model-predicted values for the composites. This phenomenon arises from the presence of larger metal-enriched regions within the composites, devoid of ceramic phases, thereby significantly diminishing the constraining effect of the ceramic phase. In their subsequent studies[131], ceramic preform with varying content (34%-60%) were prepared using the same method. Al12Si/alumina IPCs were subsequently produced via squeeze casting. Anisotropy was observed in the thermal expansion behavior of the IPCs, primarily attributed to the elastic anisotropy inherent in both the ceramic preform and the IPCs. At low temperatures, the coefficient of thermal expansion is biased towards the metal matrix due to elastic deformation of the phases. However, at high temperatures, the matrix undergoes plastic deformation, and the rigid ceramic phases exert greater control over the thermal expansion behavior of the material, resulting in a bias towards the ceramic reinforcement in the coefficient of thermal expansion.

SiC/Al-Si-Mg IPCs with a coefficient of thermal expansion of approximately 7.03 × 10^{-6}/°C were fabricated using mold-forming and pressureless infiltration techniques by Wang et al[132]. They attributed the reduction in CTE to three factors: the hindrance of thermal expansion in Al alloys and composites by network-structured SiC; the restraint of thermal expansion in Al and composites by Si and Mg; and the mitigation of plastic deformation in Al alloys due to micropores within the composites at temperatures ranging from room temperature up to 100°C. The influence of Mg on the thermal expansion behavior of Al and composites, along with the presence of micropores in the composites counteracting the plastic deformation of Al alloys, was observed at temperatures ranging from room temperature up to 100°C.

Regarding heat conduction in 3D interpenetrating network structured composites, the continuous nature of metal and ceramic phases fosters the creation of efficient thermal conduction pathways. Specifically, phonons propagate within the ceramic phase, while electrons migrate within the metal phase. Additionally, compared to particle-filled composites, these composites exhibit fewer phase boundaries, resulting in reduced hindrance to the movement of phonons and electrons.

Wang et al.[132] examined the heat transfer properties of SiC/Al-Si-Mg composites featuring a 3D interpenetrating network structure. These composites demonstrate a remarkable thermal conductivity of 233.6 W/(m-K), substantially surpassing that of particle-filled composites in similar conditions. This enhancement primarily stems from the formation of a network structure in the former, which promotes efficient heat transfer. Conversely, particle-filled composites exhibit increased phase interfaces, with the SiC phase enveloped by SiO2 on the surface, impeding phonon transfer and resulting in inferior thermal conductivity.

Zhang et al.[133] prepared oriented porous SiC ceramics using high-temperature recrystallization and SiC/Cu-Si IPCs via spontaneous infiltration. They observed anisotropy in thermal conductivity, which decreased with rising experimental temperature. This decline results from the narrowing gap between the ceramic phase's thermal conductivity and that of the matrix.

Li et al.[130] studied the thermal conductivity of two structural composites: 3D-SiC/Al and SiCp/Al. They demonstrated that the thermal conductivity of the former is greater than that of the latter. This difference is primarily ascribed to the interface's impact on the material's heat transfer performance, which is inferior to that of the latter under similar conditions.

1.5 Objective of this thesis

Since the inception of three-dimensional network interpenetrating phase composites, they have garnered significant attention from scholars and researchers. Over the past few decades, various types of IPCs including metal-ceramic, metal-polymer, metal-metal, ceramic-polymer, and polymer-polymer compositions have been developed. Among these, metal-ceramic IPCs have witnessed the widest applications and garnered the most attention. The unique structure of IPCs effectively amalgamates ceramic's wear resistance, high hardness, high-temperature resistance, and dimensional stability with metal's advantageous traits such as good plasticity, high toughness, and excellent thermal and electrical conductivity. Consequently, metal-ceramic IPCs exhibit exceptional mechanical and thermal properties.

Aluminum and its alloys possess numerous advantages including low density, high specific strength, excellent thermal conductivity, corrosion resistance, and environmental friendliness. Thus, their application as metallic phases in metal-ceramic IPCs has been a focal point of research. Extensive research has explored the mechanical and thermal properties of aluminum-based IPCs using experimental and simulation techniques. However, the ceramic phases predominantly consist of Al_2O_3 and SiC, with minimal investigation conducted on AlN. AlN offers advantages such as high hardness, stiffness, thermal conductivity, and a coefficient of thermal expansion compatible with SiC. Its chemical stability prevents adverse reactions with aluminum alloy at the interface, which could hinder interfacial bonding. Consequently, Al/AlN IPCs hold significant promise for applications in aerospace and electronic packaging industries. Therefore, conducting a systematic investigation into the mechanical and thermal properties of Al/AlN IPCs is imperative.

In this study, porous AlN ceramics with varying porosities were fabricated as precast bodies for interpenetrating phase composites using slurry infiltration method. Additionally, Al/AlN IPCs were produced via the low-pressure casting method. The microstructures of the IPCs were examined through X-ray diffractometry (XRD), scanning electron microscopy (SEM), and electron probe microanalysis (EPMA). The mechanical properties of IPCs were assessed through nanoindentation and room temperature compression testing apparatus. A vertical direct dilatometer was used to determine the thermal expansion coefficient. 3D representative volume elements (RVEs) are created to model the microstructures of Al/AlN IPCs and the finite element models generated from RVEs are used to study thermal expansion behavior. CTE was predicted using finite element method (FEM) and thermoelastic models. The thermal conductivity of the IPCs was measured and subsequently analyzed.

This study deeply investigates the structure, mechanical properties, thermal expansion behavior, and thermal conductivity of IPCs with varying preform porosity. Revealing the effect of preform porosity on mechanical and thermal properties. This study offers theoretical insights for the application and development of Al/AlN IPCs.

1.6 Outline of this thesis

Chapter 1 Background and Objective

This chapter introduces Interpenetrating Phase Composites (IPCs) and their preparation methods. It provides an overview of porous ceramics used as preforms for IPCs, covering their classification, preparation methods, and applications. Additionally, it presents research progress on the mechanical and thermal properties of metal-ceramic IPCs, and refines the research objectives of this study.

Chapter 2 Microstructure and mechanical properties of Al/AlN interpenetrating phase composites with different preform porosity

In this chapter, Al/AlN interpenetrating phase composites (IPCs) was fabricated by infiltrating the alloy melt into AlN preform via low pressure casting method. Open cell porous AlN preforms, fabricated via the slurry infiltration method, and have four different preform porosity were used for IPCs fabrication. The microstructures of porous AlN preforms and Al/AlN interpenetrating phase composites were characterized using scanning electron microscopy (SEM). The phase compositions of preforms and composites were analyzed by X-ray diffraction (XRD). The interface between AlN and Al matrix was found to have no visible defects, indicating good interfacial bonding. Compression tests were conducted, and the results showed that the material strength and toughness increased with increasing porosity. Additionally, the composites changed from brittle fracture to ductile fracture. Nanoindentation tests indicate that an increase in AlN content enhances the hardness of the IPCs components.

Chapter 3 Thermal expansion behavior and analysis of Al/AlN interpenetrating phase composites with different preform porosity

In this chapter, the coefficient of thermal expansion (CTE) of Al/AlN interpenetrating phase composites (IPCs) has been measured based on the length change from room temperature (RT) to 200 ◦C. 3D representative volume elements (RVEs) are created to model the microstructures of Al/AlN IPCs and the finite element models generated from RVEs are used to study thermal expansion behavior. CTE was predicted utilizing the finite element method (FEM) and thermo-elastic models of Kerner, Turner and Schapery, after which the results were compared with the experimental values. According to experimental results, a notable reduction in the CTE of IPCs is observed as preform porosity decreases. This shows that an AlN preform can effectively enhance dimensional stability. A comparative analysis of extant literature indicates that IPCs may attain a lower CTE compared to particle-reinforced composites. Experimental data align closely with analytical models. The FE simulation results demonstrate better consistency with experimental data only under conditions of high preform porosity, since residual thermal stresses and plastic deformation were not considered.

Chapter 4 Thermal conductivity of Al/AlN interpenetrating phase composites with different preform porosity

. In this chapter, the thermal Conductive Properties of the Al/AlN interpenetrating phase composites (IPCs) with varying preform porosity was studied. Evaluated the thermal conductivity (TC) of IPCs at different temperatures (20°C to 200°C). The TC values obtained through experimentation were compared to predictions generated by analytical models. IPCs with higher preform porosity exhibit higher TC. The TC of IPCs exhibits an inverse temperature dependence. Theoretical models accurately predict the thermal conductivity of IPCs with high preform porosity.

Chapter 5 Conclusions

This chapter presents a synthesis of the findings from the aforementioned studies.

1.7 reference

[1] V. Chak, H. Chattopadhyay, T.L. Dora, A review on fabrication methods, reinforcements and mechanical properties of aluminum matrix composites, Journal of Manufacturing Processes 56 (2020) 1059–1074. https://doi.org/10.1016/j.jmapro.2020.05.042.

[2] A. Kumar, K. Sharma, A.R. Dixit, A review on the mechanical properties of polymer composites reinforced by carbon nanotubes and graphene, Carbon Lett. 31 (2021) 149–165. https://doi.org/10.1007/s42823-020-00161-x.

[3] J. Zhu, W. Jiang, G. Li, F. Guan, Y. Yu, Z. Fan, Microstructure and mechanical properties of SiCnp/Al6082 aluminum matrix composites prepared by squeeze casting combined with stir casting, Journal of Materials Processing Technology 283 (2020) 116699. https://doi.org/10.1016/j.jmatprotec.2020.116699.

[4] V. Khanna, V. Kumar, S.A. Bansal, Mechanical properties of aluminium-graphene/carbon nanotubes (CNTs) metal matrix composites: Advancement, opportunities and perspective, Materials Research Bulletin 138 (2021) 111224. https://doi.org/10.1016/j.materresbull.2021.111224.

[5] T. Liu, X. Liu, P. Feng, A comprehensive review on mechanical properties of pultruded FRP composites subjected to long-term environmental effects, Composites Part B: Engineering 191 (2020) 107958. https://doi.org/10.1016/j.compositesb.2020.107958.

[6] Ö. Güler, N. Bağcı, A short review on mechanical properties of graphene reinforced metal matrix composites, Journal of Materials Research and Technology 9 (2020) 6808–6833. https://doi.org/10.1016/j.jmrt.2020.01.077.

[7] M.K. Surappa, Aluminium matrix composites: Challenges and opportunities, Sadhana 28 (2003) 319–334. https://doi.org/10.1007/BF02717141.

[8] A. Ramanathan, P.K. Krishnan, R. Muraliraja, A review on the production of metal matrix composites through stir casting – Furnace design, properties, challenges, and research opportunities, Journal of Manufacturing Processes 42 (2019) 213–245. https://doi.org/10.1016/j.jmapro.2019.04.017.

[9] O.S. Salih, H. Ou, W. Sun, D.G. McCartney, A review of friction stir welding of aluminium matrix composites, Materials & Design 86 (2015) 61–71. https://doi.org/10.1016/j.matdes.2015.07.071.

[10] B.-X. Dong, Q. Li, Z.-F. Wang, T.-S. Liu, H.-Y. Yang, S.-L. Shu, L.-Y. Chen, F. Qiu, Q.-C. Jiang, L.-C. Zhang, Enhancing strength-ductility synergy and mechanisms of Al-based composites by size-tunable in-situ TiB2 particles with specific spatial distribution, Composites Part B: Engineering 217 (2021) 108912. https://doi.org/10.1016/j.compositesb.2021.108912.

[11] A. Gholampour, T. Ozbakkaloglu, A review of natural fiber composites: properties, modification and processing techniques, characterization, applications,

J Mater Sci 55 (2020) 829–892. https://doi.org/10.1007/s10853-019-03990-y.

[12] J. Le, Y. Han, P. Qiu, G. Huang, J. Mao, W. Lu, The impact of matrix texture and whisker orientation on property anisotropy in titanium matrix composites: Experimental and computational evaluation, Composites Part B: Engineering 212 (2021) 108682. https://doi.org/10.1016/j.compositesb.2021.108682.

[13] X. Li, Y.H. Tan, P. Wang, X. Su, H.J. Willy, T.S. Herng, J. Ding, Metallic microlattice and epoxy interpenetrating phase composites: Experimental and simulation studies on superior mechanical properties and their mechanisms, Composites Part A: Applied Science and Manufacturing 135 (2020) 105934. https://doi.org/10.1016/j.compositesa.2020.105934.

[14] M.T. Isa, A.S. Ahmed, B.O. Aderemi, R.M. Taib, I.A. Mohammed-Dabo, Effect of fiber type and combinations on the mechanical, physical and thermal stability properties of polyester hybrid composites, Composites Part B: Engineering 52 (2013) 217–223. https://doi.org/10.1016/j.compositesb.2013.04.018.

[15] H. Ahlatci, T. Koçer, E. Candan, H. Çimenoğlu, Wear behaviour of Al/(Al2O3p+SiCp) hybrid composites, Tribology International 39 (2006) 213–220. https://doi.org/10.1016/j.triboint.2005.01.029.

[16] J. Liu, J. Binner, R. Higginson, Dry sliding wear behaviour of co-continuous ceramic foam/aluminium alloy interpenetrating composites produced by pressureless infiltration, Wear 276–277 (2012) 94–104. https://doi.org/10.1016/j.wear.2011.12.008.

[17] L.D. Wegner, L.J. Gibson, The mechanical behaviour of interpenetrating phase composites – I: modelling, International Journal of Mechanical Sciences 42 (2000) 925–942. https://doi.org/10.1016/S0020-7403(99)00025-9.

[18] J.M. Gómez de Salazar, M.I. Barrena, G. Morales, L. Matesanz, N. Merino, Compression strength and wear resistance of ceramic foams–polymer composites, Materials Letters 60 (2006) 1687–1692. https://doi.org/10.1016/j.matlet.2005.11.092.

[19] F. Scherm, R. Völkl, A. Neubrand, F. Bosbach, U. Glatzel, Mechanical characterisation of interpenetrating network metal–ceramic composites, Materials Science and Engineering: A 527 (2010) 1260–1265. https://doi.org/10.1016/j.msea.2009.09.063.

[20] M. Pavese, P. Fino, M. Valle, C. Badini, Preparation of C4 ceramic/metal composites by reactive metal penetration of commercial ceramics, Composites Science and Technology 66 (2006) 350–356. https://doi.org/10.1016/j.compscitech.2005.04.046.

[21] G.S. Daehn, M.C. Breslin, Co-continuous composite materials for friction and braking applications, JOM 58 (2006) 87–91. https://doi.org/10.1007/s11837-006-0235-1.

[22] B. Wang, Z.-Y. Xu, W.-Z. Lu, F. Jin, J.-F. Yang, K. Niihara, Effect of porous Si3N4 preform on the mechanical properties of Si3N4/Al composites with interpenetrating network structure, Materials Science and Engineering: A 607 (2014) 307–312. https://doi.org/10.1016/j.msea.2014.04.022.

[23] Z. Di, X. Xian-qing, F. Tong-xiang, S. Bing-he, T. Sakata, H. Mori, T. Okabe, Microstructure and properties of ecoceramics/metal composites with interpenetrating networks, Materials Science and Engineering: A 351 (2003) 109–116. https://doi.org/10.1016/S0921-5093(02)00822-5.

[24] S. Li, G. Wang, K. Zhang, X. Zhang, L. Zhang, W. Wang, R. He, Mechanical properties of Al2O3 and Al2O3/Al interpenetrated functional gradient structures by 3D printing and melt infiltration, Journal of Alloys and Compounds 950 (2023) 169948. https://doi.org/10.1016/j.jallcom.2023.169948.

[25] S. Li, Y. Li, Q. Wang, K. Miao, X. Liang, Z. Lu, D. Li, Fabrication of 3D-SiC/aluminum alloy interpenetrating composites by DIW and pressureless infiltration, Ceramics International 47 (2021) 24340–24347. https://doi.org/10.1016/j.ceramint.2021.05.147.

[26] S.B. Hein, Powder injection moulding of metal ceramic interpenetrating phase composites, Powder Metallurgy 57 (2014) 348–356. https://doi.org/10.1179/1743290114Y.0000000116.

[27] Y. Lu, J. Yang, W. Lu, R. Liu, G. Qiao, C. Bao, The mechanical properties of co-continuous Si3N4/Al composites manufactured by squeeze casting, Materials Science and Engineering: A 527 (2010) 6289–6299. https://doi.org/10.1016/j.msea.2010.06.047.

[28] A.P. Amosov, A.F. Fedotov, E.I. Latukhin, V.A. Novikov, TiC–Al interpenetrating composites by SHS pressing, Int. J Self-Propag. High-Temp. Synth. 24 (2015) 187–191. https://doi.org/10.3103/S1061386215040032.

[29] X. Zhang, X.-Y. Yue, H.-Q. Ru, Effect of in-situ synthesized TiB2 on microstructure and mechanical property of Al/TiB2-SiC interpenetrating phase composites, Journal of Asian Ceramic Societies 10 (2022) 531–544. https://doi.org/10.1080/21870764.2022.2082643.

[30] Y. Guo, X. Xie, Z. Liu, L. Zhuo, J. Zhang, S. Wang, Q. Duan, Q. Jia, D. Xu, W. Xue, D. Duan, F. Berto, Z. Zhang, R. Yang, Wear-resistant Ag-MAX phase 3D interpenetrating-phase composites: Processing, structure, and properties, Nano Res. 17 (2024) 806–819. https://doi.org/10.1007/s12274-023-6015-1.

[31] X. Zhang, C. Hong, J. Han, H. Zhang, Microstructure and mechanical properties of TiB2/(Cu, Ni) interpenetrating phase composites, Scripta Materialia 55 (2006) 565–568. https://doi.org/10.1016/j.scriptamat.2006.04.048.

[32] M. Leverkoehne, V.S.R. Murthy, R. Janssen, N. Claussen, Electrical resistivity of Cr–Al2O3 and ZrxAly–Al2O3 composites with interpenetrating microstructure, Journal of the European Ceramic Society 22 (2002) 2149–2153. https://doi.org/10.1016/S0955-2219(01)00539-8.

[33] Y. Zheng, Y. Zhou, Y. Feng, X. Teng, S. Yan, R. Li, W. Yu, Z. Huang, S. Li, Z. Li, Synthesis and mechanical properties of TiC-Fe interpenetrating phase composites fabricated by infiltration process, Ceramics International 44 (2018) 21742–21749. https://doi.org/10.1016/j.ceramint.2018.08.268.

[34] N.K. Bhoi, H. Singh, S. Pratap, Developments in the aluminum metal matrix composites reinforced by micro/nano particles – A review, Journal of Composite Materials 54 (2020) 813–833. https://doi.org/10.1177/0021998319865307.

[35] P. Samal, P.R. Vundavilli, A. Meher, M.M. Mahapatra, Recent progress in aluminum metal matrix composites: A review on processing, mechanical and wear properties, Journal of Manufacturing Processes 59 (2020) 131–152. https://doi.org/10.1016/j.jmapro.2020.09.010.

[36] W. Zhou, Thermal and dielectric properties of the AlN particles reinforced linear low-density polyethylene composites, Thermochimica Acta 512 (2011) 183–188. https://doi.org/10.1016/j.tca.2010.10.003.

[37] E. Bedolla, J. Lemus-Ruiz, A. Contreras, Synthesis and characterization of Mg-AZ91/AlN composites, Materials & Design 38 (2012) 91–98. https://doi.org/10.1016/j.matdes.2012.02.001.

[38] Y.Q. Liu, H.T. Cong, W. Wang, C.H. Sun, H.M. Cheng, AlN nanoparticle-reinforced nanocrystalline Al matrix composites: Fabrication and mechanical properties, Materials Science and Engineering: A 505 (2009) 151–156. https://doi.org/10.1016/j.msea.2008.12.045.

[39] N. Kota, M.S. Charan, T. Laha, S. Roy, Review on development of metal/ceramic interpenetrating phase composites and critical analysis of their properties, Ceramics International 48 (2022) 1451–1483. https://doi.org/10.1016/j.ceramint.2021.09.232.

[40] M. Basista, J. Jakubowska, W. Węglewski, Processing Induced Flaws in Aluminum-Alumina Interpenetrating Phase Composites, Adv. Eng. Mater. 19 (2017) 1700484. https://doi.org/10.1002/adem.201700484.

[41] T. Etter, P. Schulz, M. Weber, J. Metz, M. Wimmler, J.F. Löffler, P.J. Uggowitzer, Aluminium carbide formation in interpenetrating graphite/aluminium composites, Materials Science and Engineering: A 448 (2007) 1–6. https://doi.org/10.1016/j.msea.2006.11.088.

[42] P. Tran, T.D. Ngo, A. Ghazlan, D. Hui, Bimaterial 3D printing and numerical analysis of bio-inspired composite structures under in-plane and transverse loadings, Composites Part B: Engineering 108 (2017) 210–223. https://doi.org/10.1016/j.compositesb.2016.09.083.

[43] A.P. Jackson, J.F.V. Vincent, R.M. Turner, R.M. Alexander, The mechanical design of nacre, Proceedings of the Royal Society of London. Series B. Biological Sciences 234 (1997) 415–440. https://doi.org/10.1098/rspb.1988.0056.

[44] N. Suksangpanya, N.A. Yaraghi, D. Kisailus, P. Zavattieri, Twisting cracks in Bouligand structures, Journal of the Mechanical Behavior of Biomedical Materials 76 (2017) 38–57. https://doi.org/10.1016/j.jmbbm.2017.06.010.

[45] J.C. Weaver, G.W. Milliron, A. Miserez, K. Evans-Lutterodt, S. Herrera, I. Gallana, W.J. Mershon, B. Swanson, P. Zavattieri, E. DiMasi, D. Kisailus, The Stomatopod Dactyl Club: A Formidable Damage-Tolerant Biological Hammer, Science 336 (2012) 1275–1280. https://doi.org/10.1126/science.1218764.

[46] W. Yang, G. Zhang, H. Liu, X. Li, Microstructural Characterization and Hardness Behavior of a Biological *Saxidomus purpuratus* Shell, Journal of Materials Science & Technology 27 (2011) 139–146. https://doi.org/10.1016/S1005-0302(11)60039-X.

[47] D. Jiao, Z.Q. Liu, R.T. Qu, Z.F. Zhang, Anisotropic mechanical behaviors and their structural dependences of crossed-lamellar structure in a bivalve shell, Materials Science and Engineering: C 59 (2016) 828–837. https://doi.org/10.1016/j.msec.2015.11.003.

[48] I. Hussain, O. Al-Ketan, F. Renda, M. Malvezzi, D. Prattichizzo, L. Seneviratne, R.K. Abu Al-Rub, D. Gan, Design and prototyping soft–rigid tendon-driven modular grippers using interpenetrating phase composites materials, The International Journal of Robotics Research 39 (2020) 1635–1646. https://doi.org/10.1177/0278364920907697.

[49] M. Zhang, N. Zhao, Q. Yu, Z. Liu, R. Qu, J. Zhang, S. Li, D. Ren, F. Berto, Z. Zhang, R.O. Ritchie, On the damage tolerance of 3-D printed Mg-Ti interpenetrating-phase composites with bioinspired architectures, Nat Commun 13 (2022) 3247. https://doi.org/10.1038/s41467-022-30873-9.

[50] G.I. Dzhardimalieva, I.E. Uflyand, Preparation of metal-polymer nanocomposites by chemical reduction of metal ions: functions of polymer matrices, J Polym Res 25 (2018) 255. https://doi.org/10.1007/s10965-018-1646-8.

[51] A. Chaturvedi, Recent developments in the field of metal foam-polymer hybrid materials: A brief overview, Journal of Metals, Materials and Minerals 28 (2018). https://www.jmmm.material.chula.ac.th/index.php/jmmm/article/view/341 (accessed March 27, 2024).

[52] A.V. Okulov, A.S. Volegov, J. Weissmüller, J. Markmann, I.V. Okulov, Dealloying-based metal-polymer composites for biomedical applications, Scripta Materialia 146 (2018) 290–294. https://doi.org/10.1016/j.scriptamat.2017.12.022.

[53] J. Li, Y. Yang, H. Jiang, Y. Wang, Y. Chen, S. Jiang, J.-M. Wu, G. Zhang, 3D interpenetrating piezoceramic-polymer composites with high damping and piezoelectricity for impact energy-absorbing and perception, Composites Part B: Engineering 232 (2022) 109617. https://doi.org/10.1016/j.compositesb.2022.109617.

[54] A. Coldea, M.V. Swain, N. Thiel, Mechanical properties of polymer-infiltrated-ceramic-network materials, Dental Materials 29 (2013) 419–426. https://doi.org/10.1016/j.dental.2013.01.002.

[55] A. Singh, O. Al-Ketan, N. Karathanasopoulos, Mechanical performance of solid and sheet network-based stochastic interpenetrating phase composite materials, Composites Part B: Engineering 251 (2023) 110478. https://doi.org/10.1016/j.compositesb.2022.110478.

[56] Y. Zhang, M.-T. Hsieh, L. Valdevit, Mechanical performance of 3D printed interpenetrating phase composites with spinodal topologies, Composite Structures 263 (2021) 113693. https://doi.org/10.1016/j.compstruct.2021.113693.

[57] A. Asar, W. Zaki, A comprehensive review of the mechanisms and structure of interpenetrating phase composites with emphasis on metal-metal and polymer-metal variants, Composites Part B: Engineering 275 (2024) 111314. https://doi.org/10.1016/j.compositesb.2024.111314.

[58] L.D. Wegner, L.J. Gibson, The fracture toughness behaviour of interpenetrating phase composites, International Journal of Mechanical Sciences 43 (2001) 1771–1791. https://doi.org/10.1016/S0020-7403(01)00016-9.

[59] I.V. Okulov, P.-A. Geslin, I.V. Soldatov, H. Ovri, S.-H. Joo, H. Kato, Anomalously low modulus of the interpenetrating-phase composite of Fe and Mg obtained by liquid metal dealloying, Scripta Materialia 163 (2019) 133–136. https://doi.org/10.1016/j.scriptamat.2019.01.017.

[60] J. Bauer, M. Sala-Casanovas, M. Amiri, L. Valdevit, Nanoarchitected metal/ceramic interpenetrating phase composites, Science Advances 8 (2022) eabo3080. https://doi.org/10.1126/sciadv.abo3080.

[61] Z. Hu, H. Yin, M. Li, J. Li, H. Zhu, Research and developments of ceramic-reinforced steel matrix composites—a comprehensive review, Int J Adv Manuf Technol 131 (2024) 125–149. https://doi.org/10.1007/s00170-024-13123-8.

[62] M. Khodaei, M.H. Enayati, F. Karimzadeh, Mechanochemically synthesized Fe3Al–Al2O3 nanocomposite, Journal of Alloys and Compounds 467 (2009) 159–162. https://doi.org/10.1016/j.jallcom.2007.11.123.

[63] M.S. Newkirk, A.W. Urquhart, H.R. Zwicker, E. Breval, Formation of Lanxide, Journal of Materials Research 1 (1986) 81–89. https://doi.org/10.1557/JMR.1986.0081.

[64] F. Wagner, D.E. Garcia, A. Krupp, N. Claussen, Interpenetrating Al2O3-TiAl3 alloys produced by reactive infiltration, Journal of the European Ceramic Society 19 (1999) 2449–2453. https://doi.org/10.1016/S0955-2219(99)00133-8.

[65] L.Q. Chen, Q. Dong, M.J. Zhao, J. Bi, N. Kanetake, Synthesis of TiC/Mg composites with interpenetrating networks by in situ reactive infiltration process, Materials Science and Engineering: A 408 (2005) 125–130. https://doi.org/10.1016/j.msea.2005.07.036.

[66] D. Wang, Z. Zheng, J. Lv, G. Xu, S. Zhou, W. Tang, Y. Wu, Interface design in 3D-SiC/Al-Si-Mg interpenetrating composite fabricated by pressureless infiltration, Ceramics International 44 (2018) 11956–11965. https://doi.org/10.1016/j.ceramint.2018.03.016.

[67] A. Mattern, B. Huchler, D. Staudenecker, R. Oberacker, A. Nagel, M.J. Hoffmann, Preparation of interpenetrating ceramic–metal composites, Journal of the European Ceramic Society 24 (2004) 3399–3408. https://doi.org/10.1016/j.jeurceramsoc.2003.10.030.

[68] A. Mortensen, 3.20 - Melt Infiltration of Metal Matrix Composites, in: A. Kelly, C. Zweben (Eds.), Comprehensive Composite Materials, Pergamon, Oxford, 2000: pp. 521–554. https://doi.org/10.1016/B0-08-042993-9/00019-X.

[69] J. Zhu, Y. Wang, C. Bao, B. Lu, Effect of oxidization of 3D-SiC preforms on the interfacial structure and mechanical properties of co-continuous SiC/Al composites, Ceramics International 47 (2021) 14635–14646. https://doi.org/10.1016/j.ceramint.2021.02.047.

[70] R.J. Moon, M. Tilbrook, M. Hoffman, A. Neubrand, Al–Al2O3 Composites with Interpenetrating Network Structures: Composite Modulus Estimation, Journal of the American Ceramic Society 88 (2005) 666–674. https://doi.org/10.1111/j.1551-2916.2005.00115.x.

[71] A. Shaga, P. Shen, L.-G. Xiao, R.-F. Guo, Y.-B. Liu, Q.-C. Jiang, High damage-tolerance bio-inspired ZL205A/SiC composites with a lamellar-interpenetrated structure, Materials Science and Engineering: A 708 (2017) 199–207. https://doi.org/10.1016/j.msea.2017.09.114.

[72] M. Merzkirch, Ch. Blümel, R. Rössler, K.G. Schell, E.C. Bucharsky, K.A. Weidenmann, Manufacturing and Characterization of Interpenetrating SiC Lightweight Composites, Procedia CIRP 18 (2014) 102–107. https://doi.org/10.1016/j.procir.2014.06.115.

[73] Y. Sahin, M. Acılar, Production and properties of SiCp-reinforced aluminium alloy composites, Composites Part A: Applied Science and Manufacturing 34 (2003) 709–718. https://doi.org/10.1016/S1359-835X(03)00142-8.

[74] F. Gul, M. Acilar, Effect of the reinforcement volume fraction on the dry sliding wear behaviour of Al–10Si/SiCp composites produced by vacuum infiltration technique, Composites Science and Technology 64 (2004) 1959–1970. https://doi.org/10.1016/j.compscitech.2004.02.013.

[75] D. Cree, M. Pugh, Production and characterization of a three-dimensional cellular metal-filled ceramic composite, Journal of Materials Processing Technology 210 (2010) 1905–1917. https://doi.org/10.1016/j.jmatprotec.2010.07.002.

[76] P. Gao, M. Xu, Z. Yuan, L. Cheng, J. Liang, H. Xiao, R. Chen, Temperature dependence of the mechanical and thermal expansion behaviors of

MoSi2-RSiC composites with a three-dimensionally (3D) interpenetrated network structure, Journal of Alloys and Compounds 731 (2018) 1103–1111. https://doi.org/10.1016/j.jallcom.2017.09.219.

[77] Q.M. Zhang, Research on Ceramic Matrix Composites (CMC) for Aerospace Aplications, Advanced Materials Research 284–286 (2011) 324–329. https://doi.org/10.4028/www.scientific.net/AMR.284-286.324.

[78] Z. Dong, J. Liu, Y. Wang, D. Song, R. Cao, X. Yang, Enhanced sound absorption characteristic of aluminum-polyurethane interpenetrating phase composite foams, Materials Letters 323 (2022) 132595. https://doi.org/10.1016/j.matlet.2022.132595.

[79] N. Kota, P. Jana, S. Sahasrabudhe, S. Roy, Processing and characterization of Al-Si alloy/SiC foam interpenetrating phase composite, Materials Today: Proceedings 44 (2021) 2930–2933. https://doi.org/10.1016/j.matpr.2021.01.923.

[80] R. Ramesh, A.S. Prasanth, M. Ragavan, M. Likhith, SiC/Aluminium Co-Continuous Composite Synthesized by Reactive Metal Penetration, Applied Mechanics and Materials 592–594 (2014) 847–853. https://doi.org/10.4028/www.scientific.net/AMM.592-594.847.

[81] R.E. Newnham, D.P. Skinner, L.E. Cross, Connectivity and piezoelectric-pyroelectric composites, Materials Research Bulletin 13 (1978) 525–536. https://doi.org/10.1016/0025-5408(78)90161-7.

[82] Y. Liu, X. Gong, Compressive behavior and energy absorption of metal porous polymer composite with interpenetrating network structure, Transactions of Nonferrous Metals Society of China 16 (2006) s439–s443. https://doi.org/10.1016/S1003-6326(06)60229-X.

[83] S.-J. Tan, X.-X. Zeng, Q. Ma, X.-W. Wu, Y.-G. Guo, Recent Advancements in Polymer-Based Composite Electrolytes for Rechargeable Lithium Batteries, Electrochem. Energ. Rev. 1 (2018) 113–138. https://doi.org/10.1007/s41918-018-0011-2.

[84] A.T. Sidambe, Biocompatibility of Advanced Manufactured Titanium Implants—A Review, Materials 7 (2014) 8168–8188. https://doi.org/10.3390/ma7128168.

[85] T. Kraus, S.F. Fischerauer, A.C. Hänzi, P.J. Uggowitzer, J.F. Löffler, A.M. Weinberg, Magnesium alloys for temporary implants in osteosynthesis: In vivo studies of their degradation and interaction with bone, Acta Biomaterialia 8 (2012) 1230–1238. https://doi.org/10.1016/j.actbio.2011.11.008.

[86] F. Witte, V. Kaese, H. Haferkamp, E. Switzer, A. Meyer-Lindenberg, C.J. Wirth, H. Windhagen, In vivo corrosion of four magnesium alloys and the associated bone response, Biomaterials 26 (2005) 3557–3563. https://doi.org/10.1016/j.biomaterials.2004.09.049.

[87] Problem of Stress Shielding and Improvement to the Hip Implant Designs: A Review, (n.d.). https://doi.org/10.3923/jms.2007.460.467.

[88] A. Bansiddhi, T.D. Sargeant, S.I. Stupp, D.C. Dunand, Porous NiTi for bone implants: A review, Acta Biomaterialia 4 (2008) 773–782. https://doi.org/10.1016/j.actbio.2008.02.009.

[89] M.H. Elahinia, M. Hashemi, M. Tabesh, S.B. Bhaduri, Manufacturing and processing of NiTi implants: A review, Progress in Materials Science 57 (2012) 911–946. https://doi.org/10.1016/j.pmatsci.2011.11.001.

[90] A.N. Alagha, S. Hussain, W. Zaki, Additive manufacturing of shape memory alloys: A review with emphasis on powder bed systems, Materials & Design 204 (2021) 109654. https://doi.org/10.1016/j.matdes.2021.109654.

[91] Q. Li, J. Li, G. He, Compressive properties and damping capacities of magnesium reinforced with continuous steel wire, Materials Science and Engineering: A 680 (2017) 92–96. https://doi.org/10.1016/j.msea.2016.10.089.

[92] L.L. Poole, M. Gonzales, M.R. French, W.A. Yarberry, A.R. Moustafa, Z.C. Cordero, Hypervelocity impact of PrintCast 316L/A356 composites, International Journal of Impact Engineering 136 (2020) 103407. https://doi.org/10.1016/j.ijimpeng.2019.103407.

[93] L.-H. He, M. Swain, A novel polymer infiltrated ceramic dental material, Dental Materials 27 (2011) 527–534. https://doi.org/10.1016/j.dental.2011.02.002.

[94] D.W. Abueidda, A.S. Dalaq, R.K. Abu Al-Rub, I. Jasiuk, Micromechanical finite element predictions of a reduced coefficient of thermal expansion for 3D periodic architectured interpenetrating phase composites, Composite Structures 133 (2015) 85–97. https://doi.org/10.1016/j.compstruct.2015.06.082.

[95] D.J. Green, MECHANICAL BEHAVIOR OF CELLULAR CERAMICS, in: W.R. Tyson, B. Mukherjee (Eds.), Proceedings of the Metallurgical Society of the Canadian Institute of Mining and Metallurgy, Pergamon, 1988: pp. 191–192. https://doi.org/10.1016/B978-0-08-035764-5.50019-5.

[96] L.C. Hwa, S. Rajoo, A.M. Noor, N. Ahmad, M.B. Uday, Recent advances in 3D printing of porous ceramics: A review, Current Opinion in Solid State and Materials Science 21 (2017) 323–347. https://doi.org/10.1016/j.cossms.2017.08.002.

[97] E.C. Hammel, O.L.-R. Ighodaro, O.I. Okoli, Processing and properties of advanced porous ceramics: An application based review, Ceramics International 40 (2014) 15351–15370. https://doi.org/10.1016/j.ceramint.2014.06.095.

[98] Design and formulation of polyurethane foam used for porous alumina ceramics | Journal of Polymer Research, (n.d.). https://link.springer.com/article/10.1007/s10965-018-1535-1 (accessed March 27, 2024).

[99] E. Gregorová, W. Pabst, Porous ceramics prepared using poppy seed as a pore-forming agent, Ceramics International 33 (2007) 1385–1388. https://doi.org/10.1016/j.ceramint.2006.05.019.

[100] F. Xue, K. Zhou, N. Wu, H. Luo, X. Wang, X. Zhou, Z. Yan, I. Abrahams,

D. Zhang, Porous SiC ceramics with dendritic pore structures by freeze casting from chemical cross-linked polycarbosilane, Ceramics International 44 (2018) 6293–6299. https://doi.org/10.1016/j.ceramint.2018.01.019.

[101] N. Wang, Y. Liu, Y. Zhang, Y. Du, J. Zhang, Control of pore structure during freeze casting of porous SiC ceramics by different freezing modes, Ceramics International 45 (2019) 11558–11563. https://doi.org/10.1016/j.ceramint.2019.03.025.

[102] Fabrication and Structure Characterization of Alumina-Aluminum Interpenetrating Phase Composites | Journal of Materials Engineering and Performance, (n.d.). https://link.springer.com/article/10.1007/s11665-016-1901-2 (accessed March 27, 2024).

[103] J. Yang, J. Yu, Y. Huang, Recent developments in gelcasting of ceramics, Journal of the European Ceramic Society 31 (2011) 2569–2591. https://doi.org/10.1016/j.jeurceramsoc.2010.12.035.

[104] Y. Dong, X. Dong, L. Li, J. Wu, L. Yan, J. Liu, A. Guo, Lightweight and thermally insulating aluminum borate nanofibrous porous ceramics, Ceramics International 47 (2021) 21029–21037. https://doi.org/10.1016/j.ceramint.2021.04.104.

[105] F. Zhang, Z. Li, M. Xu, S. Wang, N. Li, J. Yang, A review of 3D printed porous ceramics, Journal of the European Ceramic Society 42 (2022) 3351–3373. https://doi.org/10.1016/j.jeurceramsoc.2022.02.039.

[106] H. Zhou, J. Xie, F. Yan, W. Guo, P. Gao, H. Qin, H. Xiao, Porous Al2O3 ceramics with directional gradient pore structure modified by cobweb-bridged WO3 nanowires for oil/water emulsions separation, Ceramics International 48 (2022) 18753–18764. https://doi.org/10.1016/j.ceramint.2022.03.150.

[107] G. Zhang, B. Zou, X. Wang, Y. Yu, Q. Chen, Design, manufacturing and properties of controllable porosity of ceramic filters based on SLA-3D printing technology, Ceramics International 49 (2023) 1009–1019. https://doi.org/10.1016/j.ceramint.2022.09.076.

[108] H. Yang, X. Min, S. Xu, J. Bender, Y. Wang, Development of Effective and Fast-Flow Ceramic Porous Media for Point-of-Use Water Treatment: Effect of Pore Size Distribution, ACS Sustainable Chem. Eng. 8 (2020) 2531–2539. https://doi.org/10.1021/acssuschemeng.9b07177.

[109] C. Young, C. Zhang, A. Nisar, B. Boesl, A. Agarwal, Spark plasma sintered porous aluminum oxide for filtration applications, Ceramics International 47 (2021) 21822–21827. https://doi.org/10.1016/j.ceramint.2021.04.199.

[110] M. Biesuz, M. Tomasi, B. Santhosh, V.M. Sglavo, G.D. Sorarù, Polymer-derived Si3N4 nanofelts as a novel oil spills clean-up architecture, Journal of Environmental Chemical Engineering 8 (2020) 104134. https://doi.org/10.1016/j.jece.2020.104134.

[111] Y. Tian, Y. Tang, J. Wang, R. Zhang, X. Yan, G. Peng, L. Fang, Q. Jing,

Open-cell porous sound-absorbing ceramics prepared by a new procedure that combines foamed and templated methods, International Journal of Applied Ceramic Technology 17 (2020) 1033–1043. https://doi.org/10.1111/ijac.13468.

[112] J.H. Chen, P.S. Liu, J.X. Sun, Sound absorption performance of a lightweight ceramic foam, Ceramics International 46 (2020) 22699–22708. https://doi.org/10.1016/j.ceramint.2020.06.033.

[113] G.-R. Li, C.-H. Li, J.-A. Liu, Y. Zou, L. Hu, Y.-S. Shi, High sound absorption characteristics of foamed alumina ceramics fabricated by gelcasting-foaming process, Journal of the Ceramic Society of Japan 128 (2020) 387–394. https://doi.org/10.2109/jcersj2.19227.

[114] M. Assefi, S. Maroufi, I. Mansuri, V. Sahajwalla, High strength glass foams recycled from LCD waste screens for insulation application, Journal of Cleaner Production 280 (2021) 124311. https://doi.org/10.1016/j.jclepro.2020.124311.

[115] A. Dutto, M. Zanini, E. Jeoffroy, E. Tervoort, S.A. Mhatre, Z.B. Seibold, M. Bechthold, A.R. Studart, 3D Printing of Hierarchical Porous Ceramics for Thermal Insulation and Evaporative Cooling, Advanced Materials Technologies 8 (2023) 2201109. https://doi.org/10.1002/admt.202201109.

[116] S. Li, B. Chang, M. Li, S. Ran, Fabrication of high strength and thermal insulation porous ceramics via adjusting the fiberglass contents, International Journal of Applied Ceramic Technology 20 (2023) 2321–2330. https://doi.org/10.1111/ijac.14343.

[117] F.B. Löffler, F.J. Altermann, E.C. Bucharsky, K.G. Schell, M.L. Vera, H. Traid, A. Dwojak, M.I. Litter, Morphological characterization and photocatalytic efficiency measurements of pure silica transparent open-cell sponges coated with TiO2, International Journal of Applied Ceramic Technology 17 (2020) 1930–1939. https://doi.org/10.1111/ijac.13504.

[118] J. Liu, C. Tian, T. Jiang, E.I. Ricohermoso, Z. Yu, E. Ionescu, L. Molina-Luna, J.P. Hofmann, R. Riedel, Polymer-derived SiOC ceramics: A potential catalyst support controlled by the sintering temperature and carbon content, Journal of the European Ceramic Society 43 (2023) 3191–3200. https://doi.org/10.1016/j.jeurceramsoc.2023.02.045.

[119] C. Huo, X. Tian, Y. Nan, D. Li, Hierarchically porous alumina ceramic catalyst carrier prepared by powder bed fusion, Journal of the European Ceramic Society 40 (2020) 4253–4264. https://doi.org/10.1016/j.jeurceramsoc.2020.03.059.

[120] K.K. Sahu, Y.K. Modi, Multi response optimization for compressive strength, porosity and dimensional accuracy of binder jetting 3D printed ceramic bone scaffolds, Ceramics International 48 (2022) 26772–26783. https://doi.org/10.1016/j.ceramint.2022.05.375.

[121] N. Raja, A. Sung, H. Park, H. Yun, Low-temperature fabrication of

calcium deficient hydroxyapatite bone scaffold by optimization of 3D printing conditions, Ceramics International 47 (2021) 7005–7016. https://doi.org/10.1016/j.ceramint.2020.11.051.

[122] Novel Porous Barium Titanate/Nano-bioactive Glass Composite with High Piezoelectric Coefficient for Bone Regeneration Applications | Journal of Materials Engineering and Performance, (n.d.). https://link.springer.com/article/10.1007/s11665-020-05016-0 (accessed March 27, 2024).

[123] S. Roy, K.G. Schell, E.C. Bucharsky, K.A. Weidenmann, A. Wanner, M.J. Hoffmann, Processing and characterization of elastic and thermal expansion behaviour of interpenetrating Al12Si/alumina composites, Materials Science and Engineering: A 743 (2019) 339–348. https://doi.org/10.1016/j.msea.2018.11.100.

[124] W. Gao, Y. Zhou, S. Wu, R. Cai, Y. Zhao, S. Li, Z. Huang, Preparation, microstructure and mechanical properties of steel matrix composites reinforced by a 3D network TiC ceramics, Ceramics International 48 (2022) 20848–20857. https://doi.org/10.1016/j.ceramint.2022.04.074.

[125] S. Vaucher, J. Kuebler, O. Beffort, L. Biasetto, F. Zordan, P. Colombo, Ceramic foam-reinforced Al-based micro-composites, Composites Science and Technology 68 (2008) 3202–3207. https://doi.org/10.1016/j.compscitech.2008.08.004.

[126] J. Schukraft, D. Horny, K. Schulz, K.A. Weidenmann, 3D modeling and experimental investigation on the damage behavior of an interpenetrating metal ceramic composite (IMCC) under compression, Materials Science and Engineering: A 844 (2022) 143147. https://doi.org/10.1016/j.msea.2022.143147.

[127] S. Roy, J. Gibmeier, K.G. Schell, E.C. Bucharsky, K.A. Weidenmann, A. Wanner, M.J. Hoffmann, Internal load transfer in an interpenetrating metal/ceramic composite material studied using energy dispersive synchrotron X-ray diffraction, Materials Science and Engineering: A 753 (2019) 247–252. https://doi.org/10.1016/j.msea.2019.03.049.

[128] V. Imbeni, I.M. Hutchings, M.C. Breslin, Abrasive wear behaviour of an Al2O3–Al co-continuous composite, Wear 233–235 (1999) 462–467. https://doi.org/10.1016/S0043-1648(99)00188-X.

[129] E. del Rio, J.M. Nash, J.C. Williams, M.C. Breslin, G.S. Daehn, Co-continuous composites for high-temperature applications, Materials Science and Engineering: A 463 (2007) 115–121. https://doi.org/10.1016/j.msea.2006.07.162.

[130] S. Li, D. Xiong, M. Liu, S. Bai, X. Zhao, Thermophysical properties of SiC/Al composites with three dimensional interpenetrating network structure, Ceramics International 40 (2014) 7539–7544. https://doi.org/10.1016/j.ceramint.2013.12.105.

[131] S. Roy, A. Nagel, K.A. Weidenmann, Anisotropic thermal expansion behavior of an interpenetrating metal/ceramic composite, Thermochimica Acta

684 (2020) 178488. https://doi.org/10.1016/j.tca.2019.178488.

[132] D. Wang, Z. Zheng, J. Lv, G. Xu, S. Zhou, W. Tang, Y. Wu, Enhanced thermal conductive 3D-SiC/Al-Si-Mg interpenetrating composites fabricated by pressureless infiltration, Ceramics International 43 (2017) 1755–1761. https://doi.org/10.1016/j.ceramint.2016.10.104.

[133] K. Zhang, Z. Shi, H. Xia, K. Wang, G. Liu, G. Qiao, J. Yang, Preparation and thermophysical properties of directional SiC/Cu–Si composite via spontaneous infiltration, Ceramics International 42 (2016) 996–1001. https://doi.org/10.1016/j.ceramint.2015.08.173.

Chapter2

Microstructure and mechanical properties of Al/AlN interpenetrating phase composites with different preform porosity

2.1 Introduction

Among the variety of metal matrix materials, aluminum matrix composites (AMCs) stand out for their light weight, great durability, good thermal properties and relative low cost. Aluminum matrix composites are widely employed in automotive components, aerospace, electronic packaging, and other applications for these reasons[1–5]. Traditional composite reinforcements are primarily particles, fibers, and whiskers that are discontinuously dispersed in the composite as the second phase[6–11]. In contrast, the individual components of interpenetrating composites exhibit continuity in three dimensions and possess an interconnected network structure. This structural feature enables the remaining phases to maintain a stable and self-supporting structure even if one phase is eliminated.[12,13]. IPCs often offer enhanced physical and mechanical characteristics because to their unique structure, including increased Young's modulus, hardness, and wear resistance[14–16]. Moreover, IPCs exhibit higher thermal conductivity and lower Coefficient of Thermal Expansion (CTE) compared to particle-reinforced composites with equal component content. This is attributed to the distinctive interconnected structure, which features a relatively smaller interfacial region. The two separately contiguous phases create two independent heat transfer channels, enhancing thermal conductivity efficiency. Furthermore, this structure enables the ceramic phase to more effectively restrict the expansion of the metal phase [17–20].

So far, silicon carbide (SiC), aluminum oxide (Al_2O_3), silicon nitride (Si_3N_4), and Titanium carbide (TiC) have been the most widely explored second phase used to strengthen Al matrix interpenetrating composites[3,12,19,21–28]. At present, there are few investigations on Al/AlN IPCs. AlN has outstanding thermophysical characteristics, strong interfacial adhesion without interfacial reaction with aluminum alloy, high thermal conductivity, high electrical resistivity, low coefficient of thermal expansion, high specific strength and stiffness[29–32]. Al/AlN IPCs therefore also offer desirable mechanical, electrical, and thermal properties. A356 is a widely used low-cost aluminum casting alloy with excellent casting properties. The addition of magnesium enhances the wettability at the interface between the aluminum alloy and the reinforcing material, making it highly suitable for serving as the matrix in IPCs[33,34].

In this study, we aim to investigate the microstructure and mechanical properties of A356/AlN interpenetrating phase composites (IPCs) with varying porosity of the AlN preform. To achieve this, open-cell AlN preform with different porosity were fabricated using the slurry infiltration method. Subsequently, Al/AlN composites with an interpenetrating structure were produced via low-pressure casting. The microstructures and compositions of the AlN preforms and A356/AlN IPCs were thoroughly examined. Finally, the mechanical properties of the composites were evaluated via compression testing and nanoindentation test.

2.2 Experimental procedures

2.2.1 Preparation of AlN preforms

AlN powder (Tokuyama Co, Ltd., average particle diameter: 1.17 μm), Al_2O_3 sol binder (Nissan Chemical Industries Co, Ltd.) and polyurethane foam (Achilles Co, Ltd., cell diameter is 500 μm and cell wall size is 100 μm) were used in the present work. In a typical fabrication process, AlN powder was mixed with Al_2O_3 sol binder (1.5:1) to form a slurry. Then infiltrate the PU foam into the slurry, press and release the PU foam to make it suck the slurry. The weight of preform should be weighted to control the porosity. Excess slurry is removed by squeezing the foam. Preforms of four weights were prepared (2.30 g, 3.39 g, 3.72 g, 4.40 g). Thereafter these preforms were dried at 343 K for 12 h. Then preforms were sintered at 1923 K for 1h in Ar atmosphere by carbon embedded method. The dimensions of the foams used for the fabrication of IPCs were Φ 20 mm × 10 mm. The preform porosity (θ) was obtained by(2.1).

$$\theta = \frac{\rho_m}{\rho_t} \tag{2.1}$$

where ρ_m is the measured density of preform and ρ_t is the theoretical density of preform. Furthermore, the measured density of preform (ρ_m) was calculated according to (2.2).

$$\rho_m = \frac{M_m}{V_m} \tag{2.2}$$

where M_m is the measured mass of preform and V_m is the measured volume which can calculated based on external dimension of the sintered preform. The flow chart for preparing preform is shown in Fig. 2-1.

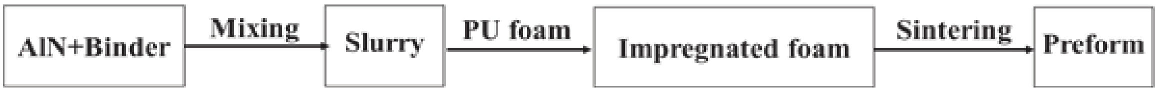

Fig. 2-1 Flow chart for the fabrication of AlN preform.

2.2.2 Fabrication of IPCs

The Al/AlN IPCs were prepared by low pressure casting process. Commercially available aluminum alloy (A356) was used as a matrix material. The preform was placed in the bottom of graphite mould and the aluminum alloy block was placed above the preform. Then the sample was heated to 1123 K, the Al alloy was infiltrated into the preform under the pressure of 0.4 MPa for 1h under Ar atmosphere.

2.2.3 Characterization

The phase characterization of the AlN preforms and Al/AlN IPCs was carried out using an X-ray diffractometer (Rigaku D/max-2500) with Cu Kα radiation (k = 0.15406 nm). The microstructures and element distribution were examined with an electron probe micro-analyzer (EPMA, JEOL JXA-ISP100). The density and porosity of Al/AlN IPCs were measured by Archimedes method. The Al/AlN IPCs were cut into compression specimens with a size of 6 × 6 × 6 mm. The compression strength of Al/AlN IPCs were measured in a WDW-50 universal testing machine with a strain rate of 0.001 s^{-1}. The hardness of composites was tested using G200 nano indenter. For conducting the nanoindentation test, we employed a Berkovich diamond indenter with a tip curvature radius of 20 nm. We performed a total of eight indentations on each sample, with each indentation separated by a distance of 25 μm from the next. The maximum load applied during the indentations was 5000 μN, and each loading had a duration of 5 seconds. All tests are performed at room temperature.

2.3 Results and discussion

2.3.1 Microstructure and phase composition

Fig. 2-2 shows the microstructure of 84% porosity AlN preform. The 3D network topology of the open-cell AlN preform is representative, and the open-cell structure has an almost spherical shape. A higher magnification SEM image of the AlN strut is shown in Fig. 2b. This image confirms that the effective bonding of the AlN powders, and the presence of sintered necks is evident.

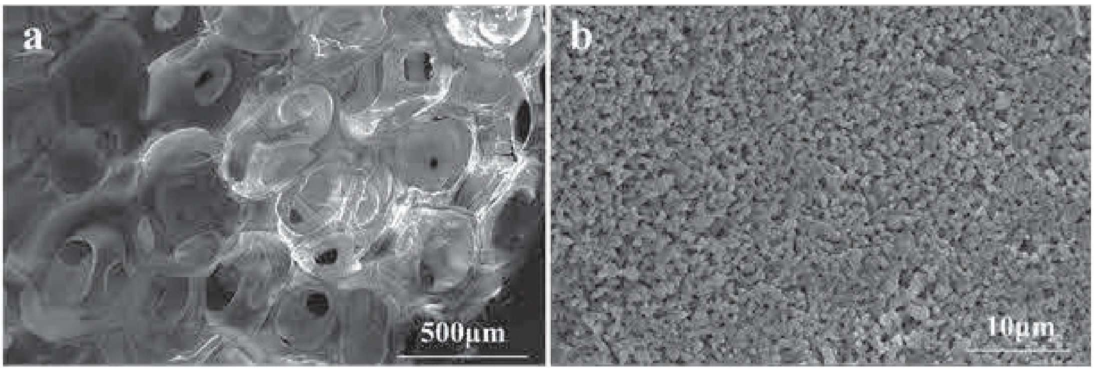

Fig. 2-2 SEM image of preform with 84% porosity: a. low magnification, b. high magnification.

Fig. 2-3 displays the X-ray diffraction pattern of an AlN preform with 84% porosity. As observed in the figure, the sintered sample consists of two phases: Al_2O_3 and AlN. Notably, the content of Al_2O_3 is relatively low. Furthermore, it is worth mentioning that the carbon embedded method was utilized to prevent the oxidation of AlN during the sintering process. Based on XRD data, the jade software estimates an alumina content of approximately 14% for the preform, while the theoretically alumina content calculated based on component ratios is about 12%. This demonstrates a minimal degree of oxidation in the preform during sintering, and the carbon embeded method effectively inhibits oxidation behavior throughout the sintering process.

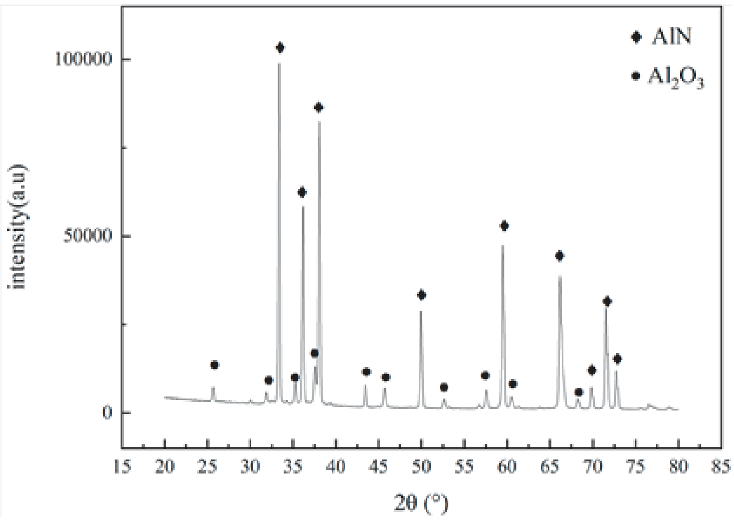

Fig. 2-3 XRD patterns of the sintered porous preforms with 84% porosity.

The relative density variation curve with preform porosity is shown in Fig. 2-4. It can be observed that the relative density decreases as the preform porosity decreases. In particular, a significant reduction in relative density is observed when the preform porosity decreases from 79% to 76%. This phenomenon can be attributed to the substantial increase in the number of closed cells when the preform porosity falls below 76%. The increased number of closed cells consequently leads to a considerable decrease in the relative density of the IPCs. Moreover, the reduced cell size may also pose a challenge for the aluminum alloy to penetrate the preform, which can further contribute to the reduction in relative density.

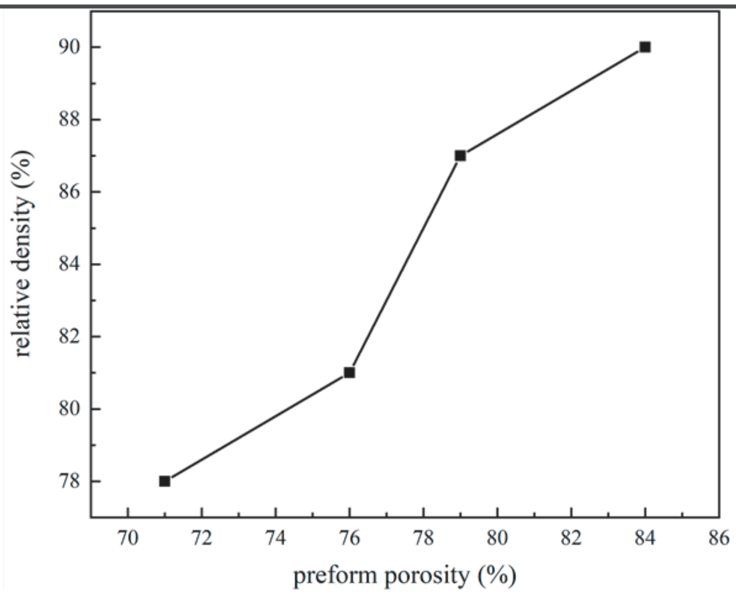

Fig. 2-4 Relationship between preform porosity and relative density of IPCs.

Fig. 2-5 depicts the microstructure of prepared Al/AlN IPCs with varying preform porosity. The figure demonstrates that the Al alloy was able to infiltrate the preform effectively while retaining its porous structure. As observed, the aluminum alloy not only permeates the circular pores but also infiltrates the triangular and quadrilateral holes. The triangular and quadrilateral holes represent hollow arms remaining from the polymer strut's sintering process[35]. The size of the cell walls increased as the preform porosity decreased. Additionally, the interface between the preform and matrix was well-bonded, and no visible defects, such as pores or gaps, were detected. While there are some pores visible in Fig. 2-5a and b, these pores are primarily located within the aluminum nitride preform. This results from a reduction in porosity within the preform. With reduced porosity, the preform develops more closed pores, which become visible during composites processing involving procedures like grinding and polishing that disrupt these closed pores.

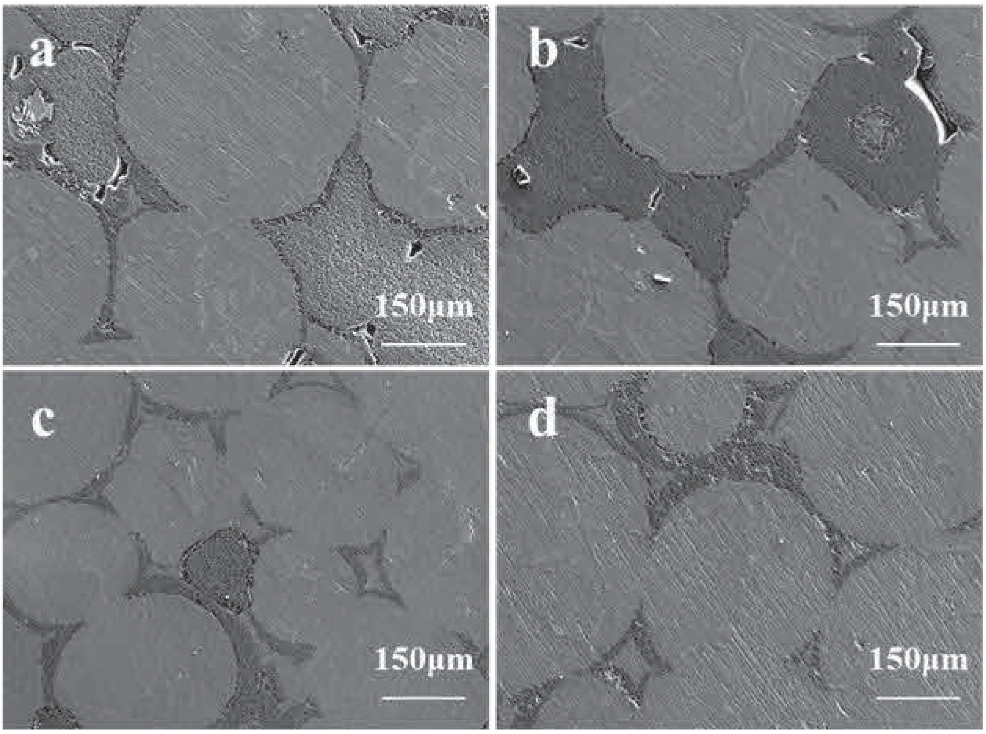

Fig. 2-5 SEM image of the IPCs with different preform porosity: a. 71%, b. 76%, c. 79% and d. 84%.

The EPMA map of 84% preform porosity IPCs is shown in Fig. 2-6. The mapping reveals that oxygen (O) and magnesium (Mg) elements are mainly concentrated at the interface. This observation indicates that magnesium in the aluminum alloy reacts with alumina in the preform, thereby promoting interfacial bonding. In addition, silicon (Si) is distributed within the matrix in the form of precipitates.

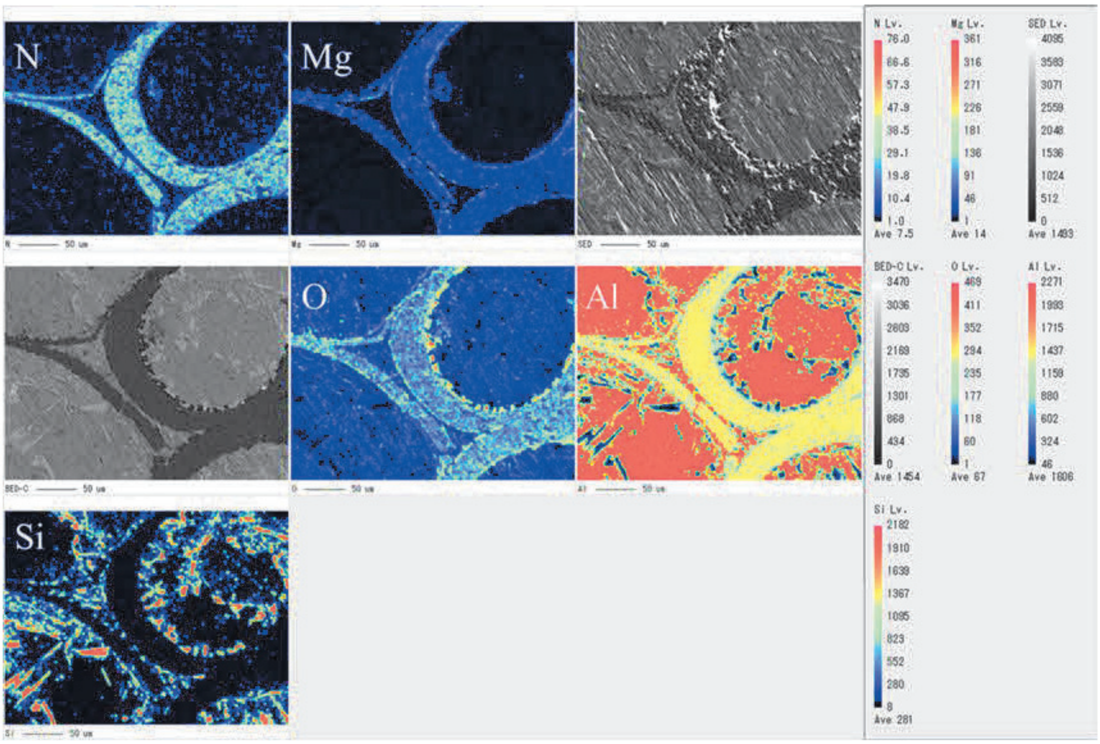

Fig. 2-6 The EPMA image of 84% preform porosity IPCs.

Fig. 2-7a shows the XRD pattern of 84% preform porosity IPCs, which confirms the presence of Al, Si, $MgAl_2O_4$, and AlN phases. Notably, no Al_2O_3 phase was detected, indicating that the Al_2O_3 on the preform reacted with the Mg in the alloy. This reaction enhances the wettability between the matrix and the preform. The resultant $MgAl_2O_4$ spinel contributes to an increase in strength and wear resistance to some degree[36,37]. 3D XRD patterns of IPCs with different preform porosity are illustrated in Fig. 2-7b.

Although the diffraction peak positions of the four samples are essentially the same, the peak shapes differ more significantly. This difference is due to the lower relative density and increased internal porosity of the 71% and 76% preform porosity samples. These pores also scatter X-rays, leading to broadening and reduced intensity of the diffraction peaks. Texture development during processing and preparation could contribute to variations in the intensity of diffraction peaks.

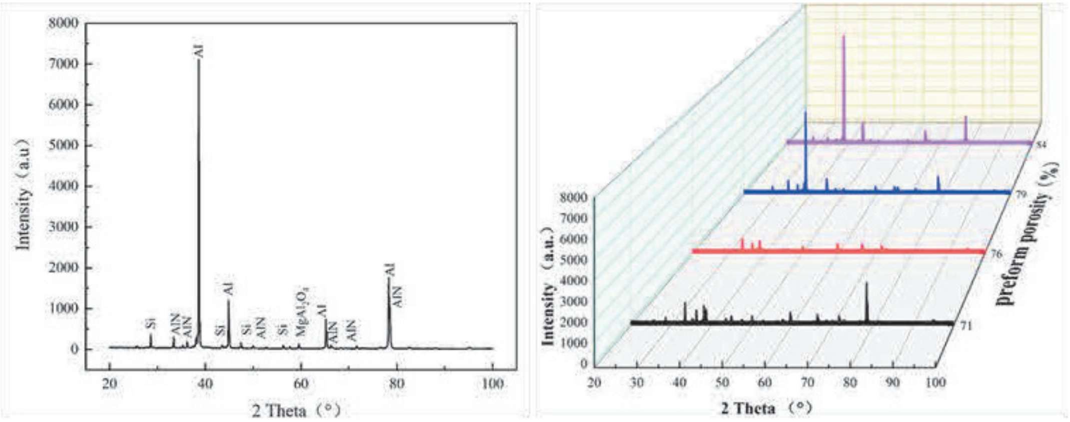

Fig. 2-7 XRD patterns: a. IPCs with 84% preform porosity, b. 3D of IPCs.

2.3.2 Compression test

Fig. 2-8a shows representative engineering compressive stress-strain curve of IPCs with different preform porosity. And the stress-strain curves of A356 and preforms with 84% porosity are provided for comparison. Similar to the foam metal and other IPCs[38,39], the stress-strain curves for the 84% and 76% samples exhibit three regions, indicating good strength and toughness. Conversely, the stress-strain curves for the 76% and 71% samples decrease rapidly and end after the stress peaks due to apparent brittle fracture. This can be attributed partly to the increased content of the brittle phase AlN, which reduces material toughness, and partly to the large number of pores in the 76% and 71% samples, leading to their brittle fracture. Due to their porous structure and inherent brittleness, AlN preforms exhibit notably low strength and ductility in their stress-strain curves. Since the Al alloy is a dense plastic material, the stress-strain curve exhibits greater strength, with stress increasing as strain rises; however, there is no notable compressive strength value. Later, we will delve into a more detailed examination of compression performance. Fig. 2-8b illustrates the variation of true strain and work hardening rate with true strain for the 84% preform porosity sample. The entire deformation process can be divided into five stages which is similar to 3D printed Mg-NiTi interpenetrating-phase composites[40]. In stage I, both Al matrix and AlN ceramic strut are principally deformed elastically. As the stress increases, the aluminum matrix begins to yield while the aluminum nitride ceramic continues to undergo elastic deformation, resulting in a mixed mode deformation of the composite. With an increase in deformation, the dislocation density in the Al matrix rises, leading to work hardening. Consequently, there is a corresponding rise in the rate of work hardening during this stage. The stress then enters a plateau stage, during which the cells composed of aluminum matrix and ceramic skeleton begin to collapse, leading to yielding and fracture, while the stress and work-hardening rate remains relatively constant. After all the cells collapse, further deformation increases the density of the composite, causing the stress and work-hardening rate to rise sharply.

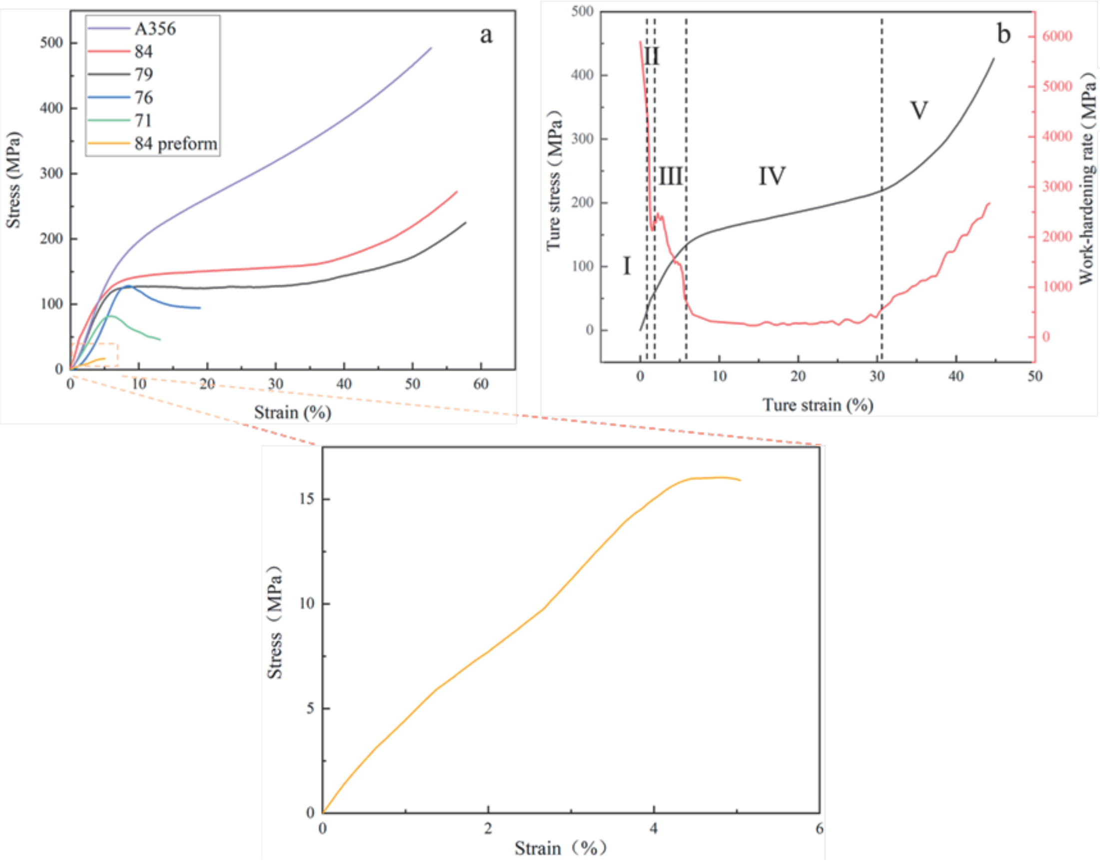

Fig. 2-8 Compression properties: a. representative engineering compressive stress-strain curve of IPCs, A356 and preform, b. variation of true strain and work hardening rate with true strain for IPCs with 84% preform porosity.

The Compression properties are shown in Table 2-1. The toughness of each IPCs sample was determined by calculating the area under the stress-strain curve before the end of stress plateau stage. Toughness signifies a material's capacity to absorb energy under compression[41,42]. The elastic modulus, i.e. Young's modulus, is calculated as the ratio of stress to strain observed in the elastic stage. As aluminum alloys display a stress-strain curve that rises continuously without a stable plateau phase, the area under the stress-strain curve prior to reaching the yield strain is commonly employed to depict its energy absorption capacity[40]. The results indicate that the compressive strength, yield strength, and toughness of the samples increase with an increase in preform porosity. Notably, the toughness of samples with preform porosity below 76% is significantly lower than that of samples with preform porosity above 76%. This disparity is attributed to the low relative density of the samples with preform porosity below 76%, as the presence of more closed pores within these samples can significantly compromise their compression properties, leading to brittle fracture. A356 alloy demonstrates higher yield strength, attributed in part to the lower strength of the AlN preform and likely due to the reaction between Al_2O_3 and Mg in the matrix. This reaction consumes nearly all Mg, preventing the formation of Mg_2Si precipitates within the matrix, consequently reducing the strength of the IPCs. Compared to A356 alloys, the 84% and 79% preform porosity IPCs have slightly lower yield strengths, but much higher energy absorption capacities. The 84% preform porosity samples also have higher elastic modulus, which is due to the special structure of IPCs. Despite ceramic preforms offering a higher elastic modulus the lower relative density of IPCs with 79%-71% preform porosity results in increased internal pore content. These non-load-bearing pores can decrease the overall cross-sectional area. Simultaneously, stress concentrations commonly occur around the pores, potentially causing material damage or failure in those regions. Consequently, the modulus of elasticity is lower compared to A356 alloys.

Sekar et al.[43] used stirring and squeeze casting methods to prepare A356/ Al_2O_3 particle-reinforced composites, which had compressive yield strengths ranging from 110 to 200 MPa. Using a liquid pressing process, Lee et al.[44] prepared A356/SiC_P composites that had compressive yield strengths of 297-450 MPa, but low plasticity with a total strain of only 3.0%-4.3%. The composites investigated in this study exhibit commendable energy absorption capabilities; however, their strength is somewhat lacking. Enhancing the strength constitutes our primary research objective moving forward.

Table 2-1 Compression properties of IPCs, A356 and preform.

Preform porosity (%)	**Yield strength (MPa)**	**Compressive strength (MPa)**	**Toughness (MJm^3)**	**Elastic modulus (GPa)**
71	66	81	7.2	1.42
76	100	128	16.1	1.39
79	110	127	39.2	2.18
84	130	140	49.0	3.61
A356	142	--	3.6	2.55
Preform	--	16	0.4	0.44

Photographs of fractured IPC specimens with 84% and 71% preform porosity are shown in Fig. 2-9a and b, respectively. Upon compression testing, it was observed that the sample with 71% preform porosity broke along a 45° angle with respect to the loading direction and had a rough surface, indicating poor ductility. Conversely, the sample with 84% preform porosity did not break into multiple pieces, like the sample with 71% preform porosity, but instead underwent significant deformation, resulting in multiple cracks on the surface. Despite this, it remained relatively intact, indicating good toughness. Fig. 2-9c shows an SEM image of the fracture surface of 71% preform porosity IPCs. The image reveals a significant presence of closed-cells with windows, indicating that debonding had occurred between the AlN closed-cells and the Al matrix. An enlarged view (Fig. 2-9d) shows numerous cracks in the struts and gaps between cells and struts. The presence of a large number of closed cells severely impacted the connectivity of the IPCs, resulting in poor entanglement between the preform and the matrix. This, in turn, prevented the Al matrix with good toughness from protecting the brittle AlN ceramics during deformation, leading to the generation of numerous cracks and frequent debonding, resulting in brittle fracture of the material.

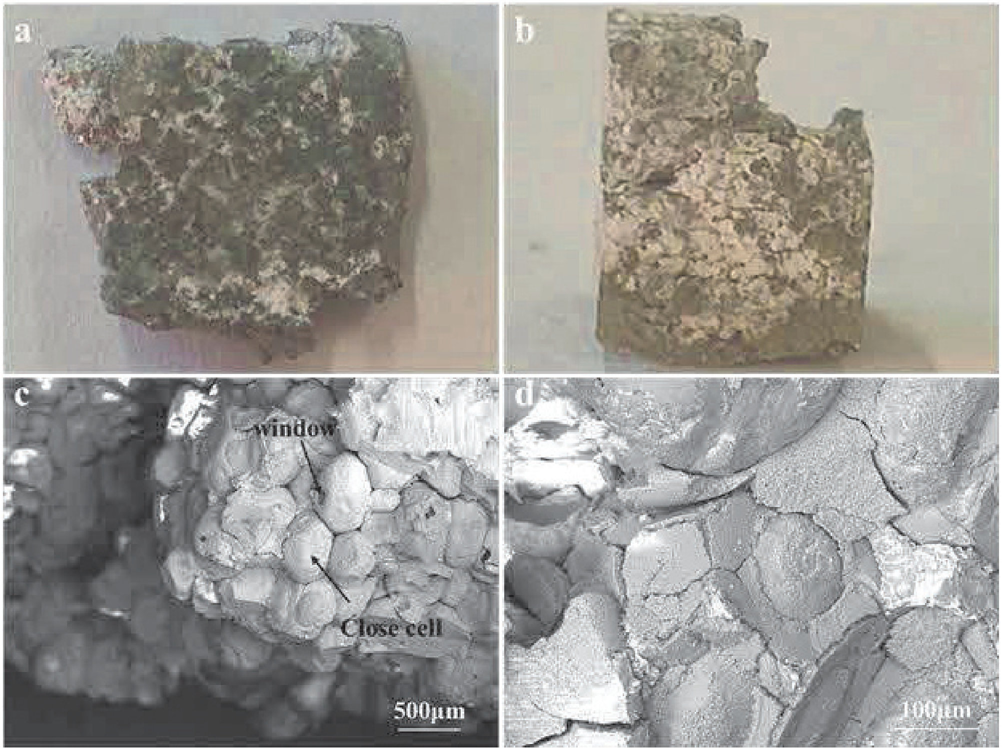

Fig. 2-9 Fracture morphology: photographs of fractured IPC specimens a.84%, b.71%, c. SEM image of the fracture surface of IPCs with 71% preform porosity, d. an enlarge view of c.

2.3.3 Nanoindentation test

Fig. 2-10 shows the hardness of IPCs with different preform porosity. The 1st-3rd points are at AlN reinforcement, the 4th point at the interface, the 5th-8th points are distributed at Al alloy matrix. Hardness generally increases from the eighth to the first point, with a significant rise observed from the fifth to the fourth point. The higher interfacial hardness indicates a strong bond between the reinforcement and the matrix. Good interfacial bonding facilitates internal load transfer from the metal matrix phase to the ceramic reinforced phase, resulting in better mechanical properties[45]. Roy et al.[46] examined the internal load transfer mechanism in interpenetrating metal/ceramic composites through energy dispersive synchrotron X-ray diffraction. They observed that at low applied pressure, each phase undergoes elastic deformation, and the load distribution among the phases remains constant. At high applied stress, the metal phase undergoes plastic deformation, transferring the load to the ceramic phase. With further stress increase, the ceramic phase undergoes destruction, imposing additional load on the metal matrix. Notably, there is no significant load transfer within the metal alloy itself during this process. As the preform porosity decreases, the hardness of the composites increases gradually. This trend inconsistent with the relationship between compressive strength and preform porosity, indicating that nanoindentation hardness is less influenced by the relative density compared to compressive strength.

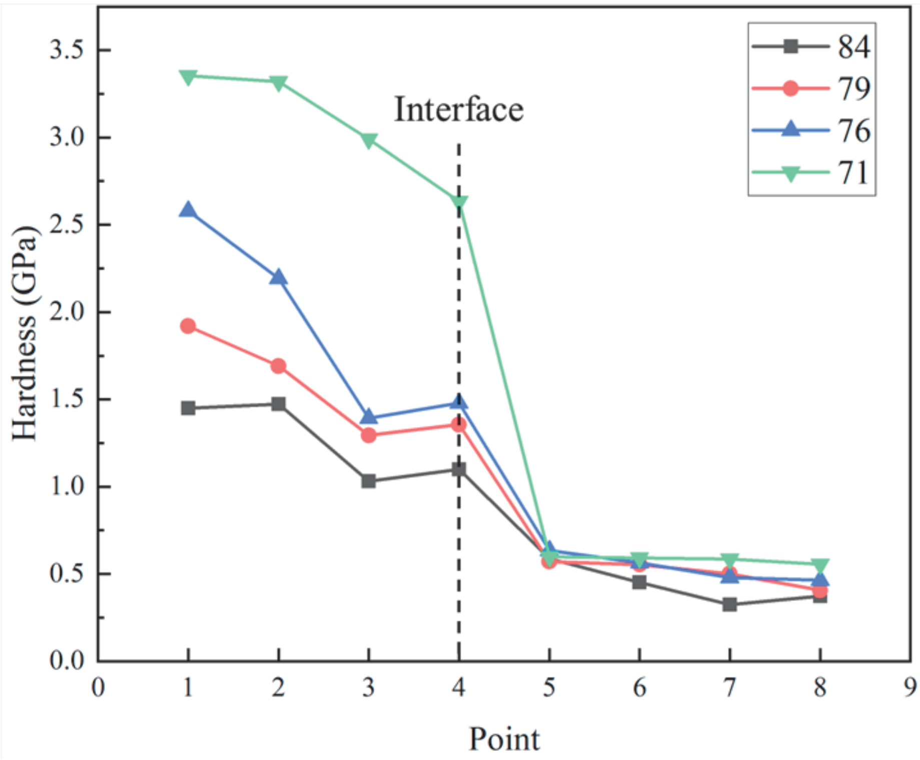

Fig. 2-10 Hardness of IPCs with different preform porosity.

2.4 Summary

This study investigated the microstructure and mechanical properties of Al/AlN interpenetrating phase composites (IPCs) with different preform porosity. After analysis and discussion, the main conclusions were obtained as follows:

(1) Al/AlN IPCs were successfully fabricated by infiltrating molten A356 alloy into AlN preforms with different porosity (71%, 76%, 79%, and 84%) using the low-pressure casting method. The Al alloy effectively infiltrated the preforms, and a clean, well-bonded interface was observed between the components.

(2) The relative density of the composites increased with increasing preform porosity. The compression behavior varied greatly, with samples having 84% and 79% preform porosity exhibiting ductile fracture, while those with 76% and 71% porosity exhibited brittle fracture. Compressive strength, yield strength, and toughness increased with increasing preform porosity. The 84% preform porosity IPCs demonstrated the highest compressive strength (140 MPa) and the best toughness (48.98 MJm^{-3}).

(4) Nanoindentation hardness was minimally affected by the presence of pores but increased with decreasing preform porosity. Higher interfacial hardness indicated effective interfacial bonding.

2.5 References

[1] L. Ren, T. Gao, J. Nie, G. Liu, X. Liu, A novel core-shell TiCx particle by modifying TiCx with B element and the preparation of the (TiCx + AlN)/Al composite, Journal of Alloys and Compounds 894 (2022) 162448. https://doi.org/10.1016/j.jallcom.2021.162448.

[2] J. Maj, W. Węglewski, K. Bochenek, Ł. Rogal, S. Woźniacka, M. Basista, A Comparative Study of Mechanical Properties, Thermal Conductivity, Residual Stresses, and Wear Resistance of Aluminum-Alumina Composites Obtained by Squeeze Casting and Powder Metallurgy, Metall Mater Trans A 52 (2021) 4727–4736. https://doi.org/10.1007/s11661-021-06401-7.

[3] J. Maj, M. Basista, W. Węglewski, K. Bochenek, A. Strojny-Nędza, K. Naplocha, T. Panzner, M. Tatarková, F. Fiori, Effect of microstructure on mechanical properties and residual stresses in interpenetrating aluminum-alumina composites fabricated by squeeze casting, Materials Science and Engineering: A 715 (2018) 154 – 162. https://doi.org/10.1016/j.msea.2017.12.091.

[4] R. Zheng, X. Hao, Y. Yuan, Z. Wang, K. Ameyama, C. Ma, Effect of high volume fraction of B4C particles on the microstructure and mechanical properties of aluminum alloy based composites, Journal of Alloys and Compounds 576 (2013) 291–298. https://doi.org/10.1016/j.jallcom.2013.04.141.

[5] N. Kota, P. Jana, S. Sahasrabudhe, S. Roy, Processing and characterization of Al-Si alloy/SiC foam interpenetrating phase composite, Materials Today: Proceedings 44 (2021) 2930–2933. https://doi.org/10.1016/j.matpr.2021.01.923.

[6] A. Mortensen, J. Llorca, Metal Matrix Composites, Annu. Rev. Mater. Res. 40 (2010) 243–270. https://doi.org/10.1146/annurev-matsci-070909-104511.

[7] H. Wang, G. Li, Y. Zhao, G. Chen, In situ fabrication and microstructure of Al2O3 particles reinforced aluminum matrix composites, Materials Science and Engineering: A 527 (2010) 2881–2885. https://doi.org/10.1016/j.msea.2010.01.022.

[8] R. Taherzadeh Mousavian, R. Azari Khosroshahi, S. Yazdani, D. Brabazon, A.F. Boostani, Fabrication of aluminum matrix composites reinforced with nano- to micrometer-sized SiC particles, Materials & Design 89 (2016) 58–70. https://doi.org/10.1016/j.matdes.2015.09.130.

[9] V. Chak, H. Chattopadhyay, T.L. Dora, A review on fabrication methods, reinforcements and mechanical properties of aluminum matrix composites, Journal of Manufacturing Processes 56 (2020) 1059–1074. https://doi.org/10.1016/j.jmapro.2020.05.042.

[10] H. Naji, S.M. Zebarjad, S.A. Sajjadi, The effects of volume percent and aspect ratio of carbon fiber on fracture toughness of reinforced aluminum matrix composites, Materials Science and Engineering: A 486 (2008) 413–420. https://doi.org/10.1016/j.msea.2007.09.030.

[11] F.A. Girot, J.M. Quenisset, R. Naslain, Discontinuously-reinforced aluminum matrix composites, Composites Science and Technology 30 (1987) 155–184. https://doi.org/10.1016/0266-3538(87)90007-8.

[12] M. Basista, J. Jakubowska, W. Węglewski, Processing Induced Flaws in Aluminum-Alumina Interpenetrating Phase Composites, Adv. Eng. Mater. 19 (2017) 1700484. https://doi.org/10.1002/adem.201700484.

[13] O. Al-Ketan, R.K.A. Al-Rub, R. Rowshan, Mechanical Properties of a New Type of Architected Interpenetrating Phase Composite Materials, Adv. Mater. Technol. 2 (2017) 1600235. https://doi.org/10.1002/admt.201600235.

[14] D.W. Abueidda, A.S. Dalaq, R.K. Abu Al-Rub, I. Jasiuk, Micromechanical finite element predictions of a reduced coefficient of thermal expansion for 3D periodic architectured interpenetrating phase composites, Composite Structures 133 (2015) 85–97. https://doi.org/10.1016/j.compstruct.2015.06.082.

[15] M. Kouzeli, D.C. Dunand, Effect of reinforcement connectivity on the elasto-plastic behavior of aluminum composites containing sub-micron alumina particles, Acta Materialia 51 (2003) 6105–6121. https://doi.org/10.1016/S1359-6454(03)00431-

2.

[16]C. San Marchi, M. Kouzeli, R. Rao, J.A. Lewis, D.C. Dunand, Alumina–aluminum interpenetrating-phase composites with three-dimensional periodic architecture, Scripta Materialia 49 (2003) 861–866. https://doi.org/10.1016/S1359-6462(03)00441-X.

[17]S. Li, D. Xiong, M. Liu, S. Bai, X. Zhao, Thermophysical properties of SiC/Al composites with three dimensional interpenetrating network structure, Ceramics International 40 (2014) 7539–7544. https://doi.org/10.1016/j.ceramint.2013.12.105.

[18]D. Cree, M. Pugh, Production and characterization of a three-dimensional cellular metal-filled ceramic composite, Journal of Materials Processing Technology 210 (2010) 1905–1917. https://doi.org/10.1016/j.jmatprotec.2010.07.002.

[19]D. Wang, Z. Zheng, J. Lv, G. Xu, S. Zhou, W. Tang, Y. Wu, Enhanced thermal conductive 3D-SiC/Al-Si-Mg interpenetrating composites fabricated by pressureless infiltration, Ceramics International 43 (2017) 1755–1761. https://doi.org/10.1016/j.ceramint.2016.10.104.

[20]N. Kota, M.S. Charan, T. Laha, S. Roy, Review on development of metal/ceramic interpenetrating phase composites and critical analysis of their properties, Ceramics International 48 (2022) 1451–1483. https://doi.org/10.1016/j.ceramint.2021.09.232.

[21]L. Xie, T. Sun, C. He, J. Deng, H. Yi, X. Yang, Q. Qin, Q. Peng, Enhancement of toughness of SiC through compositing SiC–Al interpenetrating phase composites, Nanotechnology 31 (2020) 135706. https://doi.org/10.1088/1361-6528/ab6468.

[22]H. Chang, R. Higginson, J. Binner, Microstructure and property characterisation of 3-3 Al(Mg)/Al2O3 interpenetrating composites produced by a pressureless infiltration technique, J Mater Sci 45 (2010) 662–668. https://doi.org/10.1007/s10853-009-3983-9.

[23]J. Schukraft, D. Horny, K. Schulz, K.A. Weidenmann, 3D modeling and experimental investigation on the damage behavior of an interpenetrating metal ceramic composite (IMCC) under compression, Materials Science and Engineering: A 844 (2022) 143147. https://doi.org/10.1016/j.msea.2022.143147.

[24] Y. Lu, J. Yang, W. Lu, R. Liu, G. Qiao, C. Bao, The mechanical properties of co-continuous Si3N4/Al composites manufactured by squeeze casting, Materials Science and Engineering: A 527 (2010) 6289–6299. https://doi.org/10.1016/j.msea.2010.06.047.

[25] B.-L. He, Y.-F. Zhu, Microstructure and Properties of TiC/Ni $_3$ Al Composites Prepared by Pressureless Melt Infiltration with Porous TiC/Ni $_3$ Al Preforms, Materials and Manufacturing Processes 26 (2011) 586–591. https://doi.org/10.1080/10426910903229339.

[26] A.P. Amosov, A.F. Fedotov, E.I. Latukhin, V.A. Novikov, TiC–Al interpenetrating composites by SHS pressing, Int. J Self-Propag. High-Temp. Synth. 24 (2015) 187–191. https://doi.org/10.3103/S1061386215040032.

[27] S. Roy, K.G. Schell, E.C. Bucharsky, K.A. Weidenmann, A. Wanner, M.J. Hoffmann, Processing and characterization of elastic and thermal expansion behaviour of interpenetrating Al12Si/alumina composites, Materials Science and Engineering: A 743 (2019) 339–348. https://doi.org/10.1016/j.msea.2018.11.100.

[28] P.C. Morbitzer, J. Schukraft, C. Lohr, K.A. Weidenmann, In-situ SEM investigation on the damage behavior of an interpenetrating metal ceramic composite, Composite Structures 321 (2023) 117278. https://doi.org/10.1016/j.compstruct.2023.117278.

[29] C.-H. Li, L.-H. Kao, M.-J. Chen, Y.-F. Wang, C.-H. Tsai, Rapid preparation of aluminum nitride powders by using microwave plasma, Journal of Alloys and Compounds 542 (2012) 78–84. https://doi.org/10.1016/j.jallcom.2012.07.086.

[30] Q. Zheng, R.G. Reddy, Mechanism of in situ formation of AlN in Al melt using nitrogen gas, Journal of Materials Science 39 (2004) 141–149. https://doi.org/10.1023/B:JMSC.0000007738.14116.fd.

[31] L. Jia, K. Kondoh, H. Imai, M. Onishi, B. Chen, S. Li, Nano-scale AlN powders and AlN/Al composites by full and partial direct nitridation of aluminum in solid-state, Journal of Alloys and Compounds 629 (2015) 184–187. https://doi.org/10.1016/j.jallcom.2014.12.220.

[32] G. Pezzotti, I. Kamada, S. Miki, Thermal conductivity of AlN/polystyrene

interpenetrating networks, Journal of the European Ceramic Society 20 (2000) 1197–1203. https://doi.org/10.1016/S0955-2219(99)00282-4.

[33] S.A. Sajjadi, H.R. Ezatpour, M. Torabi Parizi, Comparison of microstructure and mechanical properties of A356 aluminum alloy/Al2O3 composites fabricated by stir and compo-casting processes, Materials & Design 34 (2012) 106–111. https://doi.org/10.1016/j.matdes.2011.07.037.

[34] P.K. Krishnan, J.V. Christy, R. Arunachalam, A.-H.I. Mourad, R. Muraliraja, M. Al-Maharbi, V. Murali, M.M. Chandra, Production of aluminum alloy-based metal matrix composites using scrap aluminum alloy and waste materials: Influence on microstructure and mechanical properties, Journal of Alloys and Compounds 784 (2019) 1047–1061. https://doi.org/10.1016/j.jallcom.2019.01.115.

[35] S. Roy, Recent developments in processing techniques and morphologies of bulk macroporous ceramics for multifunctional applications, Materials Today Communications 38 (2024) 107752. https://doi.org/10.1016/j.mtcomm.2023.107752.

[36] H. Scholz, R. Gonther, J. Rodel, P. Greil, Formation of AI20z fibre-reinforced AIN/AI-matrix composites by Al(Mg)-melt nitridation, (n.d.).

[37] B. Srinivasa Rao, V. Jayaram, Pressureless infiltration of Al–Mg based alloys into Al2O3 preforms: mechanisms and phenomenology, Acta Materialia 49 (2001) 2373–2385. https://doi.org/10.1016/S1359-6454(01)00158-6.

[38] Y. Hangai, S. Otazawa, T. Utsunomiya, Aluminum alloy foam-filled aluminum tube fabricated by friction stir back extrusion and its compression properties, Composite Structures 183 (2018) 416–422. https://doi.org/10.1016/j.compstruct.2017.04.048.

[39] R. Jhaver, H. Tippur, Processing, compression response and finite element modeling of syntactic foam based interpenetrating phase composite (IPC), Materials Science and Engineering: A 499 (2009) 507–517. https://doi.org/10.1016/j.msea.2008.09.042.

[40] M. Zhang, Q. Yu, Z. Liu, J. Zhang, G. Tan, D. Jiao, W. Zhu, S. Li, Z. Zhang, R.

Yang, R.O. Ritchie, 3D printed Mg-NiTi interpenetrating-phase composites with high strength, damping capacity, and energy absorption efficiency, Sci. Adv. 6 (2020) eaba5581. https://doi.org/10.1126/sciadv.aba5581.

[41] A.S. Dalaq, D.W. Abueidda, R.K. Abu Al-Rub, Mechanical properties of 3D printed interpenetrating phase composites with novel architectured 3D solid-sheet reinforcements, Composites Part A: Applied Science and Manufacturing 84 (2016) 266–280. https://doi.org/10.1016/j.compositesa.2016.02.009.

[42] A.A. Yar, M. Montazerian, H. Abdizadeh, H.R. Baharvandi, Microstructure and mechanical properties of aluminum alloy matrix composite reinforced with nano-particle MgO, Journal of Alloys and Compounds 484 (2009) 400–404. https://doi.org/10.1016/j.jallcom.2009.04.117.

[43] K. Sekar, K. Allesu, M.A. Joseph, Effect of T6 Heat Treatment in the Microstructure and Mechanical Properties of A356 Reinforced with Nano Al2O3 Particles by Combination Effect of Stir and Squeeze Casting, Procedia Materials Science 5 (2014) 444–453. https://doi.org/10.1016/j.mspro.2014.07.287.

[44] H. Lee, S.S. Sohn, C. Jeon, I. Jo, S.-K. Lee, S. Lee, Dynamic compressive deformation behavior of SiC-particulate-reinforced A356 Al alloy matrix composites fabricated by liquid pressing process, Materials Science and Engineering: A 680 (2017) 368–377. https://doi.org/10.1016/j.msea.2016.10.102.

[45] P. Maurya, N. Kota, J. Gibmeier, A. Wanner, S. Roy, Review on study of internal load transfer in metal matrix composites using diffraction techniques, Materials Science and Engineering: A 840 (2022) 142973. https://doi.org/10.1016/j.msea.2022.142973.

[46] S. Roy, J. Gibmeier, K.G. Schell, E.C. Bucharsky, K.A. Weidenmann, A. Wanner, M.J. Hoffmann, Internal load transfer in an interpenetrating metal/ceramic composite material studied using energy dispersive synchrotron X-ray diffraction, Materials Science and Engineering: A 753 (2019) 247–252. https://doi.org/10.1016/j.msea.2019.03.049.

Chapter3

Thermal expansion behavior and analysis of Al/AlN interpenetrating phase composites with different preform porosity

3.1 Introduction

Novel materials research and development is becoming more important for many industries. This is due to the ongoing advancements in science and technology. The demand for materials exhibiting exceptional performance is consistently increasing, especially within the domains of engineering, aerospace, and energy. Conventional single materials often face limitations and difficulties in satisfying the needs of diverse harsh working conditions. Composites are gaining prominence as a focal research topic in materials science, offering a solution to overcome these limitations[1–3]. One of the most promising types of composites is metal matrix composites (MMCs). They have high strength, low density, and long service life, which make them widely used in structural materials and electronic packaging. These composites are especially well-suited for thermal management applications. Metal matrices, such as aluminum and copper, exhibit high thermal conductivity. Ceramic reinforcements, such as silicon carbide and aluminum nitride, possess low coefficients of thermal expansion and high temperature stability, rendering them ideal for fulfilling application requirements[4–11]. In this paper, we aim to investigate the thermal expansion behavior of a novel type of composite material, namely interpenetrating phase composites (IPCs).

Extensive experimental research has been conducted to investigate the thermal expansion behavior of MMCs[5,12–15]. Additionally, researchers have developed various thermal-elastic models, including the Turner model and the Kerner model, to better understand the thermal expansion behavior of composites[16,17]. Finite element analysis has been used to simulate the thermal expansion behavior of materials and to improve the prediction of their thermal expansion coefficients. This topic has received a lot of research attention[18–23]. Empirical measurements and theoretical modeling can be combined to analyze material characteristics and design materials effectively. However, despite the extensive research on MMCs, the thermal expansion behavior of

IPCs has been relatively understudied. IPCs have attracted a lot of research interest. This material consists of two components, each of which extends continuously in three dimensions and contains interconnected phases. This arrangement permits each phase to remain isolated, even when the other phase is removed. Due to their unique structure, they often exhibit superior mechanical and physical properties compared to conventional composites. This includes higher Young's modulus, hardness, and wear resistance, as well as a lower coefficient of thermal expansion and higher thermal conductivity[24–30]. Consequently, numerous experiments have been conducted by researchers to investigate the thermal expansion behavior of IPCs. However, most of these tests have focused on IPCs reinforced with SiC and Al_2O_3[31–36]. The thermal expansion behavior of IPCs reinforced with AlN has been rarely studied, especially by combining experimental and numerical analysis.

To address this research gap, we conducted a comprehensive and systematic analysis of the thermal expansion behavior of Al/AlN IPCs. In our previous study[37], the AlN preform with varying porosity were fabricated by slurry infiltration method, and the Al/AlN IPCs were produced via low-pressure casting. The microstructure and mechanical properties of IPCs were investigated. In present paper, the linear coefficient of thermal expansion of Al/AlN IPCs with different preform porosity were measured. Representative volume element (RVE) was generated to model the microstructure of IPCs and numerically investigate the thermal expansion behavious. The results obtained from 3D FEM are compared with the experimental results and thermo-elastic models. Our study contributes to the existing body of research by offering a comprehensive analysis of Al/AlN IPCs, including the exploration of preform porosity effects, integration of experimental and numerical analyses, comparison with analytical models, and insights into thermal stress distribution.

3.2 Experimental procedures

3.2.1 Materials

A356/AlN IPCs with preforms of varying porosity were employed to investigate thermal expansion behaviors. Porous AlN preform with different porosities were prepared using the slurry impregnation method. Subsequently, they were sintered at 1923K for 1h in an Ar atmosphere using the carbon-embedded method. The Al/AlN IPCs were manufactured using the low-pressure casting method. The samples were heated to 1123K, and the Al alloy was infiltrated into the preform at 0.4MPa for 1h in an Ar atmosphere. Relative density (The ratio of the theoretical density to the actual density of the sample) and preform porosity of the composites are show in Table 3-1. Fig. 3-1 shows the morphology of the IPCs. The light gray circular areas represent the Al alloy matrix, while the dark areas indicate AlN struts.

Table 3-1. Relative density and preform porosity of IPCs.

sample	Preform porosity (%)	Relative density (%)
71	71	78
76	76	81
79	79	87
84	84	89

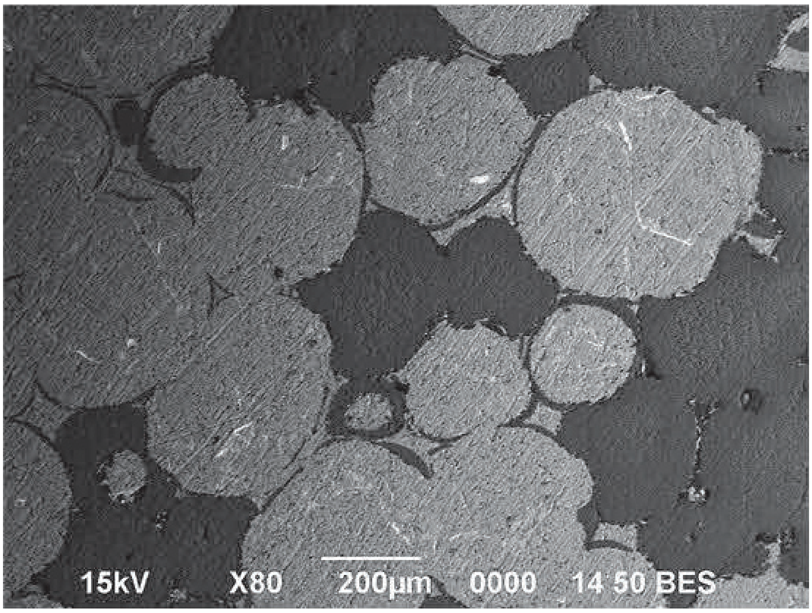

Fig. 3-1 micro structure of IPCs.

3.2.2 Thermal expansion measurement

A vertical direct dilatometer (LINSEIS DIL L75 VS) was used to determine the thermal expansion coefficient. The average dimension of the rectangular specimens for CTE testing was 6 mm × 6 mm × 6 mm. The samples were heated at a rate of 5 ℃/min to a temperature of 200 ℃ in a protected argon environment. The thermal expansion coefficient was calculated as follows:

$$\alpha = \frac{dL}{L_0 dT} \tag{3.1}$$

where L_0 is the original length of the specimen at room temperature, L is the actual length of specimen at T, and dL is the elongation at the temperature interval of dT.

3.3 Finite element analysis of composites

3.3.1 3D microstructure modelling of IPCs

To conduct the FE analysis, RVEs of A356/AlN IPCs with different preform porosity are generated. To model the complex IPCs structure more realistically and facilitate modeling, we constructed the model shown in Fig. 3-2. Initially, a porous aluminum nitride framework is established, followed by the creation of a filled aluminum alloy model using Boolean operations within Abaqus to guarantee the continuity of both phases in three dimensions. AlN forms a porous framework with spherical voids, within which aluminum alloy is distributed. Both phases interconnect continuously and become entangled. Preform porosity adjustment by changing framework dimensions.

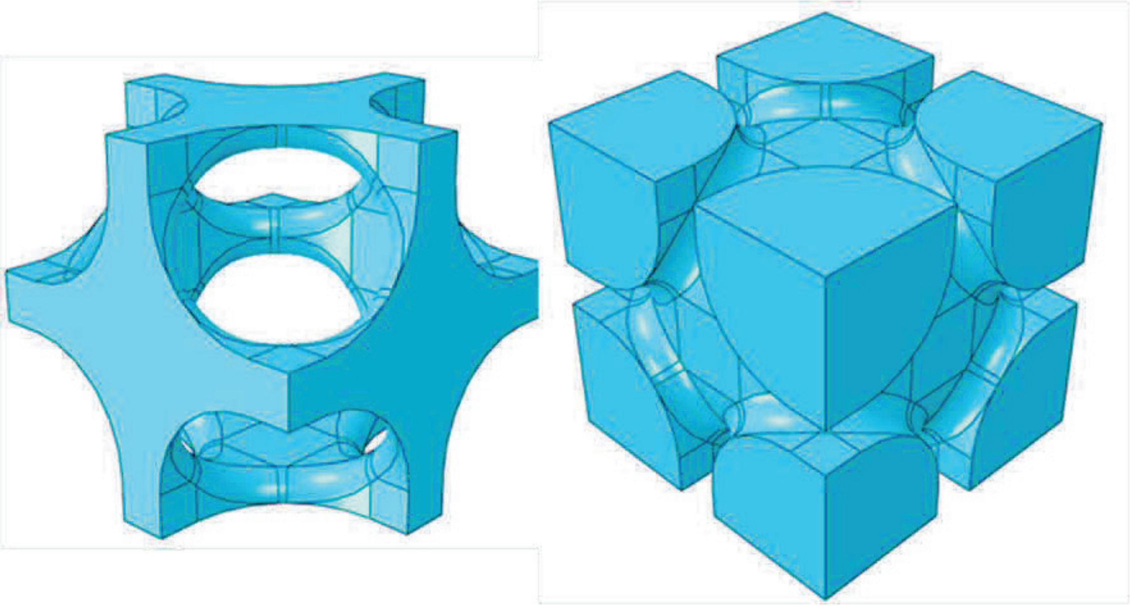

Fig. 3-2 FE model of IPCs.

3.3.2 Meshing and boundary conditions

The generated RVEs underwent meshing and was subsequently analyzed using the commercial software Abaqus. Because of the intricacy in constructing the RVEs, the two phases are meshed with modified 10-node tetrahedral elements (C3D10M). The RVEs are geometrically periodic, so periodic boundary conditions (PBC) are adopted in this study to ensure accuracy of thermal expansion behavior of IPCs. To calculate the coefficient of thermal expansion, we restrict the displacement of the three orthogonal boundary surfaces in the x, y, and z directions, allowing their opposing surfaces to expand freely. the RVEs without stresses were heated by 200°C (T) from 25 °C (T_r) and the corresponding strain (volumetric mean) was measured in x, y and z direction. The average strains were calculated (ε_{avg}) and the linear CTE (α) were computed:

$$\alpha = \frac{\varepsilon_{avg}}{\Delta T} \tag{3.2}$$

where $\Delta T = T - T_r$

The average strain is computed as:

$$\varepsilon_{avg} = \frac{\varepsilon_{xx} + \varepsilon_{yy} + \varepsilon_{zz}}{3} \tag{3.3}$$

Where ε_{xx}, ε_{yy}, ε_{zz} are the volumetric mean of linear strain components along x, y and z directions.

The calculation of the average volumetric linear strain in the x, y, and z axes is as follows (in terms of ε_{xx}):

$$\varepsilon_{xx} = \frac{\sum v_i \varepsilon_{xxi}}{\sum v_i} \tag{3.4}$$

The term v_i represents the volume of element ‘i’, while ε_{xxi} denotes the linear strain of element ‘i’ in the x direction.

3.4 Analytical models

3.4.1 Turner model

The Turner model makes the assumption that, under thermal action, only uniform static stresses are produced between adjacent regions in the heated composite material, while disregarding shear strains[17]. The Turner formula is expressed as follows:

$$\alpha_{\mathrm{C}}=\frac{\alpha_{\mathrm{p}}V_{\mathrm{p}}K_{\mathrm{p}}+\alpha_{\mathrm{m}}V_{\mathrm{m}}K_{\mathrm{m}}}{V_{\mathrm{p}}K_{\mathrm{p}}+V_{\mathrm{m}}K_{\mathrm{m}}} \tag{3.5}$$

where α is linear CTE and V is volume fraction. The subscripts m, c and p refer to the matrix, composite and preform, respectively. K is the bulk modulus.

3.4.2 Kerner model

The Kerner model assumes isotropy for both the matrix and reinforcement materials. It also posits that the reinforcement and matrix coexist in a spherically encapsulated state with a tightly integrated interface, where the matrix comprises the outer layer, and the reinforcement resides in the inner layer[16]. The Kerner model can be expressed as:

$$\alpha_{\mathrm{C}}=\alpha_{\mathrm{p}}V_{\mathrm{p}}+\alpha_{\mathrm{m}}V_{\mathrm{m}}+\left(\alpha_{\mathrm{p}}-\alpha_{\mathrm{m}}\right)V_{\mathrm{p}}V_{\mathrm{m}}\times\frac{K_{\mathrm{p}}-K_{\mathrm{m}}}{V_{\mathrm{p}}K_{\mathrm{p}}+V_{\mathrm{m}}K_{\mathrm{m}}+\frac{3}{4}K_{\mathrm{p}}K_{\mathrm{m}}G_{\mathrm{m}}} \tag{3.6}$$

where V is the volume fraction and the subscripts m, c and p refer to the matrix, composite and preform, respectively. K is the bulk modulus and G is the shear modulus of the constituents of composite.

3.4.3 Schapery model

Schapery developed models based on the Hashin-Shtrikman model to determine the upper and lower bounds of the effective CTE. These models for bounds are derived from the principle of elastic energy and are applicable to both anisotropic and isotropic composites, assuming isotropy of the constituent phases [29,38–40]. The Schapery bounds of the CTE take the following form:

$$\alpha_c^{\ u} = \frac{\alpha_m - \left(\alpha_m - \alpha_p\right) K_p \left(3K_m + 4G_m\right) V_p}{K_m \left(3K_p + 4G_m\right) + 4\left(K_p - K_m\right) G_m V_p} \tag{3.7}$$

$$\alpha_c^{\ l} = \frac{\alpha_p - \left(\alpha_p - \alpha_m\right) K_m \left(3K_p + 4G_p\right) V_m}{K_p \left(3K_m + 4G_p\right) + 4\left(K_m - K_p\right) G_p V_m} \tag{3.8}$$

where V is the volume fraction and the subscripts m, c and p refer to the matrix, composite and preform, respectively. The bulk modulus K and the shear modulus G can be calculated as follow:

$$K = \frac{E}{3\left(1-2\nu\right)} \tag{3.9}$$

$$G = \frac{E}{2\left(1+\nu\right)} \tag{3.10}$$

where E is the Young’s modulus and ν is the Poisson’s ratio of the constituents of composite.

The thermo-mechanical properties of the IPCs ingredients used for the calculation of the CTEs of the investigated materials by means of analytical thermo-elastic models and FE analysis are presented in Table 3-2.

Table 3-2 The temperature dependence of elastic moduli *E* (GPa), Poisson’s ratio *ν*, and α (10^{-6}/K) of Al matrix and AlN preform for the modelling[7,8].

T (°C)	A356			AlN		
	E	ν	α	E	ν	α
50	74.4	0.33	21.3	310	0.21	4.8
100	71.2	0.33	22.3	310	0.21	4.9
200	67.3	0.33	24	310	0.21	5.0

3.5 Results and discussion

3.5.1 Thermal expansion

Fig. 3-3 shows the CTE and relative elongation of the Al/AlN IPCs prepared from the AlN preform with different preform porosity. Examination of Fig. 3-3a reveals that thermal expansion increases with temperature across all samples, yet it gradually decreases with decreasing preform porosity. Fig. 3-3b shows temperature dependence of the IPCs' CTE with different preform porosity. Clearly, elevating the test temperature resulted in a corresponding increase in Coefficient of Thermal Expansion (CTE). As an illustration, consider the CTE variation in specimen 84 in response to temperature fluctuations. The CTE increases from 15.49 (10^{-6}/K) at 50°C to 19.08 (10^{-6}/K) at 200°C. As the preform porosity decreases, the CTE of IPCs also decreases. Moreover, the CTE for all IPCs are markedly lower than those observed in aluminum alloys[8]. The incorporation of an AlN preform was observed to reduce the coefficient of thermal expansion and improve the dimensional stability of the IPCs.

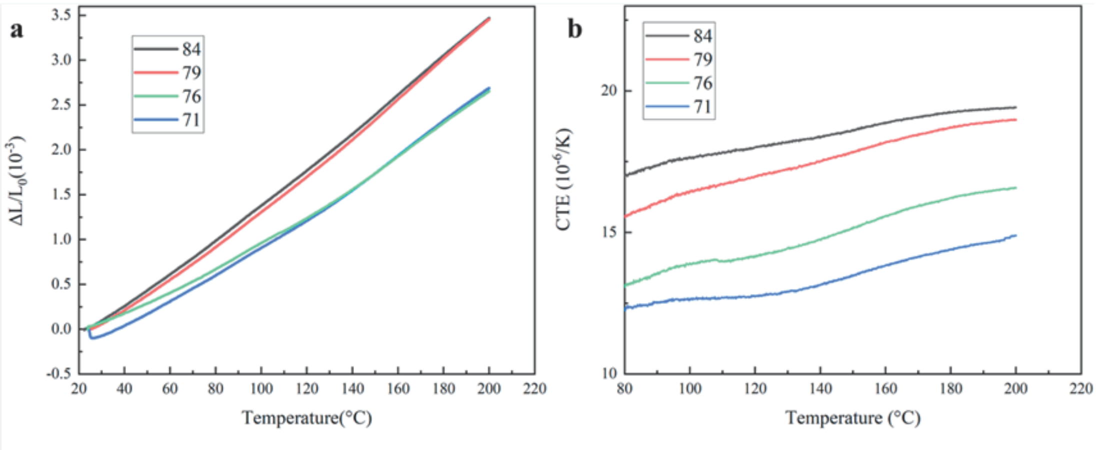

Fig. 3-3 Relative elongation and CTE of the Al/AlN IPCs with different preform porosity.

Fig. 3-4 contrasts experimental CTE data with data available in the literature[10,11,41–43]. The figure's trend reveals that the coefficient of thermal expansion in this study is lower than that in the literature for the same AlN content. This suggests that IPCs, with their special structure, can achieve lower coefficients of thermal expansion compared to conventional particle-reinforced composites. In IPCs, a special structure where both phases are continuous proves more effective in constraining the expansion of the aluminum matrix by the low CTE reinforcement phase, consequently achieving a lower overall CTE[44].

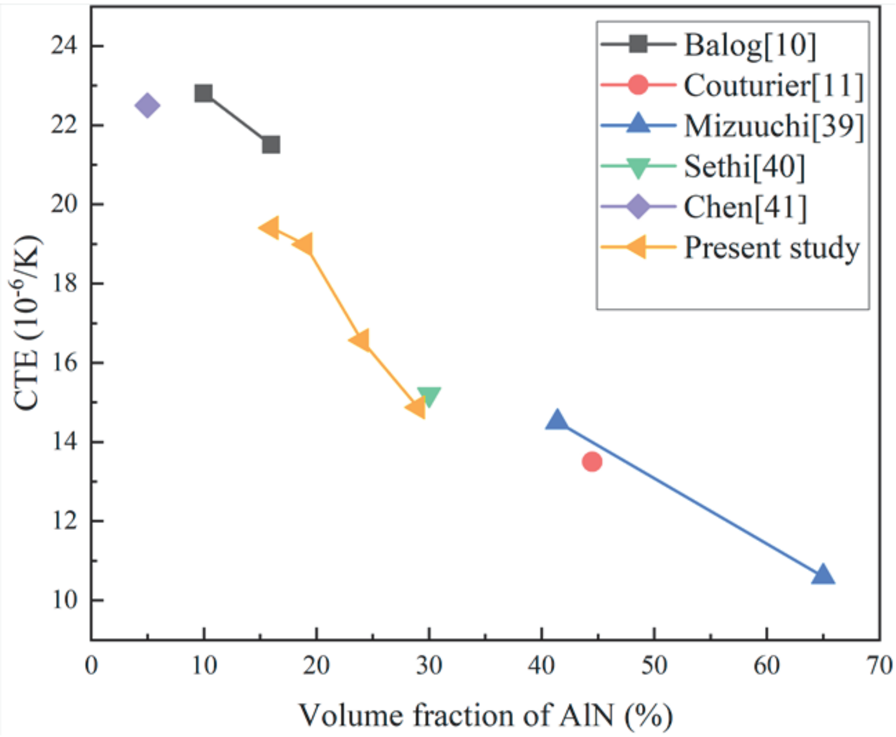

Fig. 3-4 Comparison of the CTE of IPCs in this study with CTE of other Al/AlN MMC[10,11,41–43].

3.5.2 Analytical models

Introducing theoretical models facilitates predicting a material's coefficient of thermal expansion, thereby streamlining the manufacturing process of materials customized to meet application-specific properties. Fig. 3-5 compares the theoretically predicted and the experimentally obtained CTEs for IPCs with different preform porosity. The experimental values for samples 84 and 79 mostly fall between the Schapery upper and lower bounds, whereas for samples 76 and 71, the experimental values are distributed around the Turner model. Residual thermal stresses, formed during sample preparation and processing, constrain the material's thermal expansion, leading to a reduction in the coefficient of thermal expansion[43,45]. Simultaneously, the decreased preform porosity enhances the capability of the porous AlN framework to restrict the expansion of the aluminum matrix. It also alters the ratio of the interfacial region, facilitating stress concentration and rendering the Al matrix more prone to plastic deformation, thereby lowering the CTE. Consequently, the experimental values of samples 71 and 76 exhibit proximity to the Turner model. The measured CTE shows steeper rise than that of analytical models. This is primarily attributed to the alleviation of residual stresses, as well as the decline in Young's modulus and yield strength during the heating process[5]. Concurrently, inaccuracies in the measurement device at low temperatures also have an effect[7]. Meanwhile, we observe a more rapid increase in the CTE for samples 84 and 79 between 50-100°C. This is primarily attributed to the higher proportion of AlN struts in samples 76 and 71, which effectively constrains sample expansion. Additionally, inaccuracies in instrumentation at lower temperatures contribute to this phenomenon.

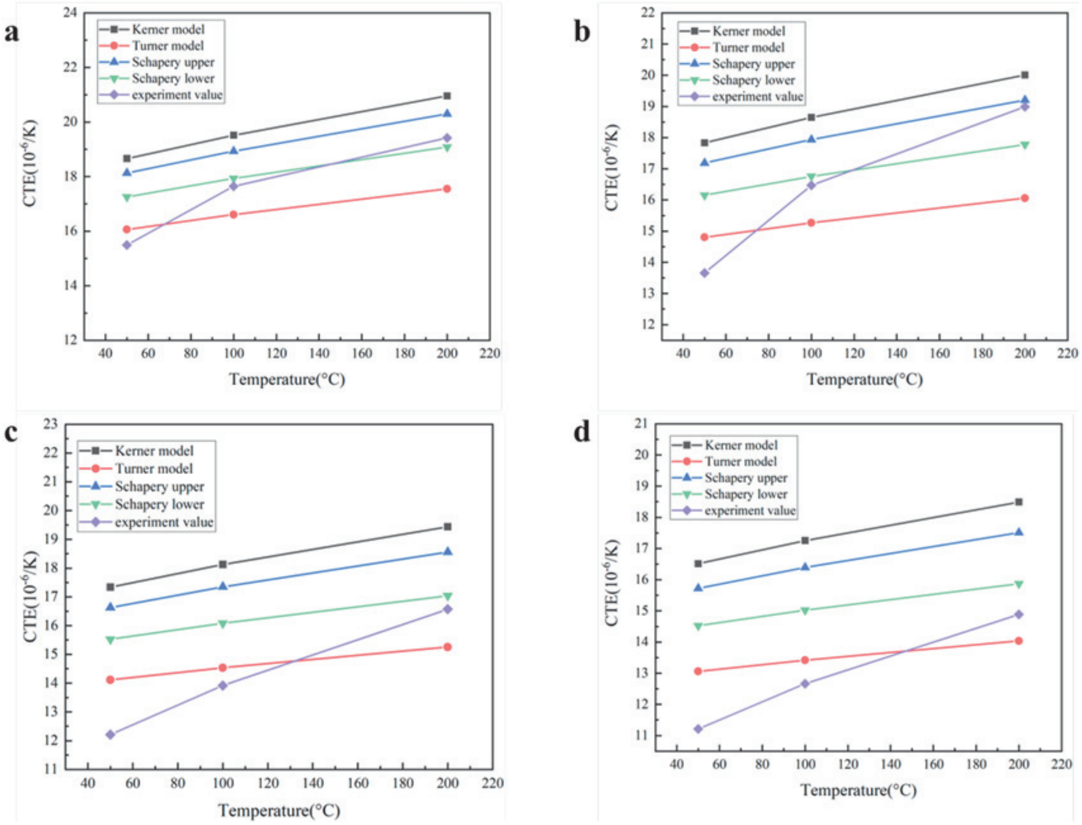

Fig. 3-5 Comparison of the calculated and measured coefficients of thermal expansion for different preform porosity: a. 84, b. 79, c. 76 and d.71.

3.5.3 Finite element analysis of 3D RVEs

3.5.3.1 Validity of the RVE model

To achieve objective and mesh-independent results when calculating the effective coefficient of thermal expansion (CTE) for IPCs through the finite element method, it is necessary to conduct a mesh sensitivity study. This study aims to identify the minimum mesh density required for various unit cells. Fig. 3-6 depicts the results of the mesh-independence verification of sample 84. The figure demonstrates that with an increasing number of elements, the coefficient of thermal expansion (CTE) gradually stabilizes, and surpassing 127,831 elements only marginally enhances accuracy (a minimal accuracy increase observed with a elements number twice as large). To conserve computational resources while maintaining calculation accuracy, a elements number of 127,831(seed size: 0.02) is chosen for subsequent analysis.

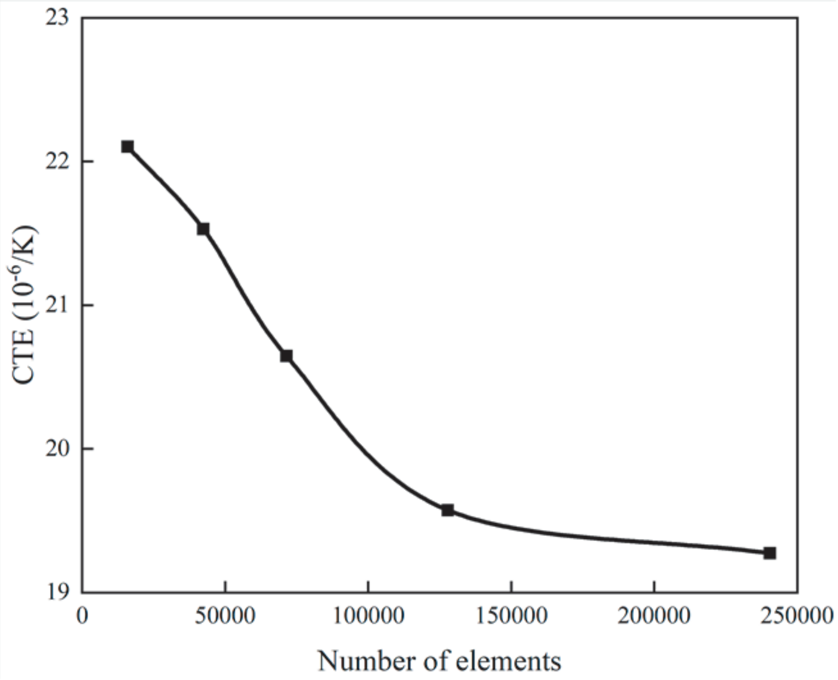

Fig. 3-6. Effect of mesh Seed size on effective CTEs of IPCs.

3.5.3.2 Simulated thermal stress

The thermal stress (S11) of IPCs with different preform porosity is shown in Fig. 3-7. Due to the isotropic nature of the material, stress distribution exhibits symmetry across all axes. Therefore, S11 is utilized for characterizing the stress distribution. The left images in this figure illustrate stresses within the Al matrix, while the right images depict stresses within the AlN preform. Heating-induced expansion generates significant thermal stress within the material. The distribution of thermal stresses within the composite material is highly intricate. The reinforcement phase of AlN primarily experiences tensile stresses, while the metal matrix undergoes predominantly compressive stresses. This can be attributed to the higher CTE of the Al matrix, causing it to rapidly expand upon heating and subjecting the reinforcement phase to tensile stresses. Furthermore, an examination of the stress contours in Fig. 3-7 reveals that as preform porosity decreases, IPCs become increasingly susceptible to thermal stress concentrations. The stress is most intense in the vicinity of the contact surface of the two phases due to the constraints between the reinforcement phase and the matrix. The decreased porosity of the preform may introduce additional interfaces, leading to heightened stress concentrations.

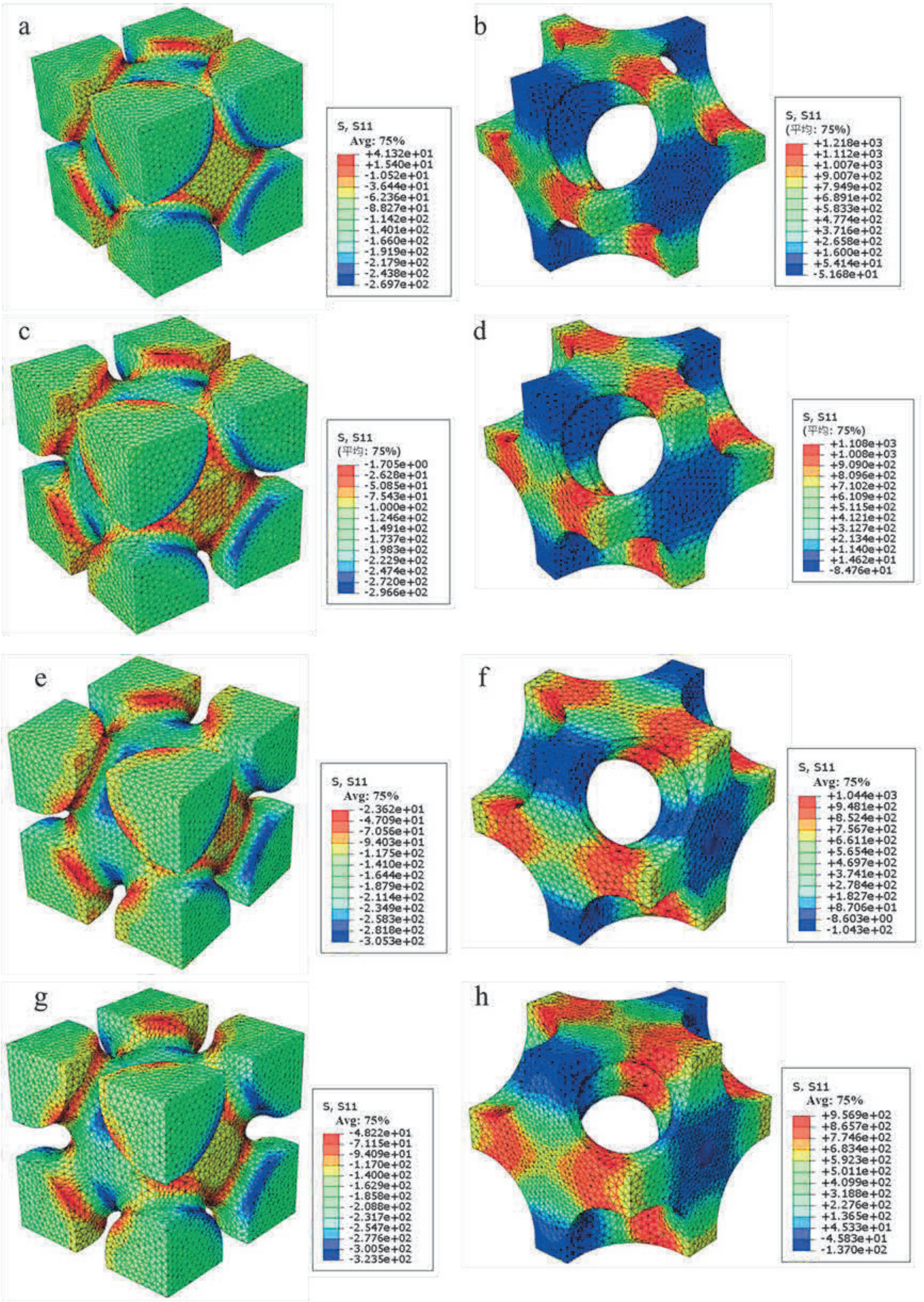

Fig. 3-7. Thermal stresses (S11, MPa) distribution in IPCs with different preform porosity: a. 84 matrix, b. 84 preform, c.79 matrix, d. 79 preform, e. 76 matrix, f. 76 preform, g. 71 matrix and h. 71preform.

Fig. 3-8 shows Probability distribution of thermal stresses in Al matrix and AlN preform for IPCs with different preform porosity. Observably, the aluminum matrix experiences predominantly compressive stress, exhibiting a unimodal stress distribution. As the preform porosity decreases, the peak shifts to the left, indicating increased stress. Conversely, AlN experiences a stress distribution characterized by multiple peaks, with these peaks predominantly located in both low-stress and high-stress regions.

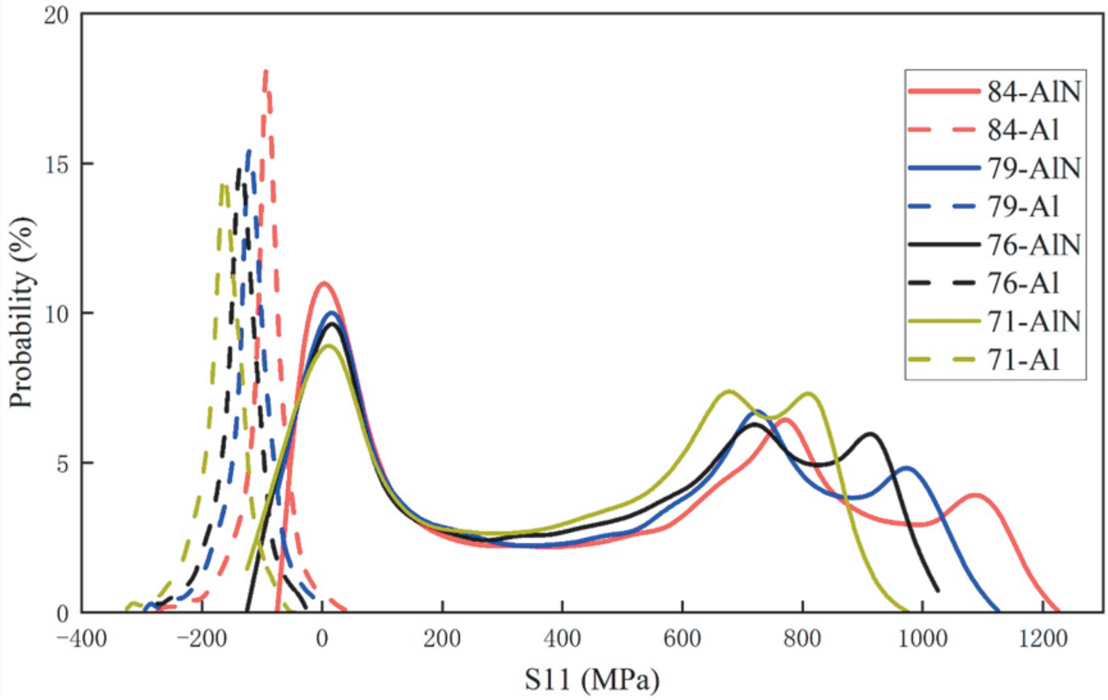

Fig. 3-8. Probability distribution of thermal stresses in Al matrix and AlN phase for IPCs with different preform porosity.

3.5.3.3 Simulated CTE

The results predicted by finite element method (FEM) and analytical models are presented in Fig. 3-9, and they are compared with the experimental values. The CTE calculated using the FEM rises as preform porosity increases. Given that only elastic deformation is considered, the CTE demonstrates a linear correlation with preform porosity. When preform porosity is high, the simulated and experimental values exhibit close agreement. However, a notable disparity arises between simulated and experimental values under low preform porosity conditions. This phenomenon arises from the material's inherent residual thermal stresses. The lower the preform porosity, the greater the generation of thermal stresses. While these residual thermal stresses contribute to a reduction in CTE[43,45], the simulation fails to consider this aspect. Simultaneously, during the actual thermal expansion process, the low preform porosity of the sample tends to induce stress concentration. This results in plastic deformation of the aluminum matrix, causing it to expand into some of the material's micro-pores and consequently reducing the CTE[46]. These factors contribute to the observed discrepancy between experimental and simulated values.

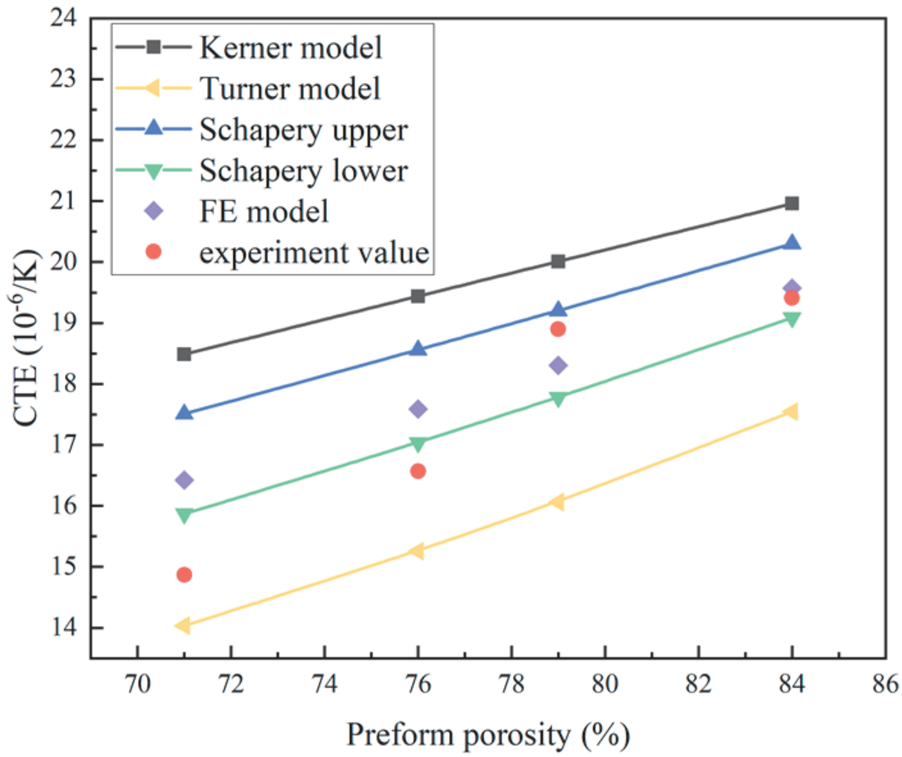

Fig. 3-9 Comparison of predicted CTEs of IPCs with different preform porosity using 3D FEM and analytical model with experimental value (200℃).

3.6 Summary

This study investigated the thermal expansion behavior of Al/AlN interpenetrating phase composites (IPCs) with different preform porosity. The thermal properties of these materials are thoroughly examined through experimental results, analytical modeling, and finite element analysis. After analysis and discussion, the main conclusions were obtained as follows:

(1) The coefficient of thermal expansion (CTE) of Al/AlN IPCs decreased with decreasing preform porosity. The incorporation of the AlN preform effectively reduced the CTE and improved dimensional stability compared to the aluminum alloy matrix.

(2) The CTEs of the Al/AlN IPCs were lower than those reported in the literature for conventional particle-reinforced Al/AlN composites with the same AlN content, attributed to the unique interpenetrating structure constraining the matrix expansion more effectively.

(3) Experimental values align with the analytical boundaries, affirming the accuracy of the analytical model's predictions.

(4) Finite element analysis of 3D RVEs validated the mesh independence and showcased the intricate distribution of thermal stresses within the IPCs. The FE model accurately predicts experimental results at high preform porosity levels. However, as preform porosity decreases, a significant disparity arises between calculated and actual values. This discrepancy is attributed to the FE simulation's omission of plastic deformation and residual thermal stresses.

3.7 References

[1] S.P. Rawal, Metal-matrix composites for space applications, JOM 53 (2001) 14–17. https://doi.org/10.1007/s11837-001-0139-z.

[2] D.K. Rajak, D.D. Pagar, R. Kumar, C.I. Pruncu, Recent progress of reinforcement materials: a comprehensive overview of composite materials, Journal of Materials Research and Technology 8 (2019) 6354–6374. https://doi.org/10.1016/j.jmrt.2019.09.068.

[3] W.H. Yu, S.L. Sing, C.K. Chua, C.N. Kuo, X.L. Tian, Particle-reinforced metal matrix nanocomposites fabricated by selective laser melting: A state of the art review, Progress in Materials Science 104 (2019) 330–379. https://doi.org/10.1016/j.pmatsci.2019.04.006.

[4] X.X. Zhang, B.L. Xiao, H. Andrä, Z.Y. Ma, Homogenization of the average thermo-elastoplastic properties of particle reinforced metal matrix composites: The minimum representative volume element size, Composite Structures 113 (2014) 459–468. https://doi.org/10.1016/j.compstruct.2014.03.048.

[5] T. Huber, H.P. Degischer, G. Lefranc, T. Schmitt, Thermal expansion studies on aluminium-matrix composites with different reinforcement architecture of SiC particles, Composites Science and Technology 66 (2006) 2206–2217. https://doi.org/10.1016/j.compscitech.2005.12.012.

[6] P. Gudlur, A. Forness, J. Lentz, M. Radovic, A. Muliana, Thermal and mechanical properties of Al/Al2O3 composites at elevated temperatures, Materials Science and Engineering: A 531 (2012) 18–27. https://doi.org/10.1016/j.msea.2011.10.001.

[7] M. Chmielewski, W. Weglewski, Comparison of experimental and modelling results of thermal properties in Cu-AlN composite materials, Bulletin of the Polish Academy of Sciences: Technical Sciences 61 (2013) 507–514. https://doi.org/10.2478/bpasts-2013-0050.

[8] T.H. Nam, G. Requena, P. Degischer, Thermal expansion behaviour of aluminum matrix composites with densely packed SiC particles, Composites Part A: Applied

Science and Manufacturing 39 (2008) 856–865. https://doi.org/10.1016/j.compositesa.2008.01.011.

[9] F. Boey, A.I.Y. Tok, Y.C. Lam, S.Y. Chew, On the effects of secondary phase on thermal conductivity of AlN ceramic substrates using a microstructural modeling approach, Materials Science and Engineering: A 335 (2002) 281–289. https://doi.org/10.1016/S0921-5093(01)01936-0.

[10] M. Balog, P. Krizik, J. Dvorak, O. Bajana, J. Krajcovic, M. Drienovsky, Industrially fabricated in-situ Al-AlN metal matrix composites (part B): The mechanical, creep, and thermal properties, Journal of Alloys and Compounds 909 (2022) 164720. https://doi.org/10.1016/j.jallcom.2022.164720.

[11] R. Couturier, D. Ducret, P. Merle, J.P. Disson, P. Joubert, Elaboration and characterization of a metal matrix composite: Al/AlN, Journal of the European Ceramic Society 17 (1997) 1861–1866. https://doi.org/10.1016/S0955-2219(97)87873-9.

[12] R. Arpón, J.M. Molina, R.A. Saravanan, C. García-Cordovilla, E. Louis, J. Narciso, Thermal expansion behaviour of aluminium/SiC composites with bimodal particle distributions, Acta Materialia 51 (2003) 3145–3156. https://doi.org/10.1016/S1359-6454(03)00126-5.

[13] K.-M. Shu, G.C. Tu, The microstructure and the thermal expansion characteristics of Cu/SiCp composites, Materials Science and Engineering: A 349 (2003) 236–247. https://doi.org/10.1016/S0921-5093(02)00788-8.

[14] J.K. Chen, I.S. Huang, Thermal properties of aluminum–graphite composites by powder metallurgy, Composites Part B: Engineering 44 (2013) 698–703. https://doi.org/10.1016/j.compositesb.2012.01.083.

[15] B. Guo, B. Chen, X. Zhang, X. Cen, X. Wang, M. Song, S. Ni, J. Yi, T. Shen, Y. Du, Exploring the size effects of Al4C3 on the mechanical properties and thermal behaviors of Al-based composites reinforced by SiC and carbon nanotubes, Carbon 135 (2018) 224–235. https://doi.org/10.1016/j.carbon.2018.04.048.

[16] E.H. Kerner, The Elastic and Thermo-elastic Properties of Composite Media, Proc.

Phys. Soc. B 69 (1956) 808–813. https://doi.org/10.1088/0370-1301/69/8/305.

[17]P.S. Turner, Thermal-expansion stresses in reinforced plastics, J. RES. NATL. BUR. STAN. 37 (1946) 239. https://doi.org/10.6028/jres.037.015.

[18]P. Kenesei, A. Borbély, H. Biermann, Microstructure based three-dimensional finite element modeling of particulate reinforced metal–matrix composites, Materials Science and Engineering: A 387–389 (2004) 852–856. https://doi.org/10.1016/j.msea.2004.02.076.

[19]Z.H. Karadeniz, D. Kumlutas, A numerical study on the coefficients of thermal expansion of fiber reinforced composite materials, Composite Structures 78 (2007) 1–10. https://doi.org/10.1016/j.compstruct.2005.11.034.

[20]Y. Hua, L. Gu, Prediction of the thermomechanical behavior of particle-reinforced metal matrix composites, Composites Part B: Engineering 45 (2013) 1464–1470. https://doi.org/10.1016/j.compositesb.2012.09.056.

[21]N.K. Sharma, R.K. Misra, S. Sharma, Thermal expansion behavior of Ni–Al2O3 composites with particulate and interpenetrating phase structures: An analysis using finite element method, Computational Materials Science 90 (2014) 130–136. https://doi.org/10.1016/j.commatsci.2014.04.008.

[22]N.K. Sharma, R.K. Mishra, S. Sharma, 3D micromechanical analysis of thermo-mechanical behavior of Al2O3/Al metal matrix composites, Computational Materials Science 115 (2016) 192–201. https://doi.org/10.1016/j.commatsci.2015.12.051.

[23]N.K. Sharma, R.K. Misra, S. Sharma, Experimental characterization and numerical modeling of thermo-mechanical properties of Al-B4C composites, Ceramics International 43 (2017) 513–522. https://doi.org/10.1016/j.ceramint.2016.09.187.

[24]M. Kouzeli, D.C. Dunand, Effect of reinforcement connectivity on the elasto-plastic behavior of aluminum composites containing sub-micron alumina particles, Acta Materialia 51 (2003) 6105–6121. https://doi.org/10.1016/S1359-6454(03)00431-2.

[25]G. Roudini, R. Tavangar, L. Weber, A. Mortensen, Influence of reinforcement

contiguity on the thermal expansion of alumina particle reinforced aluminium composites: Dedicated to Professor Dr. H.-P. Degischer on the occasion of his 65th birthday, International Journal of Materials Research 101 (2010) 1113–1120. https://doi.org/10.3139/146.110388.

[26] N. Kota, M.S. Charan, T. Laha, S. Roy, Review on development of metal/ceramic interpenetrating phase composites and critical analysis of their properties, Ceramics International 48 (2022) 1451–1483. https://doi.org/10.1016/j.ceramint.2021.09.232.

[27] Y. Chen, A. Wang, H. Fu, Z. Zhu, H. Zhang, Z. Hu, L. Wang, H. Cheng, Preparation, microstructure and deformation behavior of Zr-based metallic glass/porous SiC interpenetrating phase composites, Materials Science and Engineering: A 530 (2011) 15–20. https://doi.org/10.1016/j.msea.2011.08.063.

[28] X.-Q. Feng, Y.-W. Mai, Q.-H. Qin, A micromechanical model for interpenetrating multiphase composites, Computational Materials Science 28 (2003) 486–493. https://doi.org/10.1016/j.commatsci.2003.06.005.

[29] D.W. Abueidda, A.S. Dalaq, R.K. Abu Al-Rub, I. Jasiuk, Micromechanical finite element predictions of a reduced coefficient of thermal expansion for 3D periodic architectured interpenetrating phase composites, Composite Structures 133 (2015) 85–97. https://doi.org/10.1016/j.compstruct.2015.06.082.

[30] B. Wu, R. Chen, R. Fu, S. Agathopoulos, X. Su, H. Liu, Low thermal expansion coefficient and high thermal conductivity epoxy/Al2O3/T-ZnOw composites with dual-scale interpenetrating network structure, Composites Part A: Applied Science and Manufacturing 137 (2020) 105993. https://doi.org/10.1016/j.compositesa.2020.105993.

[31] S. Li, D. Xiong, M. Liu, S. Bai, X. Zhao, Thermophysical properties of SiC/Al composites with three dimensional interpenetrating network structure, Ceramics International 40 (2014) 7539–7544. https://doi.org/10.1016/j.ceramint.2013.12.105.

[32] Y. Jin, B. Zhang, Q. Liu, Z. Zhong, H. Zhang, F. Ye, Z. Zhang, Fabrication of co-continuous SiC/Al composites from novel SiC preforms with high porosity and controllable pore size, Ceramics International 47 (2021) 2766–2771.

https://doi.org/10.1016/j.ceramint.2020.09.130.

[33] L. Zhao, M. Zhao, H. Yan, X. Cao, J. Zhang, Mechanical behavior of SiC foam-SiC particles/Al hybrid composites, Transactions of Nonferrous Metals Society of China 19 (2009) s547–s551. https://doi.org/10.1016/S1003-6326(10)60106-9.

[34] S. Roy, K.G. Schell, E.C. Bucharsky, K.A. Weidenmann, A. Wanner, M.J. Hoffmann, Processing and characterization of elastic and thermal expansion behaviour of interpenetrating Al12Si/alumina composites, Materials Science and Engineering: A 743 (2019) 339–348. https://doi.org/10.1016/j.msea.2018.11.100.

[35] F. Scherm, R. Völkl, A. Neubrand, F. Bosbach, U. Glatzel, Mechanical characterisation of interpenetrating network metal–ceramic composites, Materials Science and Engineering: A 527 (2010) 1260–1265. https://doi.org/10.1016/j.msea.2009.09.063.

[36] R.-F. Guo, Y. Wang, P. Shen, A. Shaga, Y.-H. Ma, Q.-C. Jiang, Influence of matrix property and interfacial reaction on the mechanical performance and fracture mechanism of TiC reinforced Al matrix lamellar composites, Materials Science and Engineering: A 775 (2020) 138956. https://doi.org/10.1016/j.msea.2020.138956.

[37] X. Yan, K. Sugio, Y. Choi, T. Wang, Z. Xv, C. Zhao, G. Sasaki, Microstructure and mechanical properties of Al/AlN interpenetrating phase composites with different preform porosity, Materials Chemistry and Physics 315 (2024) 129029. https://doi.org/10.1016/j.matchemphys.2024.129029.

[38] Z. Hashin, S. Shtrikman, A variational approach to the theory of the elastic behaviour of multiphase materials, Journal of the Mechanics and Physics of Solids 11 (1963) 127–140. https://doi.org/10.1016/0022-5096(63)90060-7.

[39] Z. Hashin, S. Shtrikman, A variational approach to the theory of the elastic behaviour of polycrystals, Journal of the Mechanics and Physics of Solids 10 (1962) 343–352. https://doi.org/10.1016/0022-5096(62)90005-4.

[40] R.A. Schapery, Thermal Expansion Coefficients of Composite Materials Based on Energy Principles, Journal of Composite Materials 2 (1968) 380–404.

https://doi.org/10.1177/002199836800200308.

[41] K. Mizuuchi, K. Inoue, Y. Agari, T. Nagaoka, M. Sugioka, M. Tanaka, T. Takeuchi, J. Tani, M. Kawahara, Y. Makino, M. Ito, Processing and thermal properties of Al/AlN composites in continuous solid–liquid co-existent state by spark plasma sintering, Composites Part B: Engineering 43 (2012) 1557–1563. https://doi.org/10.1016/j.compositesb.2011.06.017.

[42] J. Sethi, S. Jena, S. Das, K. Das, Synthesis and properties of Al-AlN-CuCNT and Al-Y2W3O12-CuCNT hybrid composites, Materials Science and Engineering: A 810 (2021) 140919. https://doi.org/10.1016/j.msea.2021.140919.

[43] J. Chen, C.-G. Bao, Z.-W. Liu, B.-S. Sun, Y.-C. Shu, Q.-K. Li, Thermal Properties of Mg–Al/AlN Composites Fabricated by Powder Metallurgy, Acta Metall. Sin. (Engl. Lett.) 31 (2018) 641–649. https://doi.org/10.1007/s40195-017-0689-x.

[44] X.D. Liu, J.S. Zhang, X.M. Cao, H. Zhang, Finite element simulation of the thermal properties of particulate and continuous network-reinforced metal-matrix composites, Proceedings of the Institution of Mechanical Engineers, Part B: Journal of Engineering Manufacture 219 (2005) 111–121. https://doi.org/10.1243/095440505X8055.

[45] W.A. Uju, I.N.A. Oguocha, A study of thermal expansion of Al–Mg alloy composites containing fly ash, Materials & Design 33 (2012) 503–509. https://doi.org/10.1016/j.matdes.2011.04.056.

[46] D.K. Balch, A. Mortensen, S. Suresh, Y.-L. Shen, T.J. Fitzgerald, V.J. Michaud, Thermal expansion of metals reinforced with ceramic particles and microcellular foams, MMTA 27 (1996) 3700–3717. https://doi.org/10.1007/BF02595462.

Chapter4

Thermal conductivity of Al/AlN interpenetrating phase composites with different preform porosity

4.1 Introduction

Aluminium matrix composites, a crucial component of metal matrix composites, find extensive applications in automotive components, electronic device, aircraft structural components and various other manufacturing industries. This is attributed to the lightweight nature, high strength to density ratio, and excellent thermal conductivity inherent in the Al matrix[1–5]. Nevertheless, the relatively low hardness, wear resistance, and high coefficient of thermal expansion of Al restrict its utilization in certain specific working conditions. To address the limitations of aluminium, researchers typically opt for ceramic phases characterized by high hardness and excellent thermal dimensional stability to serve as the reinforcing phase in Al matrix composites. Aluminium nitride offers a range of benefits, including a low thermal expansion coefficient, wear resistance, good stiffness, and it is compatible and adheres well with aluminium alloys, without reacting with them. Therefore, AlN is often used as a reinforcement for aluminium matrix composites[6–10].

Researchers have recently paid extensive attention to a new type of composite materials with a special microstructure: interpenetrating phase composites (IPCs). The material typically comprises two phases, which continuously extend in three dimensions and interpenetrate to create a network structure. Within this framework, the removal of one phase allows the remaining portion to retain the ability to form an open-cell pore structure capable of withstanding external loads. The structure confers good strength and toughness to IPCs, along with outstanding wear resistance and other favourable mechanical properties. The advent of IPCs has provided new options for research in materials science, providing novel pathways for creation of customized characteristics for advanced materials. In addition to revealing the underlying principles governing IPC behaviour, research in this field attempts to fully use IPCs for a variety of applications[11–15].

In terms of thermal conduction, for IPCs, the metal matrix phase and porous ceramic preform form a continuous structure, promoting the creation of efficient thermal conduction pathways—namely, phonons in the ceramic phase and electrons in the metal phase. Simultaneously, IPCs exhibit fewer interfaces compared to particle-reinforced composites, minimizing the hindrance to phonons and electrons. Current research primarily concentrates on the thermal properties of Al/SiC IPCs[16–20], while investigation into the thermal characteristics of Al/AlN IPCs requires further development.

In present research, the thermal conductivity of the Al/AlN IPCs with different preform porosity were measured from 20℃ to 200℃. The experiment data was compared with analytical models.

4.2 Materials and methods

The interpenetrating phase composites comprises A356 Al alloy (AlSi7Mg) and porous AlN preforms. Porous AlN preform with varying porosities was prepared using the slurry impregnation method. The low-pressure casting method was applied to fabricate the IPCs. The microstructure of 84 sample is displayed in Fig. 4-1. Relative density and preform porosity of the IPCs are show in Table 4-1.

Table 4-1. Relative density and preform porosity of IPCs.

Sample	Preform porosity (%)	Relative density (%)
84	79	87
79	84	89

Fig. 4-1 Microstructure of the IPCs

Thermal conductivity is a property indicating a substance's capacity to conduct heat, quantified as the heat transferred through a unit of cross-sectional area per unit time under a unit temperature gradient. The thermal conductivity of the Al/AlN IPCs, prepared experimentally, was determined using a hyper flash thermal analysis (NETZSCH LFA467, Germany) to measure their thermal diffusion coefficient at evaluated temperature (20°C to 200°C) via the laser flash method. It was then calculated based on the conversion relationship formula between thermal conductivity and thermal diffusion coefficient:

$$\lambda = \alpha \times C_p \times \rho \tag{4.1}$$

Here, λ represents the thermal conductivity of the composite material; α denotes its thermal diffusion coefficient, which reflects the material's thermal diffusivity or heat exchange rate, measured in mm²/s; C_p stands for the specific heat capacity of the composite material, indicating the amount of energy required to raise the sample's mass by one degree Celsius (1 °C), measured in J/g°C. ρ represents the actual density of the composite material. In this case, the specific heat capacity of the composite material is ideally computed following the law of mixing of composites, which can be expressed as follows:

$$C_p = \frac{\sum V_i \rho_i \left(C_p\right)_i}{\rho} \tag{4.2}$$

where V_i and ρ_i are the theoretical density and corresponding volume fraction of phase i, respectively, and ρ is the actual density of the sample at room temperature. $(C_p)_i$ is the specific heat capacity of phase i of the composite at different temperatures.

4.3 Results and discussion

4.3.1 Measured thermal conductivity

The temperature dependence of the TC of IPCs with different preform porosity are presented in Fig. 4-2. The thermal conductivity of IPCs rises as preform porosity increases. Increasing preform porosity enhances the presence of Al matrix phases with superior heat transfer properties, consequently raising the TC of IPCs. Simultaneously, the heightened porosity creates more efficient pathways for the heat transfer of matrix, further contributing to the enhancement of TC. Furthermore, the thermal conductivity of both samples exhibited a modest decline as the temperature rose. This phenomenon may result from material inherently has inverse temperature-dependent crystalline properties, leading to increased phonon scattering[21]. Additionally, the low relative density of the IPCs and a high number of internal pores could contribute; as temperature rises, the expansion of pores might further decrease the TC.

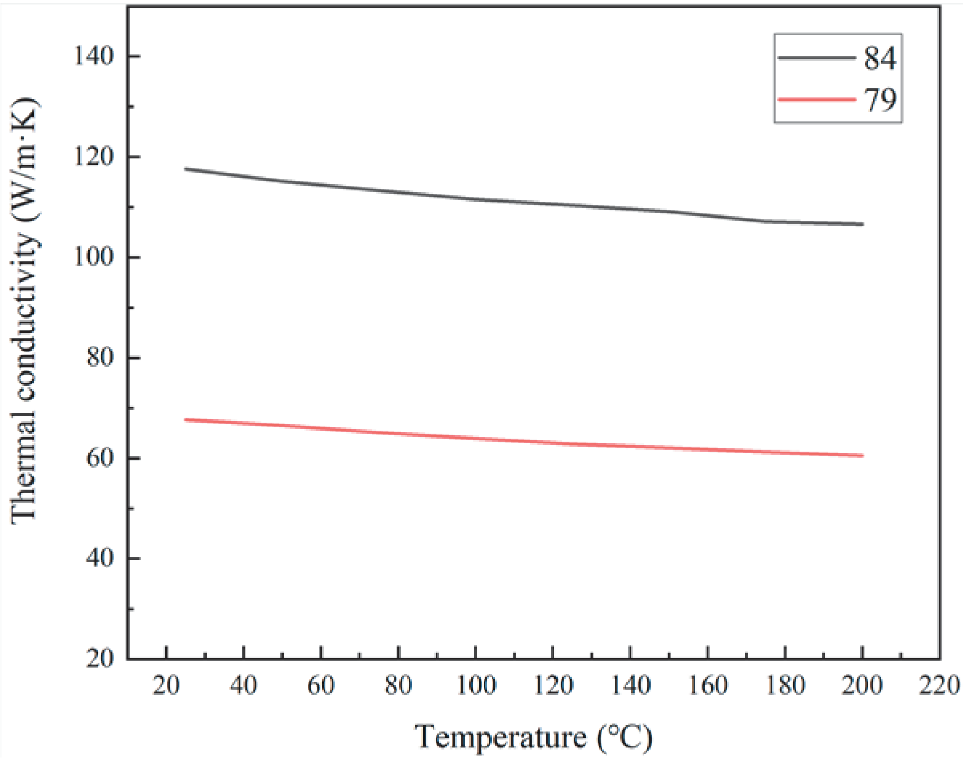

Fig. 4-2 The temperature dependence of the TC of IPCs with different preform porosity.

4.3.2 Analytical models

This paper employs various theoretical models to forecast the TC of IPCs. The Reuss model is a simple and commonly used model. It can be expressed as [6]:

$$\lambda_c = \frac{\lambda_m \lambda_p}{\lambda_m V_p + \lambda_p V_m} \tag{4.3}$$

The TC (λ) of the A356 matrix (subscript m) and the porous AlN preform (subscript p) are represented by λ_m and λ_p, respectively. V_s and V_p denote the volume fractions of each phase. The TC of the IPCs is denoted by λ_c.

The Maxwell model is founded on the theory of homogeneity. When the reinforcement is uniformly dispersed within the matrix material, the model facilitates the computation of the TC for isotropic composites. The Maxwell model equation can be expressed as follows [7]:

$$\lambda_c = \frac{2V_p(\lambda_p - \lambda_m) + \lambda_P + 2\lambda_m}{\lambda_p + 2\lambda_m - 2V_p(\lambda_p - \lambda_m)} \lambda_m \tag{4.4}$$

The Bruggeman model explains that when the volume proportion of ceramic particles in the composites increases, it reduces the spacing between reinforcing phase, resulting in stronger interactions among particles. The equation can be expressed as [8]:

$$(1 - V_p)^3 = \frac{\lambda_m}{\lambda_c} \left(\frac{\lambda_p - \lambda_c}{\lambda_p - \lambda_m}\right)^3 \tag{4.5}$$

Fig. 4-3 illustrates a comparison between the thermal conductivity fitting calculation and experimental value using the analytical model mentioned above. The theoretical model yields results surpassing the measured data. The TC of Sample 84 closely approximates the theoretical value, whereas that of Sample 79 is much lower. Changes in relative density, material structure, grain size, and other factors can be the cause. The intricate interplay among these factors significantly heightens the challenge of forecasting sample TC using these theoretical models. To enhance analytical model prediction, we will now consider the impact of pores.

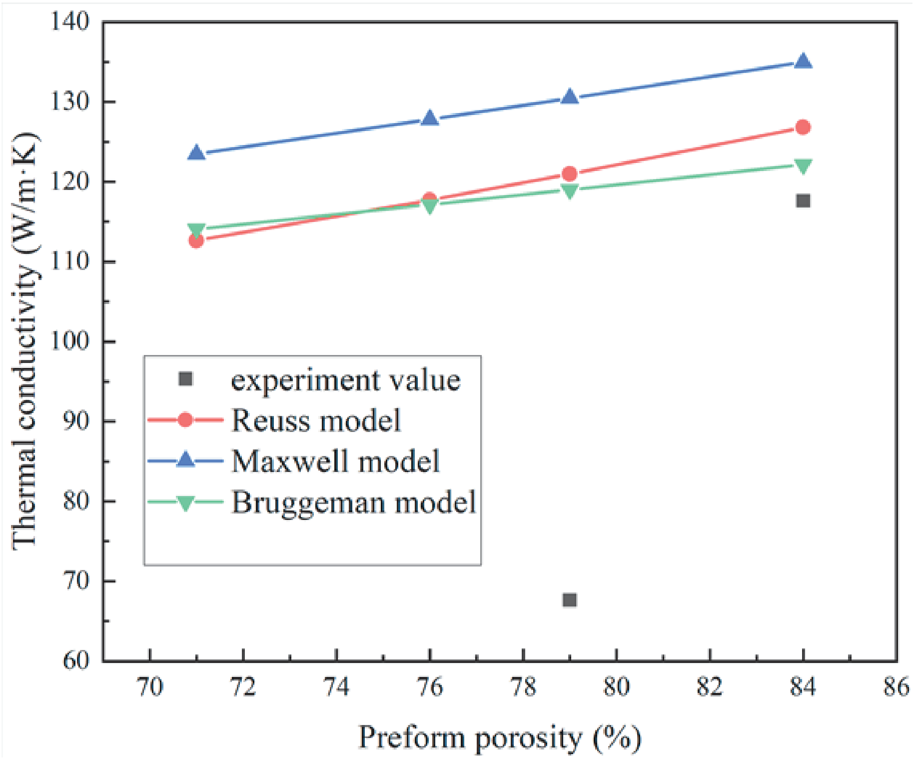

Fig. 4-3 Comparative analysis of the experimental and theoretical TC of IPCs with varying preform porosity.

Taking porosity into account, the TC of the A356 matrix is adjusted through the application of the following model[23]:

$$\lambda_{eff}=\frac{1}{4}\left[\lambda_m\left(3V_m-1\right)+\lambda_{pore}\left(3V_{pore}-1\right)+\left(\left[\lambda_m\left(3V_m-1\right)+\lambda_{pore}\left(3V_{pore}-1\right)\right]^2+8\lambda_{pore}\lambda_m\right)^{1/2}\right]$$

(4.6)

λ_{eff} is the effective TC of the A356 matrix, λ_{pore} and V_{pore} representing the TC and volume fractions of the pores, respectively.

The corrected result is depicted in Fig. 4-4. The TC of sample 84 is marginally higher than the theoretical value, whereas for sample 79, the disparity with the theoretical value remains substantial. This implies that predicting thermal conductivity is challenging due to numerous intricate factors beyond porosity influencing the material's thermal conductivity. While pores do influence the heat transfer of IPCs, focusing solely on them is insufficient for a comprehensive understanding and precise prediction of its thermal behaviour.

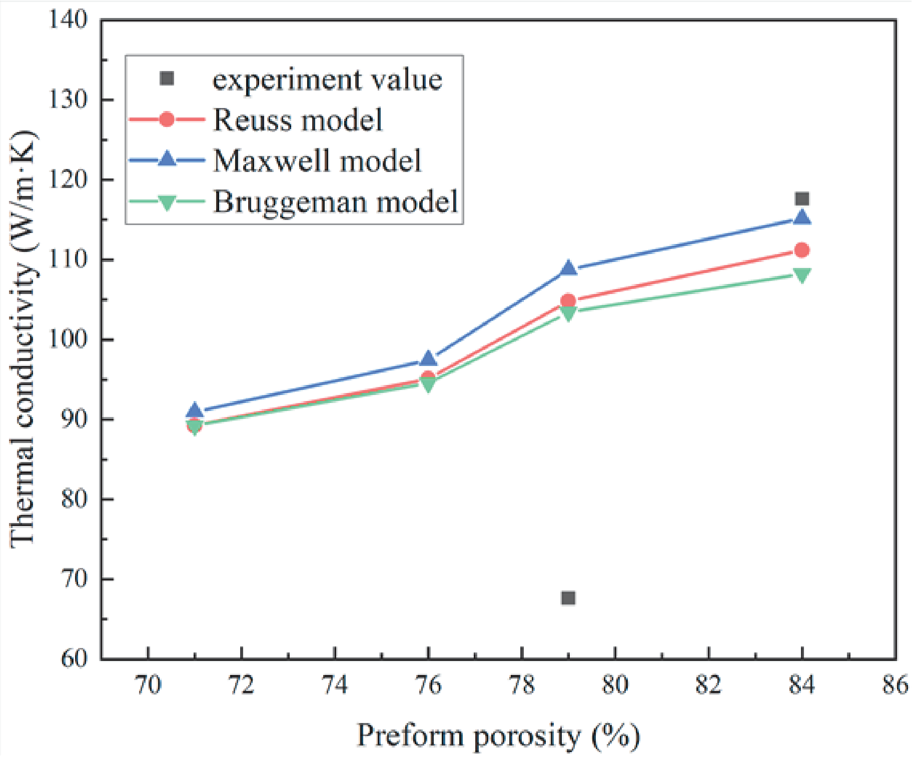

Fig. 4-4 Comparative analysis of the experimental and corrected theoretical TC of IPCs with varying preform porosity.

Metals and ceramics in solid materials exhibit distinct thermal conductivity mechanisms based on their properties, specifically electron and phonon conductivity mechanisms. Metals conduct heat via the movement of numerous free electrons within them. Due to their light mass and high speed, electrons facilitate rapid heat transfer, resulting in metals typically possessing high thermal conductivity. Ceramics possess minimal free electrons or are too bound to function as heat carriers, thus predominantly transferring heat through lattice waves generated by lattice vibrations. In metal-ceramic composites, both electrons in the metal and phonons in the ceramic contribute to heat conduction, while the interface between the metal and ceramic induces scattering effects on electron and phonon movement, consequently impeding heat conduction, a phenomenon referred to as interfacial thermal resistance. Consequently, during heat conduction, a temperature gradient forms at the interface, where temperature changes linearly within the material on both sides, while a sharp drop occurs at the interface of the material on both sides. For a more precise prediction of the thermal conductivity of IPCs using theoretical models, it's essential to account for interfacial thermal resistance. Thus, replacing the thermal conductivity of AlN with the effective thermal conductivity (λ_p^{eff}), which incorporates interfacial thermal resistance, is required. The effective thermal conductivity (λ_p^{eff}) can be determined by the following equation[16]:

$$\lambda_p^{eff} = \frac{\lambda_p}{\frac{2\lambda_p}{h \bullet d} + 1} \tag{4.7}$$

where d is the diameter of the AlN grains in the preform, λ_p is the TC of the corresponding AlN grains in the preform, h is the interfacial thermal conductance (i.e. the reciprocal of the interfacial thermal resistance). The parameter h can be calculated using the acoustic mismatch model (AMM) [25]. This model employs continuum mechanics to address interfacial heat transfer by computing the likelihood of phonon transmission across the interface[26]:

$$h \cong \frac{1}{2}\rho_m c_m \frac{v_m^3}{v_p^2} \frac{\rho_m v_m \rho_m v_m}{\left(\rho_m v_m + \rho_m v_m\right)^2} \tag{4.8}$$

where ν, ρ, c are the phonon velocity, density and specific heat capacity, respectively. The h of the AlN /Al can be calculated by (4.8).

Fig. 4-5 illustrates a comparison between the calculated value of the theoretical model and experimental values, factoring in interfacial thermal resistance and porosity. The difference between theoretical model results and experimental thermal conductivity values of 79 samples decreases when accounting for interfacial thermal resistance. Experimental values fall within the range defined by the Maxwell and Bruggeman models. Theoretical predictions better align with experimental values for these samples. However, for sample 84, the disparity between experimental and theoretical values widens, with experimental values surpassing those predicted by the theoretical model. This difference may stem from the lower porosity of sample 79's precast body, resulting in increased interface between phases and smaller pore sizes. Consequently, the cross-sectional area of the thermal channel within the aluminum substrate, with superior thermal conductivity, diminishes, making it more susceptible to interface effects. Conversely, sample 84's precast body exhibits higher porosity, reduced interface, and larger pore sizes, leading to a larger cross-sectional area for the aluminum substrate's thermal channel, thus minimizing interface impact.

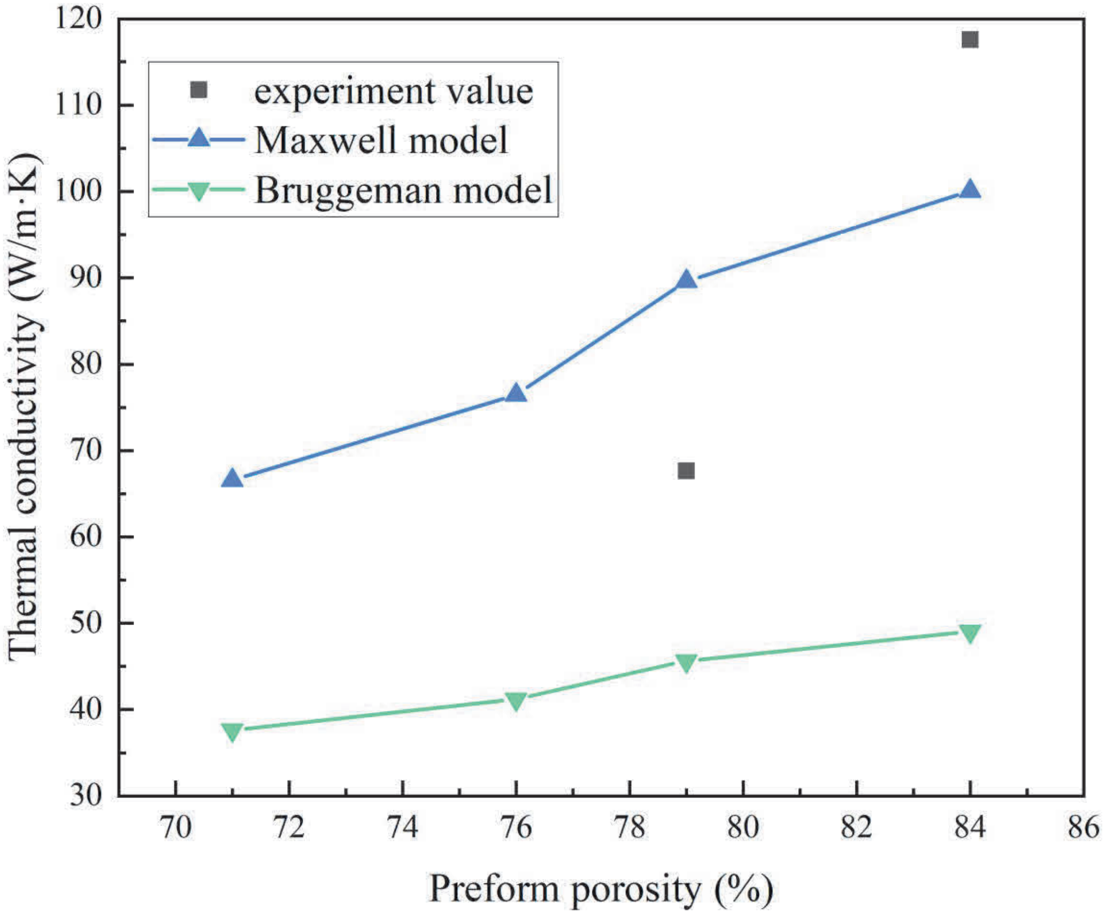

Fig. 4-5 Comparative analysis of the experimental and calculated values of the theoretical model, incorporating interfacial thermal resistance and porosity.

4.4 Summary

This study investigated the thermal conductivity of Al/AlN interpenetrating phase composites (IPCs) with varying preform porosity. The key findings are:

(1) The thermal conductivity of the IPCs increases with higher preform porosity, as the increased porosity enhances the presence of the higher thermal conductivity Al matrix phase and creates more efficient heat transfer pathways.

(2) The thermal conductivity of the IPCs exhibits a slight inverse temperature dependence, likely due to increased phonon scattering at higher temperatures and the expansion of internal pores.

(3) Theoretical models like the Reuss, Maxwell, and Bruggeman models were used to predict the thermal conductivity of the IPCs. The models were able to closely match the experimental results for the IPCs with higher preform porosity, but underestimated the thermal conductivity for the lower porosity samples.

(4) Accounting for interfacial thermal resistance and porosity effects improved the agreement between the theoretical predictions and experimental data, particularly for the lower porosity samples. However, differences remained, indicating the need for further investigation into the complex microstructural factors influencing the thermal behavior of these IPCs.

4.5 References

[1] R. Guan, Y. Wang, S. Zheng, N. Su, Z. Ji, Z. Liu, Y. An, B. Chen, Fabrication of aluminum matrix composites reinforced with Ni-coated graphene nanosheets, Materials Science and Engineering: A 754 (2019) 437–446. https://doi.org/10.1016/j.msea.2019.03.068.

[2] J. Zhu, W. Jiang, G. Li, F. Guan, Y. Yu, Z. Fan, Microstructure and mechanical properties of SiCnp/Al6082 aluminum matrix composites prepared by squeeze casting combined with stir casting, Journal of Materials Processing Technology 283 (2020) 116699. https://doi.org/10.1016/j.jmatprotec.2020.116699.

[3] P. Garg, A. Jamwal, D. Kumar, K.K. Sadasivuni, C.M. Hussain, P. Gupta, Advance research progresses in aluminium matrix composites: manufacturing & applications, Journal of Materials Research and Technology 8 (2019) 4924–4939. https://doi.org/10.1016/j.jmrt.2019.06.028.

[4] B. Jiang, L. Zhenglong, C. Xi, L. Peng, L. Nannan, C. Yanbin, Microstructure and mechanical properties of TiB2-reinforced 7075 aluminum matrix composites fabricated by laser melting deposition, Ceramics International 45 (2019) 5680–5692. https://doi.org/10.1016/j.ceramint.2018.12.033.

[5] R. Manikandan, T.V. Arjunan, A.R. Nath O. P, Studies on micro structural characteristics, mechanical and tribological behaviours of boron carbide and cow dung ash reinforced aluminium (Al 7075) hybrid metal matrix composite, Composites Part B: Engineering 183 (2020) 107668. https://doi.org/10.1016/j.compositesb.2019.107668.

[6] M. Balog, P. Krizik, P. Svec, L. Orovcik, Industrially fabricated in-situ Al-AlN metal matrix composites (part A): Processing, thermal stability, and microstructure, Journal of Alloys and Compounds 883 (2021) 160858. https://doi.org/10.1016/j.jallcom.2021.160858.

[7] A. Riquelme, P. Rodrigo, M.D. Escalera-Rodriguez, J. Rams, Effect of the process parameters in the additive manufacturing of in situ Al/AlN samples, Journal of

Manufacturing Processes 46 (2019) 271–278. https://doi.org/10.1016/j.jmapro.2019.09.011.

[8] J. Sethi, S. Das, K. Das, Study on thermal and mechanical properties of yttrium tungstate-aluminium nitride reinforced aluminium matrix hybrid composites, Journal of Alloys and Compounds 774 (2019) 848–855. https://doi.org/10.1016/j.jallcom.2018.10.017.

[9] M. Balog, P. Krizik, J. Dvorak, O. Bajana, J. Krajcovic, M. Drienovsky, Industrially fabricated in-situ Al-AlN metal matrix composites (part B): The mechanical, creep, and thermal properties, Journal of Alloys and Compounds 909 (2022) 164720. https://doi.org/10.1016/j.jallcom.2022.164720.

[10] V. Mohanavel, M. Ravichandran, Experimental investigation on mechanical properties of AA7075-AlN composites, Materials Testing 61 (2019) 554–558. https://doi.org/10.3139/120.111354.

[11] N. Kota, M.S. Charan, T. Laha, S. Roy, Review on development of metal/ceramic interpenetrating phase composites and critical analysis of their properties, Ceramics International 48 (2022) 1451–1483. https://doi.org/10.1016/j.ceramint.2021.09.232.

[12] M. Basista, J. Jakubowska, W. Węglewski, Processing Induced Flaws in Aluminum-Alumina Interpenetrating Phase Composites, Adv. Eng. Mater. 19 (2017) 1700484. https://doi.org/10.1002/adem.201700484.

[13] J. Bauer, M. Sala-Casanovas, M. Amiri, L. Valdevit, Nanoarchitected metal/ceramic interpenetrating phase composites, Science Advances 8 (2022) eabo3080. https://doi.org/10.1126/sciadv.abo3080.

[14] Y. Zhang, M.-T. Hsieh, L. Valdevit, Mechanical performance of 3D printed interpenetrating phase composites with spinodal topologies, Composite Structures 263 (2021) 113693. https://doi.org/10.1016/j.compstruct.2021.113693.

[15] M. Zhang, N. Zhao, Q. Yu, Z. Liu, R. Qu, J. Zhang, S. Li, D. Ren, F. Berto, Z. Zhang, R.O. Ritchie, On the damage tolerance of 3-D printed Mg-Ti interpenetrating-phase composites with bioinspired architectures, Nat Commun 13 (2022) 3247.

https://doi.org/10.1038/s41467-022-30873-9.

[16]Z. Zhang, Z. Shi, B. Yang, B. Ge, X. Zhang, Y. Guo, Preparation and anisotropic thermophysical properties of SiC honeycomb/Al-Mg-Si composite via spontaneous infiltration, Progress in Natural Science: Materials International 29 (2019) 177–183. https://doi.org/10.1016/j.pnsc.2019.02.004.

[17]D. Wang, Z. Zheng, J. Lv, G. Xu, S. Zhou, W. Tang, Y. Wu, Enhanced thermal conductive 3D-SiC/Al-Si-Mg interpenetrating composites fabricated by pressureless infiltration, Ceramics International 43 (2017) 1755–1761. https://doi.org/10.1016/j.ceramint.2016.10.104.

[18]J. Xie, J. Ma, M. Liao, W. Guo, L. Huang, P. Gao, H. Xiao, Reinforcement of thermally-conductive SiC/Al composite with 3D-interpenetrated network structure by various SiC foam ceramic skeletons, Ceramics International 47 (2021) 30869–30879. https://doi.org/10.1016/j.ceramint.2021.07.269.

[19]J. Xie, S. Wang, C. Guo, H. Qin, P. Gao, J. Liu, W. Guo, H. Xiao, Construction of novel plate-shaped 4H–SiC network skeleton for enhancing 3D-interpenetrated network structure SiC/Al composites, Ceramics International 48 (2022) 10251–10260. https://doi.org/10.1016/j.ceramint.2021.12.242.

[20]D. Wang, Z. Zheng, J. Lv, G. Xu, S. Zhou, W. Tang, Y. Wu, Interface design in 3D-SiC/Al-Si-Mg interpenetrating composite fabricated by pressureless infiltration, Ceramics International 44 (2018) 11956–11965. https://doi.org/10.1016/j.ceramint.2018.03.016.

[21]K. Zhang, Z. Shi, H. Xia, K. Wang, G. Liu, G. Qiao, J. Yang, Preparation and thermophysical properties of directional SiC/Cu–Si composite via spontaneous infiltration, Ceramics International 42 (2016) 996–1001. https://doi.org/10.1016/j.ceramint.2015.08.173.

[22]B.M. Caruta, New Developments in Materials Science Research, Nova Publishers, 2007.

[23]B. Nait-Ali, K. Haberko, H. Vesteghem, J. Absi, D.S. Smith, Thermal conductivity

of highly porous zirconia, Journal of the European Ceramic Society 26 (2006) 3567–3574. https://doi.org/10.1016/j.jeurceramsoc.2005.11.011.

[24] S.S. Sidhu, S. Kumar, A. Batish, Metal Matrix Composites for Thermal Management: A Review, Critical Reviews in Solid State and Materials Sciences 41 (2016) 132–157. https://doi.org/10.1080/10408436.2015.1076717.

[25] E.T. Swartz, R.O. Pohl, Thermal boundary resistance, Rev. Mod. Phys. 61 (1989) 605–668. https://doi.org/10.1103/RevModPhys.61.605.

[26] K. Chu, C. Jia, X. Liang, H. Chen, W. Gao, H. Guo, Modeling the thermal conductivity of diamond reinforced aluminium matrix composites with inhomogeneous interfacial conductance, Materials & Design 30 (2009) 4311–4316. https://doi.org/10.1016/j.matdes.2009.04.019.

Chapter5

Conclusions

In the realm of advanced materials, three-dimensional network interpenetrating phase composites (IPCs) have emerged as a subject of intense scholarly interest and research. Over the past decades, diverse compositions of IPCs, spanning metal-ceramic, metal-polymer, metal-metal, ceramic-polymer, and polymer-polymer IPCs, have been meticulously developed and investigated. Notably, metal-ceramic IPCs have garnered paramount attention owing to their exceptional amalgamation of ceramic's inherent properties, such as wear resistance, high hardness, and dimensional stability, with the advantageous traits of metals, including good plasticity, high toughness, and superior thermal and electrical conductivity. This unique synergy engenders metal-ceramic IPCs with remarkable mechanical and thermal characteristics.

Among metallic phases, aluminum and its alloys stand out due to their remarkable attributes, encompassing low density, high specific strength, excellent thermal conductivity, corrosion resistance, and eco-friendliness. Consequently, considerable research endeavors have centered on leveraging aluminum-based IPCs as promising materials. While extensive studies have delved into the mechanical and thermal properties of aluminum-based IPCs, the ceramic phases have predominantly featured compositions of Al_2O_3 and SiC, with limited exploration concerning AlN.

Aluminum Nitride (AlN) presents a compelling alternative, boasting notable advantages such as high hardness, stiffness, thermal conductivity, and a coefficient of thermal expansion compatible with SiC. Moreover, its chemical stability mitigates potential adverse reactions at the interface with aluminum alloys, thus preserving interfacial bonding integrity. Hence, the exploration of Al/AlN IPCs holds immense potential, particularly in aerospace and electronic packaging applications

Given the critical significance of this research direction, a systematic investigation into the mechanical and thermal properties of Al/AlN IPCs emerges as an imperative undertaking, promising to contribute significantly to the advancement of materials science and engineering.

In this study, AlN preform with varying porosities were fabricated via the slurry impregnation method and subsequently processed into Al/AlN IPCs utilizing low-pressure casting techniques. Microstructural analysis employed SEM, EPMA, and XRD techniques, while mechanical properties were assessed via nanoindentation and room-temperature compression. Thermal expansion behaviors were examined using finite-element simulation methods. Its thermal conductivity was also studied. This study offers a theoretical basis for the application of Al/AlN IPCs. The conclusions of this thesis can be summarized as follows:

1) Al/AlN interpenetrating phase composites with different preform porosity were successfully prepared by immersing PU foam in a mixture slurry containing AlN powder and Al_2O_3 sol, followed by infiltration with molten A356 alloy using the low-pressure casting method. SEM analysis indicated a clean and well-bonded interface between the components. As the preform porosity increased, the relative density of the composites also increased. The compression behavior of the IPCs was found to vary greatly; samples with 84% and 79% preform porosity exhibited ductile fracture, while those with 76% and 71% porosity exhibited brittle fracture. Compressive strength and yield strength showed an overall increase with increasing preform porosity. Notably, the 84% preform porosity IPCs demonstrated the highest compressive strength (140 MPa) and the best toughness (48.98 MJm^{-3}). The nanoindentation hardness is minimally affected by the presence of pores. As the porosity of the preform decreases, the nanoindentation hardness increases. Additionally, higher interfacial hardness indicates effective interfacial bonding.

2) The thermal expansion behaviors of Al/AlN IPCs with varying preform porosity have

been investigated. The experimental results, analytical models, and finite element analysis were employed to gain insights into the thermal characteristics of these materials. AlN preform effectively decreased the CTEs of Al/AlN IPCs, the reduction in preform porosity resulted in decreased CTE values for the IPCs. The unique structure of IPCs effectively constrains the expansion of the aluminum matrix, resulting in a lower CTE compared to conventional particlereinforced Al/AlN composites. Experimental values align with the analytical boundaries, affirming the accuracy of the analytical model's predictions. Finite element analysis of 3D RVEs validated the mesh independence and showcased the intricate distribution of thermal stresses within the IPCs. The FE model accurately predicts experimental results at high preform porosity levels. However, as preform porosity decreases, a significant disparity arises between calculated and actual values. This discrepancy is attributed to the FE simulation's omission of plastic deformation and residual thermal stresses.

3) Al/AlN IPCs with varying preform porosity were examined for TC. With an increase in preform porosity, the TC of IPCs also increases. The material's crystalline nature and the existence of pores contribute to a reduction in its TC as the temperature rises. The experimental results for sample 84 align well with the results derived from the theoretical models. In contrast, the experimental data for sample 79 show a considerable deviation, notably lower than the corresponding theoretical predictions. After considering interfacial thermal resistance and porosity, the disparity between the calculated results of the theoretical model and the experimental values for 79 samples decreases notably. The experimental values align with the theoretical model, whereas for 84 samples, they diverge from the calculated values. This discrepancy is primarily attributed to the decreased porosity of the prefabricated body, enlarging the interfacial region and amplifying the impact of interfacial thermal resistance. Further exploration is required to understand the impact of factors beyond porosity and interfacial thermal resistance.

Acknowledgments

During my doctoral studies, I have received a tremendous amount of help and guidance from many people, and I would like to express my sincere gratitude to all those who have supported me.

First and foremost, I would like to extend my heartfelt appreciation to Professor Sasaki for his unwavering support and mentorship. His guidance was instrumental in establishing the Ph.D. project, designing the experiment plan, advising on thesis writing, and assisting with scholarship applications. I am also deeply grateful to Assistant Professor Kenjiro Sugio and Assistant Professor Yongbum Chio for their invaluable guidance and support throughout the experimental phase of my research. Additionally, I want to express my heartfelt thanks to Professor Kazuhiro Matsugi at Hiroshima University and Professor Tiansheng Wang at Yanshan University for their technical advice and experimental assistance.

I am also thankful to Dr. Wenchuang Liu, Dr. Zixiang Qiu, Dr. Di Wu, Dr. Jia Zhao, and Dr. Wenquan Li for their kind and generous assistance. Moreover, I would like to thank all the past and present members of the Materials physics Laboratory in the Department of Mechanical Physical Engineering, Hiroshima University, for their enthusiastic help to my life and study.

I would like to extend a special thank you to Dr. Chunzhi Zhao from Harbin Institute of Technology and Dr. Xuefeng Zhou from Center for High Pressure Science & Technology Advanced Research for their unwavering support and contributions to the experimental work.

Finally, I would like to express my gratitude to my family for their steadfast support and love throughout the years. During the six-year journey from graduate school to doctoral studies, I am grateful for their understanding of my busy scientific research life.

Published Papers in Regards to This Thesis

1. Xiao Yan, Kenjiro Sugio, Yongbum Choi, Tiansheng Wang, Zhefeng Xv, Chunzhi Zhao, Gen Sasaki, Microstructure and mechanical properties of Al/AlN interpenetrating phase composites with different preform porosity, Materials Chemistry and Physics, Volume 315, 2024,129029. (Chapter 2)

2. Xiao Yan, Kenjiro Sugio, Yongbum Choi, Tiansheng Wang, Chunzhi Zhao, Gen Sasaki, Thermal expansion behavior and analysis of Al/AlN interpenetrating phase composites with different preform porosity, Journal of Materials Research and Technology, Volume 30,2024, Pages 1539-1546. (Chapter 3)

3. Xiao Yan, Chunzhi Zhao, Gen Sasaki, Thermal conductivity of Al/AlN interpenetrating phase composites with different preform porosity, 2024 3rd International Conference on Applied Mechanics and Advanced Materials (ICAMAM 2024). (Chapter 4)

Presentations

1. Characterization and preparation of open cell AlN Ceramic for MMC, Xiao Yan, Kenjiro Sugio, Gen Sasaki, 2021 年 3 月 日本金属学会 春期講演大会 ポスターセッション(オンライン開催).

2. Preparation of Al/AlN interpenetrating phase composites materials by low pressure casting, Xiao Yan, Kenjiro Sugio, Yongbum Choi, Gen Sasaki, 6th Asian Symposium on Material and Processing 2022 (ASMP2022), January 26, 2022

3. Characterization and Preparation of Al/AlN IPCs, Xiao Yan, Kenjiro Sugio, Yongbum Choi, Gen Sasaki, 2022 年 3 月 日本金属学会 秋期講演大会 オンライン開催.